Modelling diseases associated with mitochondrial proteins CHCHD10 and CHCHD2 in zebrafish

by

Virginie Petel Légaré

Integrated Program in Neuroscience

McGill University, Montréal

September 2022

A thesis submitted to McGill University in partial fulfillment of the requirements of the degree of Doctor of Philosophy

Abstract

The mitochondrial paralogues CHCHD10 and CHCHD2 have been linked to several neurodegenerative disease including most prominently amyotrophic lateral sclerosis (ALS) and Parkinson's disease (PD). Despite their linkage to disease, very little is understood of their role in the mitochondria. In the first research chapter of this thesis, we present data where we used the zebrafish to create a *chchd10* $^{-/-}$, *chchd2* $^{-/-}$ as well as a double *chchd10* $^{-/-}$ & *chchd2* $^{-/-}$ knock-out (KO) model to study the role of both proteins in the developing larvae. This chapter reveals that both proteins are important for motor behaviour, neuromuscular junction (NMJ) integrity, and survival. We also demonstrate that loss of either Chchd10 or Chchd2 leads to reduced mitochondrial respiratory chain Complex I assembly, though this defect was not observed in double *chchd10* $^{-/-}$ & *chchd2* $^{-/-}$ larvae. We speculate that activation of the mitochondrial integrated stress response (mt-ISR), which was only observed in double *chchd10* $^{-/-}$ & *chchd2* $^{-/-}$ larvae, may underlie the restoration of Complex I assembly. The first research chapter of this thesis highlights the benefits of complementing mouse models with zebrafish models when studying CHCHD10 and CHCHD2, as contrary to our findings, single CHCHD10 or CHCHD2 mouse KOs display little to no phenotypes. Importantly, we also show that previously described Complex I assembly defects in CHCHD10 and CHCHD2 models are most likely not solely responsible for the observed deficits. Indeed, while double *chchd10* $^{-/-}$ & *chchd2* $^{-/-}$ larvae did not present reduced Complex I assembly, their motor, survival, and NMJ defects were generally worse. In the second research chapter, we present data collected from studying a knock-in (KI) model expressing the orthologous ALS-associated CHCHD10 ^{P80L} variant (zebrafish Chchd10 ^{P83L}). The data presented in this chapter reveals that expression of the P83L variant leads to reduced Chchd10 levels which is coincident with defects in motor behaviour, NMJ integrity and

survival, similar to defects presented by *chchd10* $^{-/-}$ larvae in the first research chapter. This suggests that this variant likely acts through a loss-of-function disease mechanism, which contrasts with other *in vivo* studies that mostly suggest gain-of-function mechanisms. In the second research chapter, we also examined phenotypes in adult zebrafish as this would permit us to explore potential contributing factors to disease onset. Bulk spinal cord RNA sequencing revealed elevated transcript levels associated with inflammation suggesting that this pathological pathway may contribute to disease in ALS patients expressing the CHCHD10 ^{P80L} variant. Despite this finding, our KI model only displayed a muscle phenotype, which was characterized by a reduction of size and number of muscle fibers (both pre-symptomatically and at disease end stage), while motoneurons were mostly spared. This suggests that muscle pathology might contribute heavily to disease in CHCHD10 ^{P80L} patients and should be the focus for future studies investigating therapeutics. In summary, this thesis presents research findings that add to our understanding of CHCHD10 and CHCHD2 during vertebrate development and describes a new potential pathological mechanism of action of the CHCHD10 ^{P80L} variant in ALS.

Résumé

Les paralogues mitochondriaux CHCHD10 et CHCHD2 sont associés à plusieurs maladies neurodégénératives, notamment la sclérose latérale amyotrophique (SLA) et la maladie de Parkinson (MP). Malgré leur lien avec ces maladies, leurs rôles physiologiques et pathologiques sont peu définis. Dans le premier chapitre de cette thèse, nous présentons des données recueillies sur les modèles *chchd10* $^{-/-}$, *chchd2* $^{-/-}$ ainsi que double *chchd10* $^{-/-}$ & *chchd2* $^{-/-}$ knock-out (KO) que nous avons créés afin d'étudier le rôle de ces deux protéines dans les larves en développement. Ce chapitre révèle que ces protéines sont nécessaires pour la motricité, la survie et l'intégrité de la jonction neuromusculaire (JNM). Nous démontrons également que la perte de Chchd10 ou de Chchd2 entraîne une réduction de l'assemblage du Complexe I de la chaîne respiratoire mitochondriale, mais que ce défaut n'est pas présent chez les larves doubles *chchd10* $^{-/-}$ & *chchd2* $^{-/-}$. Nous proposons que l'activation de la réponse au stress intégré mitochondriale (mt-ISR), qui n'a été observée que chez les larves doubles *chchd10* $^{-/-}$ & *chchd2* $^{-/-}$, pourrait être responsable de la restauration de l'assemblage du Complexe I. Le premier chapitre de recherche démontre l'avantage d'utiliser les modèles de poissons-zèbres de manière complémentaire aux modèles de souris, lors de l'étude des protéines CHCHD10 et CHCHD2. En effet, contrairement aux observations effectuées chez les larves, les KO de souris simples de CHCHD10 ou CHCHD2 affichent peu ou pas de phénotypes. Nous démontrons également que le défaut d'assemblage du Complexe mitochondrial I, précédemment décrit dans les modèles CHCHD2 et CHCHD10, n'est pas le seul responsable des déficits, car les larves doubles *chchd10* $^{-/-}$ & *chchd2* $^{-/-}$, qui ne présentent aucune réduction de l'assemblage du Complexe I, présentent tout de même des défauts moteurs, de survie et d'intégrité de la JNM. Dans le deuxième chapitre, nous présentons les données recueillies à partir de l'étude d'un modèle knock-in (KI) exprimant le variant orthologue

CHCHD10 ^{P80L} associé à la SLA (Chchd10 ^{P83L} chez le poisson-zèbre). Nous démontrons que l'expression du variant P83L résulte à une réduction des niveaux de la protéine Chchd10, ce qui coïncide avec des défauts de comportement moteur, de survie, et d'intégrité de la JNM, similaires aux défauts observés chez les larves *chchd10* $^{-/-}$ dans le premier chapitre de cette thèse. Cela suggère que ce variant agit par le biais d'un mécanisme de perte de fonction, par opposition à d'autres études *in vivo* qui suggèrent principalement un mécanisme de gain de fonction. Dans le deuxième chapitre, nous examinons les phénotypes chez le poisson-zèbre adulte afin d'explorer les facteurs qui contribuent potentiellement au développement de la maladie. En utilisant le séquençage de masse de l'ARN de la moelle épinière, nous constatons des niveaux élevés de transcrits associés à la l'inflammation neuronale, suggérant que ce mécanisme pathologique pourrait contribuer au développement de la maladie chez les patients SLA exprimant le variant CHCHD10 ^{P80L}. Malgré cette observation, l'examen physique des muscles et motoneurones révèle que les poissons KI présentent majoritairement un phénotype musculaire, caractérisé par une réduction de la taille et du nombre de fibres musculaires (à la fois présymptomatique et au stade terminal de la maladie), alors que les corps des motoneurones sont majoritairement épargnés. Cela suggère que la pathologie musculaire pourrait contribuer plus fortement à la maladie chez les patients qui sont porteur du variant CHCHD10 ^{P80L}, ce qui devrait être au centre des futures études sur le développement thérapeutique. En résumé, cette thèse présente des résultats de recherche qui étayent notre compréhension du rôle de CHCHD10 et de CHCHD2 au cours du développement des vertébrés et décrivent de potentiels mécanismes d'action pathologiques du variant CHCHD10 ^{P80L} chez les patients SLA.

Table of contents

Abbreviation List

Abbreviation	Meaning
°C	degree Celsius
2-DG	2-deoxy-d-glucose
2D-PAGE	second dimension SDS-PAGE
Ab	antibody
aBtx	alpha-bungarotoxin
AchRs	acetylcholine receptors
AD	Alzheimer's disease
ALS	amyotrophic lateral sclerosis
BAK	BCL2 antagonist/Killer 1
BAX	BCL2 associated X protein
BCL2	B-cell lymphoma 2
C1QBP	complement component 1 Q subcomponent-binding protein
C9OR72	chromosome 9 open reading frame 72
Cas9	CRISPR-associated protein 9
CCCP	carbonyl cyanide m-chlorophenyl hydrazone
cDNA	complementary DNA
cGAS	cyclic GMP-AMP synthase
CHCH	coiled-helix coiled-helix
CHCHD10	coiled-coil-helix-coiled-coil-helix domain-containing protein 10
CHCHD2	coiled-coil-helix-coiled-coil-helix domain-containing protein 2
Chr	chromosome
CMT2	Charcot–Marie–Tooth type 2 disease
CNS	central nervous system
COX	cytochrome c oxidase
COX1	cytochrome c oxidase subunit I
COX4I2	COX subunit 4 isoform
CRISPR	clustered regularly interspaced short palindromic repeats
DA	dopaminergic
DAMPs	damage-associated molecular patterns
DAVID	Database for Annotation, Visualization and Integrated Discovery
DENN	differentially expressed in normal and neoplasia
DNA	deoxyribonucleic acid
dpf	days post fertilization
DPR	dipeptide repeat protein
eIF2α	eukaryotic translation initiation factor 2α
ER	endoplasmic reticulum

fALS	familial ALS
FTD	frontotemporal lobar degeneration
FUS	Fused in sarcoma
GR	glycine/arginine
gRNA	guide RNA
H2A.X	H2A histone family member X
hpf	hours post fertilization
IMS	Intermembrane Space
KD	knockdown
KI	knockin
KO	knockout
LRKK2	leucine rich repeat kinase 2
M	molar
MDV	mitochondrial derived vesicule
MICOS	mitochondrial contact site and cristae organizing system
MMP	mitochondrial membrane potential
MNI	montreal neurological institute
MNRR1	mitochondrial nuclear retrograde regulator 1
mPTP	mitochondrial permeability transition pore
MSA	multiple system atrophy
mt-DNA	mitchondrial DNA
mt-ISR	mitochondrial integrated stress response
MTS	mitochondrial targetting sequence
mut	mutant
n.s.	non-significant
NDUFA9	NADH:ubiquinone oxidoreductase subunit A9
NF-kB	nuclear factor kappa B
NLRP3	NLR family pyrin domain containing 3
NMJ	neuromuscular Junction
OCR	oxygen consumption rates
OMA1	metalloendopeptidase OMA1
OPA1	optic atrophy 1
ORE	oxygen-responsive elements
OXPHOS	oxydative phosphorylation
p-value	probability value
p62	ubiquitin-binding protein
PB	sodium phenylbutyrate
PBS	phosphate-buffered saline
PCR	polymerase chain reaction
PD	Parkinson's disease

PET	positron emission tomography
PFA	paraformaldehyde
qRT-PCR	quantitative real-time PCR
RNA	ribonucleic acid
ROS	reactive oxygen species
RT	room temperature
sALS	sporadic ALS
SDHA	succinate dehydrogenase complex flavoprotein subunit A
SDS	sodium dodecyl sulphate
SEM	standard error of the mean
sgRNA	single guide RNA
siRNA	small interfering RNA
SMAJ	spinal motor neuropathy Jokela type
SOD1	superoxide dismutase 1
SQSTM1	sequestosome 1
STING	stinulator of interferon genes
SYT2	synaptotagmin 2
t-test	student's statistical hypothesis test
TARDBP	Transactive Response DNA Binding Protein 43 kDa
TBST	tris-buffered saline and Tween 20
TCA	citric acid cycle
TDP-43	TAR DNA-binding protein 43
TFAM	mitochondrial transcription factor A
TL	Tübingen long fin
TLR9	toll like receptor 9
TNF-α	Tumor Necrosis Factor Alpha
Tris	tris(hydroxymethyl)aminomethane
TUBA4A	tubulin alpha 4a
TUBCCA	tauroursodeoxycholic acid
UBQLN2	ubiquilin-2
WT	wild type
µg	microgram
µL	microliter
µM	micromolar

List of figures

List of tables

Acknowledgements

I would first like to thank Dr. Gary Armstrong for his guidance throughout my Ph.D. I will be forever grateful for his scientific and financial support as well as his endless patience during the past 5 years without which this work would have not been possible. Most importantly, I would like to thank him for his trust and for giving me scientific freedom during the development of this project, which helped me develop skills which will be invaluable for the next chapter of my career.

A huge thanks also goes to the members of my lab: Christian Rampal, Esteban Rodriguez Pinto, Tyler Gunberg, and Ziyaan Harji, who were always willing to lend a helping hand when needed, and who were great people to be around in the lab.

A special thanks goes to all the past and present members of the labs on the sixth floor; Dr. Brais, Dr. Durham, Dr. Gentil, Dr. Hastings Dr. McBride, and Dr. Shoubridge. More specifically, I would like to thank those who helped me navigate my project, for the collaborations and for all the insightful discussions: Dr. Alexander Janer, Dr. Hana Antonicka, Dr. Isabella Straub, Kathleen Daigneault, Dr. Mari Aaltonen, and Dr. Rebecca Robertson. I would also like to acknowledge the members of my advisory committee for their time and their precious tips, Dr. McBride and Dr. Shoubridge.

To my family, who supported and believed in me throughout this journey, thank you for trusting that this path would be successful. To all my amazing friends, who cheered me on and kept me sane, I would not have been able to get through all those years without you. I would like to especially thank my partner, Ryan, who has been with me throughout all my graduate studies, for

his love, unwavering support, and for his ability to make me laugh, especially during all the crises that inevitably come with graduate studies. And to juju, obviously, for all the cuddles.

Lastly, I would like to thank all the institutions which granted me financial support over the years; Healthy Brain for Healthy Lives (HBHL, McGill), Internal Medicine studentship (McGill), Integrated program of neuroscience (IPN, McGill), and MITACS.

Preface

This thesis is written in accordance with the guidelines of McGill University Graduate and Postdoctoral Studies and is presented in a manuscript-based format. It is composed of 5 chapters.

Chapter 1 is a general introduction which reviews the literature relevant to the studies presented in this thesis. **Chapter 2** describes the larval phenotype of 3 models, *chchd10* $^{-/-}$, *chchd2* $^{-/-}$ and double *chchd10* $^{-/-}$ & *chchd2* $^{-/-}$. This study is in review in the journal *Developmental neurobiology*. **Chapter 3** describes the larval phenotype of a knock-in model, *chchd10* $^{P83L/P83L}$, and present data of defects present at adult stages. This study is in preparation for submission. **Chapter 4** is a general discussion around the findings of this thesis, and **Chapter 5** presents the conclusion of this work.

Contribution to original knowledge

1. Creation, characterization, and comparison of *chchd10* $^{-/-}$, *chchd2* $^{-/-}$, and double *chchd10* $^{-/-}$ *& chchd2* $^{-/-}$ in an *in vivo* model.
2. Creation and characterization of the first orthologous *chchd10* $^{P80L/P80L}$ *in vivo* knock-in (KI) model. First *in vivo* CHCHD10 KI model highlighting that a variant can act partly through loss of function.
3. Increased involvement of Chchd10 compared to Chchd2 in postsynaptic neuromuscular junction integrity at larval stages of zebrafish development.
4. Observation that activation of the mitochondrial integrated stress response (mt-ISR) is not common to all CHCHD10 variants and is activated following loss of both Chchd2 and Chchd10, but not following individual loss.
5. Mitochondrial respiratory chain Complex I deficiency following loss of either Chchd10 or Chchd2 is independent of mt-ISR activation.
6. Characterization of both a low and higher molecular weight complex of Chchd10 in an *in vivo* model
7. Observation that, though CHCHD2 is mainly linked to Parkinson's disease, it is required in muscle physiology and pathology.
8. First study to identify inflammation as potential contributor to disease in an orthologous CHCHD10 ^{P80L} model.
9. Tissue specific examination of degeneration in adult Chchd10 ^{P83L} zebrafish suggests that muscle pathology occurs pre-symptomatically and worsens during symptom onset.

Contribution of authors

With the guidance of my committee consisting of Dr. McBride, Dr. Shoubridge, and Dr. Armstrong, I designed and executed experiments included in this thesis. Listed are contributions from collaborators.

Chapter 2 : **Petel Légaré, Virginie**, Christian J. Rampal, Mari J. Aaltonen, Alexandre Janer, Lorne Zinman, Eric A. Shoubridge, and Gary A.B. Armstrong. 2022. 'Loss of mitochondrial Chchd10 or Chchd2 in zebrafish leads to an ALS-like phenotype and Complex I deficiency independent of the mt-ISR', bioRxiv: **2022**.05.02.488746. In review, Developmental Neurobiology – DNEU-00056-2022

For Chapter 2, Christian J. Rampal performed the imaging of the neuromuscular junction. Dr. Aaltonen performed the final Blue Native PAGE for publication. Dr. Janer helped with the 2D-PAGE experiment. Dr. Zinman provided funding and proofreading. Dr. Shoubridge helped with the design of experiments and proofread the manuscript.

Chapter 3: Petel Légaré, Virginie , Christian J. Rampal, Hana Antonicka, Ziyaan A. Harji, Esteban Rodriguez Pinto, Eric A. Shoubridge, and Gary A.B. Armstrong. 'CHCHD10 ^{P80L} CRISPR knock-in zebrafish model display a pre-symptomatic adult muscle phenotype. *Manuscript in preparation*

For Chapter 3, Christian J. Rampal performed the imaging of the neuromuscular junction. Dr. Hana Antonicka performed the Blue Native experiments. Ziyaan Harji helped complete the

forced swim data. Esteban Rodriguez Pinto performed the staining and imaging of both muscle and spinal cord sections.

Chapter 1: Review of the relevant literature

1. Amyotrophic lateral sclerosis

Amyotrophic Lateral Sclerosis (ALS) was first described in 1869 by Jean Martin Charcot (Kumar, Aslinia et al. 2011) and is a fatal neurodegenerative disorder. It is considered a rare disease, with an incidence of about 2/100,000 in Canada (ALS Canada) and is characterized by the progressive degeneration of lower motoneurons, located in the brainstem and spinal cord which innervate the muscles, and of the upper motoneurons in cerebral cortex. Degeneration is characterized by the histological loss of motoneurons, muscle atrophy, paralysis, and death, usually 2-5 years following diagnosis (Oskarsson, Gendron et al. 2018).

The clinical presentation of ALS is highly heterogeneous. Disease onset varies, though usually occurs between 55 and 65 years of age (Orsini, Oliveira et al. 2015). Location of symptom onset can also vary. Limb onset is the most frequent and manifests as a weakness in the arms or legs, while one third of cases develop bulbar onset, characterized by a difficulty chewing and swallowing (Brown and Al-Chalabi 2017). In some cases, neuronal degeneration also extends to the frontal and temporal cortex leading to frontotemporal lobar degeneration (FTD) (Taylor, Brown et al. 2016). FTD is the second leading cause of dementia after Alzheimer's disease (AD) (Van Langenhove, van der Zee et al. 2012, Ling, Polymenidou et al. 2013). While about 15 to 20% of ALS patients go on to develop dementia (Bang, Spina et al. 2015), 15% of FTD patients develop ALS (Ling, Polymenidou et al. 2013) leading both diseases to be considered as part of a spectrum, with overlapping clinical and pathological presentations.

There is no definitive diagnostic test for ALS. Diagnosis is usually based on progressive nature, painless weakness, examination of upper and lower motor neuronal dysfunction and electrophysiological evaluations of afflicted skeletal muscle groups (Oskarsson, Gendron et al. 2018). It also often involves differential diagnosis with other diseases such as brainstem lesion (stroke, multiple sclerosis, tumour), neuromuscular junction disorder (myasthenia gravis), bulbospinal muscular atrophy, and multifocal motor neuropathy among others (Oskarsson, Gendron et al. 2018).

Current approved treatments are largely ineffective and include Riluzole, approved since 1995 (Bensimon, Lacomblez et al. 1994), Ederavone, approved in 2017 (Cruz 2018), and more recently Albrioza approved in 2022 (Paganoni, Macklin et al. 2020, Paganoni, Hendrix et al. 2022). Riluzole, a glutamate antagonist thought to reduce excitotoxicity, has limited effect on survival and is thought to only extend life by 3-4 months (Miller, Mitchell et al. 2012, Brown and Al-Chalabi 2017). Ederavone, is a free radical scavenger that acts to suppress oxidative stress (Cruz 2018) and slows disease progression, but in a select population of patients, usually in early stages of disease (Abe, Itoyama et al. 2014, Abe, Aoki et al. 2017, Oskarsson, Gendron et al. 2018). Finally, Albrioza is a combination of two drugs, sodium phenylbutyrate (PB), a scavenger which increase excretion of excess nitrogen and can act as a chemical chaperone, and tauroursodeoxycholic acid (TUDCA), which inhibits mitochondrial apoptosis, decreases reactive oxygen species (ROS), and reduces triggering of apoptosis following endoplasmic reticulum (ER) stress. Its benefits are still mild, with the most recent trial resulting in an extension of life of 6.5 months compared to patients given placebo (Paganoni, Hendrix et al. 2021). Therefore, treatment often revolves around symptom management such as nasogastric or enteral feeding,

prevention of aspiration and ventilatory support by a multidisciplinary team (Brown and Al-Chalabi 2017). As such, there is a considerable need for drug development in ALS. One of the main deterrents to treatment discovery is the lack of basic understanding of the cellular mechanisms contributing to disease aetiology. Basic research into the pathological mechanisms involved in ALS could springboard the identification of specific targets which could subsequently be pharmacologically modulated for therapeutic development for this fatal disease.

2. Genetics of ALS and mitochondrial dysfunction

Though the majority of ALS cases are sporadic (sALS), about 10% of the cases have a familial history (fALS) (Brown and Al-Chalabi 2017). Genetic cases allow insight into the molecular mechanisms involved in disease pathogenesis. The most common genes involved in ALS are chromosome 9 open reading frame 72 (*C9ORF72*), superoxide dismutase (*SOD1),* Transactive Response DNA Binding Protein 43 kDa (*TARDBP*) and fused in sarcoma (*FUS*) (Zou, Zhou et al. 2017).

SOD1, discovered in 1993, was the first gene linked to ALS (Rosen, Siddique et al. 1993). Its protein is involved in the conversion of reactive superoxide to hydrogen peroxide or oxygen, which confers protection against oxidative stress. The most common genetic cause of ALS and FTD, is the hexanucleotide repeat "GGGGCC" expansion of *C9ORF72*, responsible for about 40% of ALS and 25% of FTD cases with European ancestry, respectively (DeJesus-Hernandez, Mackenzie et al. 2011, Brown and Al-Chalabi 2017). Its protein is part of the DENN (Differentially Expressed in Normal and Neoplasia) family and is involved in endocytosis and endosomal trafficking, though the exact mechanism of pathogenicity is still unclear (Smeyers,

Banchi et al. 2021). The last two genes, *TARDBP* (Sreedharan, Blair et al. 2008) and *FUS* (Kwiatkowski, Bosco et al. 2009) both have a role in RNA homeostasis. Interestingly, though genetic cases involving mutation in *TARDBP* are rare (~1-2%), about 97% of both sALS and fALS patients present with cytoplasmic accumulation of TDP-43, the protein encoded by *TARDBP* (Arai, Hasegawa et al. 2006, Neumann, Sampathu et al. 2006). While these genes stand out in frequency of identification in patient cohorts, over 25 genes have now been associated with ALS (https://alsod.ac.uk/) (Brown and Al-Chalabi 2017) which code for proteins known to be involved in a number of physiological processes including but not limited to protein quality control, RNA binding and homeostasis, as well as cytoskeletal dynamics (Taylor, Brown et al. 2016) (**Figure 1.1**).

One of the other major physiological pathways that has been linked to ALS pathology and other neurodegenerative diseases is mitochondrial dysfunction. Mitochondria are essential organelles responsible for several processes including apoptosis, ATP generation, calcium ion and iron ion homeostasis, ROS formation, as well as immune responses (Lezi and Swerdlow 2012, Zhong, Liang et al. 2018). Mitochondrial structural abnormalities, such as swollen and aggregated mitochondria, respiratory chain deficiencies and increased oxidative stress have been documented in ALS patient tissue (Chung and Suh 2002, Dupuis, Gonzalez de Aguilar et al. 2004, Iwata and Sasaki 2007). Some proteins involved in genetic cases of ALS such as TDP-43, SOD1, FUS, and C9ORF72 have also been proposed to potentially exert some detrimental consequences through the mitochondria with reports documenting their increased localization in mitochondria leading to oxidative stress or reduced respiration (Blokhuis, Koppers et al. 2016, Lopez-Gonzalez, Lu et al. 2016, Wang, Wang et al. 2016). Moreover, several animal models

present mitochondrial defects at early disease-like stages (Magrané, Hervias et al. 2009, Vande Velde, McDonald et al. 2011, Vinsant, Mansfield et al. 2013, Magrané, Cortez et al. 2014). Yet, whether mitochondrial dysfunction plays a central role in the disease aetiology or manifests as a downstream consequence of other cellular defects was unclear until 2014 when a protein variant was identified to segregate in fALS patients in the first exclusively mitochondrial protein (Bannwarth, Ait-El-Mkadem et al. 2014). CHCHD10 is encoded by the nuclear gene termed coiled-coil-helix-coiled-coil-helix domain containing 10 (*CHCHD10*), and was identified first in a French and Spanish family with ALS, mitochondrial myopathy, cerebellar ataxia, as well as FTD (Bannwarth, Ait-El-Mkadem et al. 2014). Though mutations in *CHCHD10* represent less than 1% of ALS cases (Traynor, Johnson et al. 2014), this protein is of interest as it can give us insight into the role that mitochondrial dysfunction plays in ALS and could offer potentially new therapeutic targets.

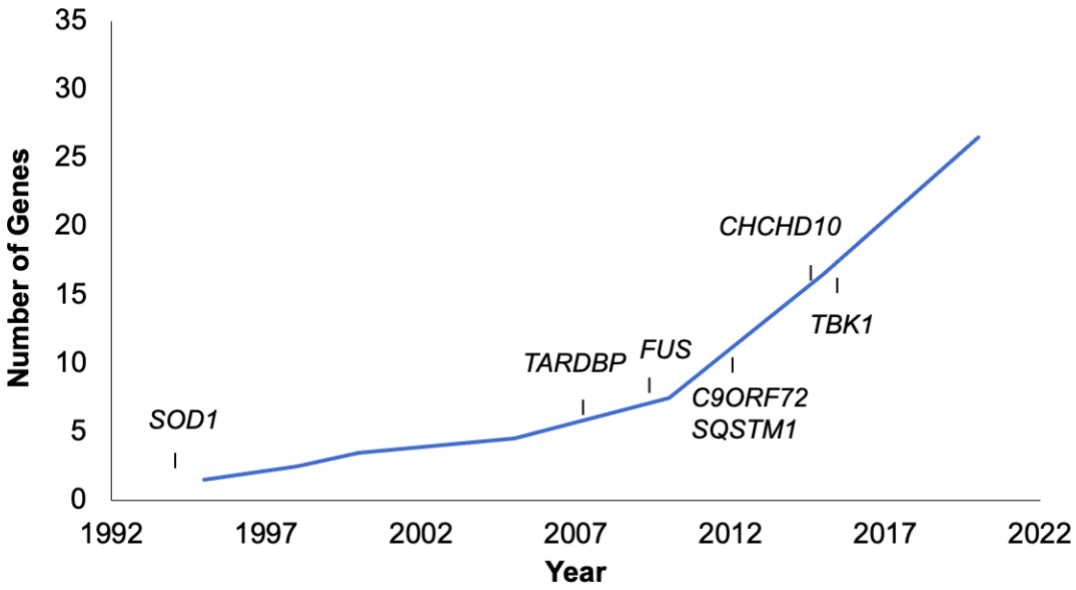

Figure 1.1 Increasing number of genes have been associated with familial ALS over the years.

2.1 CHCHD10 is associated with ALS and other neurogenerative diseases

Since the discovery of the first CHCHD10 variant, over a dozen variants have been described (https://alsod.ac.uk/) and have been associated with a spectrum of diseases, including ALS (Dols-Icardo, Nebot et al. 2015, Ronchi, Riboldi et al. 2015, Zhang, Xi et al. 2015, Perrone, Nguyen et al. 2017, Zhou, Chen et al. 2017, Lehmer, Schludi et al. 2018), FTD (Dols-Icardo, Nebot et al. 2015, Perrone, Nguyen et al. 2017), FTD-ALS (Bannwarth, Ait-El-Mkadem et al. 2014, Chaussenot, Le Ber et al. 2014), mitochondrial myopathy (Ajroud-Driss, Fecto et al. 2015), Charcot–Marie–Tooth type 2 disease (CMT2) (Auranen, Ylikallio et al. 2015), Parkinson's disease (PD) (Perrone, Nguyen et al. 2017), Alzheimer's disease (AD) (Zhang, Xi et al. 2015, Xiao, Jiao et al. 2017) and spinal motor neuropathy Jokela type (Penttilä, Jokela et al. 2015). Among those, the variants CHCHD10 ^{S59L} (Bannwarth, Ait-El-Mkadem et al. 2014, Chaussenot, Le Ber et al. 2014), CHCHD10 ^{R15L} (Müller, Andersen et al. 2014, Traynor, Johnson et al. 2014, Kurzwelly, Heneka et al. 2015) as well as the CHCHD10^{P80L} (Ronchi, Riboldi et al. 2015, Zhang, Xi et al. 2015, Perrone, Nguyen et al. 2017) have been documented in both fALS and sALS cases (Consortium 2018) (**Figure 1.2**).

2.2 CHCHD2 is a protein associated with PD and other neurogenerative diseases

Shortly after the description of *CHCHD10* mutations in ALS patients, mutations in another gene termed coiled-coil-helix-coiled-coil-helix domain containing 2 (*CHCHD2*), a paralogue of *CHCHD10*, were discovered to segregate within a Japanese family that developed PD in an autosomal dominant manner (Funayama, Ohe et al. 2015). Those findings were replicated, and *CHCHD2* mutations have now been independently identified in several familial and sporadic PD cases (Foo, Liu et al. 2015, Jansen, Bras et al. 2015, Shi, Mao et al. 2016, Ikeda, Matsushima et

al. 2017, Yang, Zhao et al. 2019). PD is a neurodegenerative disease, though degeneration occurs primarily in the dopaminergic neurons within the substantia nigra (Poewe, Seppi et al. 2017). Patients usually develop motor symptoms, mainly bradykinesia, and non-motor symptoms, such as sleep disorder and cognitive impairments (Poewe, Seppi et al. 2017). Interestingly, CHCHD2 has also been linked to FTD (Che, Zhao et al. 2018), AD (Che, Zhao et al. 2018), Lewis body dementia (Ogaki, Koga et al. 2015), and multiple system atrophy (MSA) (Nicoletti, Gagliardi et al. 2018), though a link to ALS has yet to be made (**Figure 1.2**).

3 Structure and localization of CHCHD10 and CHCHD2

CHCHD10 and CHCHD2 are paralogues with 58% sequence identity to their humans orthologues, and are thought to result from a gene duplication from their common ancestor, *mic17*, in yeast (Cavallaro 2010). Both proteins are part of the twin CX_9C-containing domain family, which are intermembrane space proteins involved in mitochondrial respiration, lipid regulation, mitochondrial dynamics, and metabolism (Modjtahedi, Tokatlidis et al. 2016). Both proteins are comprised of a putative N-terminal mitochondrial targeting sequence potentially required for import into the mitochondria (Burstein, Valsecchi et al. 2018), though some report that only the CX_9C domain is required (Becker, Böttinger et al. 2012, Lehmer, Schludi et al. 2018). Import into the intermembrane space (IMS) occurs via the Mia40/CHCHD4 machinery which catalyzes two disulfide bonds between the four cysteines residues allowing the folding and retention of the proteins inside the intermembrane space (Modjtahedi, Tokatlidis et al. 2016). Both proteins also have a hydrophobic domain, which has been described as important for protein-protein interaction, and where several documented mutations are located (**Figure 1.2**).

Both proteins also and contain highly disordered regions and the conserved the coiled-coiled helix domain (**Figure 1.3**).

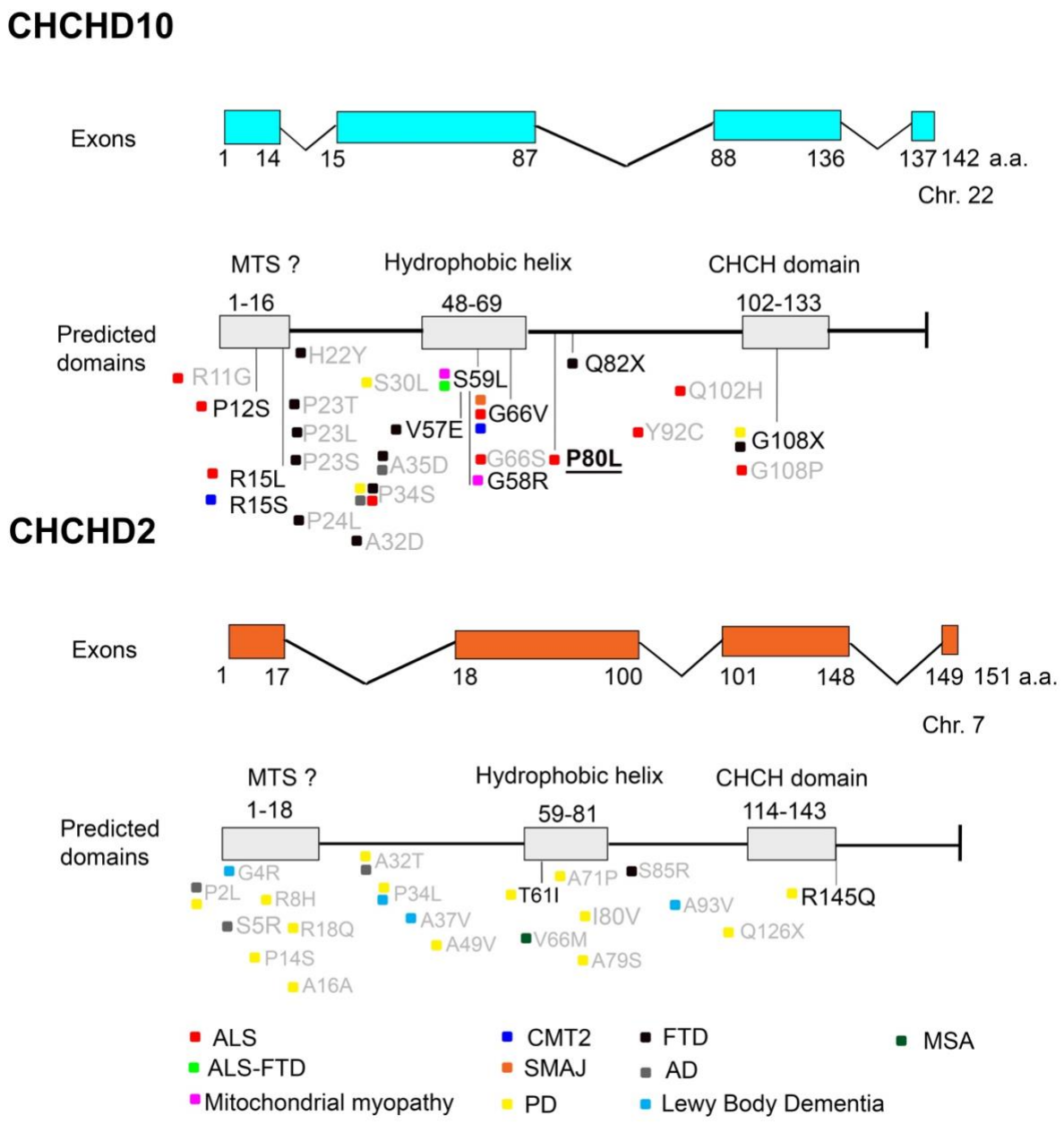

Figure 1.2 CHCHD2 and CHCHD10 structure and mutations.

Adapted from Imai, Meng et al. (2019) and Keith, Swinkin et al. (2020). The four exons of each gene are presented with their respective amino acids. Predicted domains are presented below as well as the location and nature of several documented variants documented in different diseases

(colored dots). Gray variants represent variants with low pathogenic evidence, with limited number of sporadic cases, or no familial cases. Variants in bold have greater evidence to link to disease and include familial cases. Abbreviations; ALS: amyotrophic lateral sclerosis, CMT2: Charcot Marie Tooth type 2, SMAJ: spinal motor neuropathy Jokela type, PD: Parkinson's disease, FTD: Frontotemporal dementia, AD: Alzheimer's disease, MSA: multiple system atrophy.

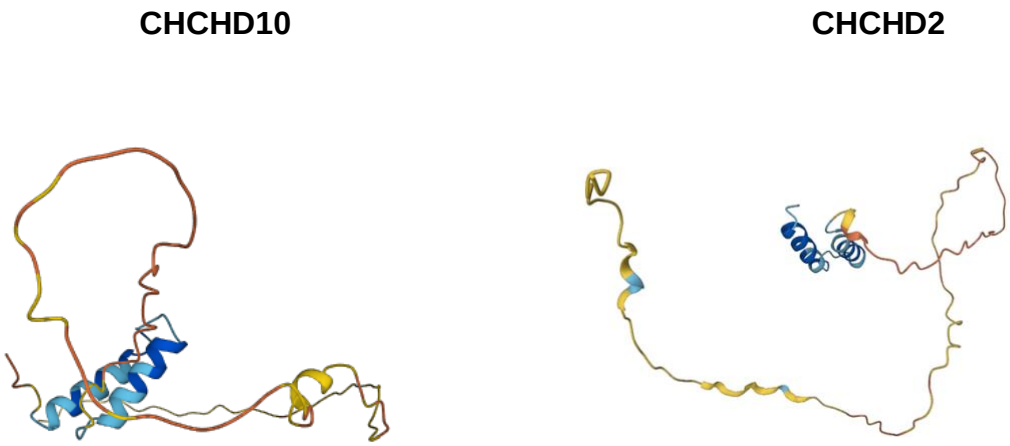

Figure 1.3 Predicted structures of CHCHD10 and CHCHD2 (https://alphafold.ebi.ac.uk/).

CHCHD10 and CHCHD2 localize mostly in the IMS of the mitochondria and are enriched at cristae junctions (Bannwarth, Ait-El-Mkadem et al. 2014, Zhou, Ma et al. 2018). Reports of localization outside the mitochondria have also been made for both proteins (Aras, Bai et al. 2015, Woo, Liu et al. 2017, Purandare, Somayajulu et al. 2018, Aras, Purandare et al. 2020). In some instances, stress seem to affect their localization. For example, CHCHD2 import has been documented to be impaired under stress condition, leading to its accumulation in the nucleus (Aras, Purandare et al. 2020). Under hypoxic conditions, CHCHD2 was also described to act as a transcription factor of the COX subunit 4 isoform (*COX4I2*) (Aras, Bai et al. 2015), while CHCHD10 was proposed to regulate transcription of oxygen-responsive elements (ORE) to increase mitochondrial respiration (Purandare, Somayajulu et al. 2018). Finally, under stress condition, both CHCHD10 and CHCHD2 have been proposed to translocate into the cytosol to regulate mitochondrial stress responses by suppressing phosphorylation of mitochondrial integrated stress response (mt-ISR) activator, eukaryotic translation initiation factor 2α (eiF2α), as described in more details in section 5.2 (Ruan, Hu et al. 2022).

4 CHCHD10/CHCHD2 complex and the impact of CHCHD10 variants

Straub et *al.* (2018) first documented that CHCHD10 and CHCHD2 formed a complex in the IMS. Both proteins have been shown to exist either as monomers or heterodimers. In addition, both proteins have also been identified in high molecular weight complexes around 170 and 220 kDa (Huang, Wu et al. 2018, Straub, Janer et al. 2018), though the composition of those complexes has yet to be resolved (Burstein, Valsecchi et al. 2018, Straub, Janer et al. 2018).

CHCHD10 variants have been documented to have various effects on their heterodimerization. CHCHD10 ^{S59L} and CHCHD10 ^{R15L} variant were reported to have no effect on the ability to form the heterodimer (Burstein, Valsecchi et al. 2018), while the CHCHD10 ^{P80L} variant was reported to result in the loss of interaction with CHCHD2 (Purandare, Somayajulu et al. 2018). Of note, increased interaction between CHCHD10 and CHCHD2 was reported in knock-in (KI) mice following the expression of the orthologous CHCHD10 ^{S59L} variant, potentially due to increased hydrophobicity (Anderson, Bredvik et al. 2019). Furthermore, a recent study showed the CHCHD10 ^{S59L} variant affected the 3D structure, where it forms more prominent β-sheet structure in comparison with the wild-type CHCHD10, promoting its oligomerization (Alici, Uversky et al. 2022). This highlights the notion that the location and nature of the variant might have an impact on pathology. Indeed, the variants being associated with specific diseases (**Figure 1.2**), both gain- and loss- of function mechanisms, have been described in the context of different variants. For example, reduced CHCHD10 protein concentrations following the expression of CHCHD10 ^{R15L} and CHCHD10 ^{G66V} has been observed (Brockmann, Freischmidt et al. 2018, Lehmer, Schludi et al. 2018, Straub, Janer et al. 2018), and both variants have been proposed to act through loss-of-function mechanisms (Woo, Liu et al. 2017, Brockmann, Freischmidt et al. 2018, Lehmer, Schludi et al. 2018, Purandare, Somayajulu et al. 2018, Straub, Janer et al. 2018) whereas unchanged levels have been described for variant CHCHD10 ^{S59L} and CHCHD10 ^{P80L} (Lehmer, Schludi et al. 2018). While one study proposed that the CHCHD10 ^{P80L} variant acted through a loss-of-function mechanism via loss of interaction with CHCHD2 as described above (Purandare, Somayajulu et al. 2018), the variant CHCHD10 ^{S59L} has been shown to act through toxic gain-of-function in several studies (Woo, Liu et al. 2017, Anderson, Bredvik et al. 2019, Genin, Madji Hounoum et al. 2019). Therefore,

diseases-associated variants of CHCHD10 should be considered individually when investigating their mechanisms of pathogenicity.

Finally, compensation has also been noted to occur between the two proteins. Loss of CHCHD10 or expression of the CHCHD10 ^{R15L} variant led to increased CHCHD2 expression *in vitro* (Huang, Wu et al. 2018, Straub, Janer et al. 2018) though this has yet to be replicated *in vivo* (Burstein, Valsecchi et al. 2018). Conversely, loss of CHCHD2 was also reported to result in increased CHCHD10 expression (Huang, Wu et al. 2018).

Taken together, those findings reveal that a complex interplay exists between CHCHD2 and CHCHD10 in cells. While sequence similarity suggests that both proteins might have some overlapping roles (Huang, Wu et al. 2018, Liu, Huang et al. 2020), they are not completely interchangeable. As CHCHD10 variants might act through different mechanisms, both proteins, as well as their complex need to be considered to properly determine the biological impact of ALS-associated CHCHD10 variants.

5 *In vitro* studies of CHCHD10 and CHCHD2

Several studies have attempted to determine the role of both proteins, with the first functional study on yeast CHCHD2/CHCHD10 orthologue Mic17. Loss of Mic17 led to decreased oxygen consumption and respiratory deficiency (Longen, Bien et al. 2009). Search for the function of both proteins was reignited following the discovery of *CHCHD10* mutations in ALS patients. One of the early proposed roles involved both CHCHD10 and CHCHD2 in the mitochondrial contact site and cristae organizing system (MICOS) complex (Genin, Plutino et al. 2016, Zhou,

Ma et al. 2018). The MICOS complex is an evolutionary conserved complex that contains a number of structural proteins which are required for the formation of the mitochondrial cristae, a structure essential for mitochondrial respiration (Khosravi and Harner 2020). This was supported by the observations that both CHCHD2 and CHCHD10 are enriched at the cristae junction, and that cristae abnormalities have been documented in patients carrying *CHCHD10* mutations (Bannwarth, Ait-El-Mkadem et al. 2014). Yet, those original findings have subsequently been challenged by independent studies which did not find evidence of either CHCHD10 or CHCHD2 within the MICOS complex (Burstein, Valsecchi et al. 2018, Huang, Wu et al. 2018, Straub, Janer et al. 2018). Furthermore, as CHCHD10 and CHCHD2 both have short half-life, of around 4 and 1.5 hours respectively (Burstein, Valsecchi et al. 2018), this likely indicates a role other than structural. There are now several proposed roles for both proteins, two of which have been replicated numerous times including a role in mitochondrial respiration and in response to stress.

5.1 Mitochondrial respiration

Numerous studies have now demonstrated that CHCHD2 and CHCHD10 are involved in mitochondrial respiration (Genin, Plutino et al. 2016, Huang, Wu et al. 2018, Lehmer, Schludi et al. 2018, Purandare, Somayajulu et al. 2018, Straub, Janer et al. 2018, Mao, Wang et al. 2019). *In vitro* basal and maximal mitochondrial respiration was decreased in CHCHD10 knockout (KO), *CHCHD2* knockdown (KD) cells, as well as patient-derived fibroblasts carrying the CHCHD10 ^{R15L} variant (Straub, Janer et al. 2018, Mao, Wang et al. 2019). This later phenotype was rescued following wild type CHCHD10 expression suggesting a loss-of-function mechanism (Straub, Janer et al. 2018). In patient fibroblasts carrying the CHCHD10 ^{R15L} variant , subjection to galactose medium, which forces reliance on mitochondrial respiration, led to an increase in

CHCHD10 and CHCHD2 concentrations in control, but not in patient fibroblasts (Straub, Janer et al. 2018). This suggests that both proteins respond to increased mitochondrial respiration demand, and highlights that CHCHD10 variants, such as the CHCHD10 ^{R15L} variant, might be unable to respond appropriately during increased oxidative phosphorylation (OXPHOS) requirements. In line with this, submitting double CHCHD2/10 KO cells to galactose led to a reduction in both basal and maximal oxygen consumption rates when compared to glucose incubation (Huang, Wu et al. 2018).

Findings of reduced respiration following loss of either protein are in line with altered mitochondrial respiratory chain complexes observed in various models of CHCHD10 and CHCHD2. Reduced Complex I subunit expression and assembly levels were observed in fibroblasts of patients carrying the CHCHD10 ^{R15L} variant (Straub, Janer et al. 2018), while reduced Complex I and IV has been observed in CHCHD2 KO cells (Meng, Yamashita et al. 2017, Huang, Wu et al. 2018).

Taken together, both proteins seem to be important for mitochondrial respiration, particularly during times of increased reliance on oxidative respiration, possibly through their influence on mitochondrial respiratory chain integrity. Yet, whether the reduction of mitochondrial respiration following loss of either protein is solely responsible for neurodegenerative phenotype, and whether other CHCHD10 variants act through other mechanisms, still needs to be clarified.

5.2 Response to stress and the mitochondrial integrated stress response (mt-ISR)

CHCHD10 and CHCHD2 have also been shown to play a role in various cellular stress responses. Loss of either CHCHD10 and/or CHCHD2 affects cell survival and/or growth following exposure to various stressors including: loss of mitochondrial membrane potential (MMP) (Huang, Wu et al. 2018), UV radiation (Liu, Clegg et al. 2014), starvation (Meng, Yamashita et al. 2017), exposure to staurosporine (Liu, Clegg et al. 2014, Mao, Wang et al. 2019) or hydrogen peroxide (Meng, Yamashita et al. 2017). Levels of both proteins have also been shown to change following various cellular stressors, such as exposure to galactose medium (Straub, Janer et al. 2018), DNA damage (Meng, Yamashita et al. 2017) and loss of MMP (Huang, Wu et al. 2018). The CHCHD10/2 containing complex also seems to respond to stressors. Increased mitochondrial respiration demands were reported to lead to the formation of a new 40 kDa complex containing both CHCHD10 and CHCHD2 which correlated with increased cell survival in both control and CHCHD10 ^{R15L} patient derived fibroblasts (Straub, Janer et al. 2018). This suggests that both proteins, as well as their complexes, respond and may be required for cells to cope with various cellular challenges. Importantly, both proteins have now also been linked to another important stress response within mitochondria: mt-ISR (Anderson, Bredvik et al. 2019, Liu, Huang et al. 2020, Straub, Weraarpachai et al. 2021, Ruan, Hu et al. 2022, Sayles, Southwell et al. 2022).

The mt-ISR is an evolutionary conversed transcriptional response activated by mitochondrial stressors including misfolded proteins, OXPHOS deficiency, ROS, and mitochondrial DNA (mt-DNA) damage (Shpilka and Haynes 2018). Upon its activation, it can promote restoration of mitochondrial homeostasis through metabolic changes and promotion of OXPHOS recovery, but

its overactivation has been shown to lead to modifications in the mitochondrial genome through mt-DNA deletion (Shpilka and Haynes 2018). In mammalian cells, mt-ISR activation is first triggered by the phosphorylation of eIF2α, which results in the preferential translation of the three main transcription factors: *CHOP*, *ATF4* and *ATF5* (Shpilka and Haynes 2018). Activation of the mt-ISR was reported in double CHCHD10/2 KO cells under steady state condition (Ruan, Hu et al. 2022). In that study, the authors propose that both CHCHD10 and CHCHD2 can translocate to the cytosol under stress conditions and prevent the phosphorylation of eiF2α and restrain the activation of mt-ISR (Ruan, Hu et al. 2022). Therefore, following loss of both proteins, activation of the mt-ISR is not prevented, a response amplified by stress. Activation of the mt-ISR was also observed in patient fibroblasts carrying the CHCHD10 ^{R15L} variant through upregulation of *ATF4* and *ATF5* (Straub, Weraarpachai et al. 2021). Interestingly, activation of this response was mostly noted when fibroblasts were subjected to galactose media, resulting in a nutrient stress (Straub, Weraarpachai et al. 2021), and suggesting that CHCHD10 ^{R15L} expression under basal conditions does not activate this response. It was also proposed that the energy deficit, such as Complex I deficiency which is particularly present in the patient fibroblasts following exposition to galactose, could lead to the activation of the mt-ISR in a cellular effort to mitigate the bioenergetic defect (Straub, Weraarpachai et al. 2021). Taken together, these *in vitro* studies suggest that both proteins play an important role in various cellular stress responses, including most notably the mt-ISR.

5.3 Other documented roles

Both proteins have also been linked to regulation of mitochondrial morphology. Mitochondrial morphology is crucial for its function and disturbances in fission and fusion has

been linked to a number of degenerative diseases including PD (Youle and van der Bliek 2012) and ALS (Jiang, Wang et al. 2015). In fact, both hyperfused (Straub, Janer et al. 2018) and fragmented mitochondria have been described (Bannwarth, Ait-El-Mkadem et al. 2014) in *CHCHD10* patient cells, and both CHCHD2 and CHCHD10 have been shown to exert an influence on the fission and fusion machinery, mostly through metalloendopeptidase OMA1 (OMA1) and optic atrophy 1 (OPA1) (Liu, Duan et al. 2020, Liu, Huang et al. 2020, Genin, Bannwarth et al. 2022, Ruan, Hu et al. 2022). Furthermore, CHCHD2 has also been proposed to be involved in apoptosis, where CHCHD2 was found to interact with Bcl-xL to inhibit BAX oligomerization, reducing apoptosis (Liu, Clegg et al. 2014).

6 Animal models of CHCHD10 and CHCHD2

In vivo models have also been created to further understand the function of both CHCHD10 and CHCHD2 in pathology in tissues relevant for specific conditions. While non-murine models mostly suggest that both loss and gain-of-function mechanisms are at play depending on the specific CHCHD10 variant studied, loss-of-function KO mouse models have shown inconsistent phenotypes, leading to disparate conclusion about CHCHD10 and CHCHD2 mechanism of pathogenicity. Moreover, animal models have highlighted the importance of each protein in various tissues, which is becoming increasingly relevant to determine pathological mechanisms in the context of CHCHD10 and CHCHD2 proteins.

6.1 CHCHD10 and CHCHD2 tissue expression and the neuromuscular junction

CHCHD10 and CHCHD2 are ubiquitously expressed, though CHCHD10 in enriched in heart and skeletal muscle (https://www.proteinatlas.org/). Within the central nervous system (CNS),

CHCHD10 and CHCHD2 have been documented to be enriched in dopaminergic neurons in the substantia nigra (Burstein, Valsecchi et al. 2018, Huang, Wu et al. 2018) as well as in spinal cord neurons colocalizing with markers of motoneurons (Burstein, Valsecchi et al. 2018), consistent with the disease affected tissues in PD and ALS, for CHCHD2 and CHCHD10, respectively.

One of the sites particularly affected in ALS is the neuromuscular junction (NMJ). The NMJ is a tripartite synapse that consists of the presynaptic motoneuron, and the postsynaptic muscle as well as terminal Schwan cell (Cappello and Francolini 2017). Degeneration processes occur at this site, leading to the loss of connection between muscle and motoneuron. One of the overreaching questions within the ALS field is whether degeneration occurs initially from the motoneuron terminal (dying back) or the cell bodies (dying forward) though both phenomena contribute to the disease eventually as both are eventually lost (Fischer, Culver et al. 2004, Moloney, de Winter et al. 2014, Cappello and Francolini 2017). While considerable focus has been placed on motoneurons in ALS research, more investigations are now being carried out on muscle and/or Schwan cell involvement in pathogenesis and degeneration. Both are still understudied and debated aspect of the disease, yet several studies point to their potential contribution (Arbour, Vande Velde et al. 2017, Cappello and Francolini 2017). Interestingly, a growing number of animal studies have noted a preferential involvement of muscle-specific defects in CHCHD10 models. As such, a conditional muscle CHCHD10 KO mouse model resulted in muscle pathology and motor deficits (Xiao, Zhang et al. 2019). In that study, the authors reported CHCHD10 expression to be particularly high in skeletal muscle endplates. It has been proposed that CHCHD10 could be required for agrin-induced clustering of acetylcholine receptors on muscle cells (Xiao et al. 2019). The observation of CHCHD10

enrichment at the post-synaptic side of NMJs in the skeletal muscle was subsequently replicated by another group (Genin, Madji Hounoum et al. 2019). A recent mouse whole CHCHD10 KO model also implicated CHCHD10 in myoblast differentiation and cold-induced browning of adipocytes in muscle (Xia, Qiu et al. 2022). Taken together, these studies suggest CHCHD10 is involved in diverse elements of muscle cell physiology and suggests that CHCHD10 variants might manifest part of their pathology specifically in skeletal muscles. The specific impact of CHCHD2 in muscle pathology has yet to be characterized.

6.2 Mice studies

Several mouse models have been created including conditional and whole animal KOs (Burstein, Valsecchi et al. 2018, Liu, Huang et al. 2020, Xiao, Zhang et al. 2020, Sato, Noda et al. 2021, Nguyen, McAvoy et al. 2022), KIs (Anderson, Bredvik et al. 2019, Genin, Madji Hounoum et al. 2019, Sayles, Southwell et al. 2022, Shammas, Huang et al. 2022), and over expressing transgenic mouse models (Liu, Woo et al. 2020, Kee, Wehinger et al. 2022, Liu, Woo et al. 2022).

The first report of whole CHCHD10 KO mice described no obvious phenotype, including no motor defects, an absence of mitochondrial defects, and no CHCHD2 compensation (Burstein, Valsecchi et al. 2018). Only a mild decrease in oxygen consumption was noted in mitochondria isolated from skeletal muscle (Burstein, Valsecchi et al. 2018), supporting its possible involvement in muscle. This was subsequently supported by another study that reported no obvious phenotype in KO mice, except muscle adipocyte browning as mentioned earlier (Xia, Qiu et al. 2022).

Similarly, CHCHD2 KO mice report varying phenotypes. The first reported CHCHD2 KO mouse was not described extensively, and authors reported no obvious phenotypes and normal development (Meng, Yamashita et al. 2017). In that study, mouse embryonic fibroblast showed no mitochondrial defect (Meng, Yamashita et al. 2017). A subsequent study challenged this, where though CHCHD2 KO mice were indistinguishable from wild type at birth, aged mice did show some parkinsonian-like traits with fragmented mitochondria in dopaminergic neurons as well as reduced mitochondrial respiration (Sato, Noda et al. 2021). A motor phenotype was also observed from 115 weeks in a runway test, with age-dependent ubiquitin-binding protein (p62) positive inclusion in neurons, irregular cristae, and reduced Complex I and III levels (Sato, Noda et al. 2021). Surprisingly, reduced CHCHD10 levels were also observed in CHCHD2 KO tissues, potentially underlying how disease expression develops at that age.

While KO mice develop few to no symptoms, KI mice models show severe phenotypes. Most of the CHCHD10 KI mice studies have focused on the CHCHD10 ^{S59L} variant which is orthologous to the CHCHD10 ^{S55L} variant in the mouse genome. In two back-to-back publications, CHCHD10 ^{S55L} KI mice were described as having a robust phenotype, which included motor deficits, myopathy, abnormal NMJs, OXPHOS deficiency in muscles, mislocalization of TDP-43 in spinal neurons, as well as reduced survival (Anderson, Bredvik et al. 2019, Genin, Madji Hounoum et al. 2019). When bred to homozygosity, mice displayed a more severe phenotype suggesting a dosage effect (Anderson, Bredvik et al. 2019). Interestingly both studies reported a severe cardiomyopathy that resulted in death of CHCHD10 ^{S55L} mice (Anderson, Bredvik et al. 2019, Genin, Madji Hounoum et al. 2019). As no heart phenotype is observed in patients (Penttilä, Jokela et al. 2015), this may suggest that the pathogenic

mechanism differs from humans and mice. Of note, a transgenic model of CHCHD10 was also created, modelling CHCHD10 ^{R15L} variant. Transgenic R15L mice developed cardiac and skeletal muscle pathology, reduced survival, and a late-stage motor phenotype (Ryan, Yan et al. 2021).

Activation of the mt-ISR has also been described in *in vivo* models of CHCHD10/2. While single CHCHD10 KO mice did not present activation of this response, CHCHD10 ^{S55L} mice did present elevated level of mt-ISR transcript markers in the heart, including the three main transcription factors *ATF4*, *ATF5* and *CHOP* (Anderson, Bredvik et al. 2019, Liu, Huang et al. 2020, Sayles, Southwell et al. 2022). Further characterization of the mice showed that activation of these transcriptional markers preceded OXPHOS defects in CHCHD10 ^{S55L} mice (Sayles, Southwell et al. 2022). As CHCHD10 ^{S55L} was shown to form aggregates with CHCHD2 within the mitochondria, the authors suggest that proteotoxic stress could be the main activator of the mt-ISR in this model, leading to the rewiring of the metabolism from oxidative to glycolytic (Sayles, Southwell et al. 2022). As the phenotype in these mice developed, it was proposed that this metabolic switch might be maladaptive, leading to OXPHOS defects, cardiomyopathy and death (Sayles, Southwell et al. 2022). This is in contrast to previous descriptions in *in vitro* studies which suggest that the mt-ISR is activated by bioenergetic defects and not *vice-versa* (Straub, Weraarpachai et al. 2021, Ruan, Hu et al. 2022).

The absence of a substantial phenotype in CHCHD10 KO mice, and robust phenotype in mice expressing the CHCHD10 ^{S55L} variant suggests that only a gain-of-function mechanism might be responsible for the pathogenic effects in the CHCHD10 KI mice. However, a recent

mouse study challenged this notion, as a double CHCHD10/CHCHD2 KO did show a phenotype with reduced respiration, disrupted mitochondrial cristae, and cardiomyopathy phenocopying several symptoms expressed by the CHCHD10 ^{S55L} KI mice (Liu, Huang et al. 2020). Interestingly, the mt-ISR was also documented in double CHCHD10/2 KO mice, suggesting that disease mechanisms other than those resulting from aggregation of CHCHD10/2 can lead to its activation *in vivo*, though the observed mt-ISR activation was less robust than in the CHCHD10 ^{S55L} mice (Liu, Huang et al. 2020). One confounding issue is that even though CHCHD10 and CHCHD2 are represented by 2 genes, it is hypothesized that there might be 9 other genes and pseudogenes representing those 2 proteins in mice, which might confer a greater capacity to compensate when one or both are lost in genetic KO models (Cavallaro 2010) (**Table 1.1**). The lack of an obvious phenotype following loss of CHCHD2 or CHCHD10 in mice is also in line with the significant number of genetic KO mouse models of mitochondrial proteins that do not adequately model neurodegenerative disease (Beal 2010). While mice have been extensively used to explore disease mechanism in ALS, it is possible that the addition of other vertebrate models may clarify disease mechanisms. Moreover, non-murine model might have an advantage in modelling neurodegeneration associated with mitochondrial genes. For example, *Drosophila melanogaster* have successfully modelled genes that have been difficult to model in mice including *PINK1, Parkin, Fbxo7, LRRK2* (Beal 2010, West, Furmston et al. 2015, Zhou, Ma et al. 2020). As for CHCHD10 and CHCHD2, non-murine models including the nematode worm (*Caenorhabditis elegans*) (Woo, Liu et al. 2017), fruit fly (*Drosophila melanogaster*) (Meng, Yamashita et al. 2017, Tio, Wen et al. 2017, Baek, Choe et al. 2021), and zebrafish (*Danio rerio*) (Brockmann, Freischmidt et al. 2018) have shown promise to model both loss- and gain-of-function phenotypes for both proteins and these will be described in the next section.

6.3 Non murine models of CHCHD10 and CHCHD2

In *Caenorhabditis elegans CHCHD2* and *CHCHD10* are represented by a single gene, *har-1* (Woo, Liu et al. 2017). Loss of *har-1* led to mitochondrial dysfunction and reduced survival. Interestingly, transgenic expression of the CHCHD10 ^{S59L} variant led to enhanced pathogenicity when compared to transgenic expression of the CHCHD10 ^{R15L} variant supporting the notion that CHCHD10 ^{S59L} variant might confer a more severe phenotype (Woo, Liu et al. 2017).

The CHCHD10/2 complex has also been modeled in *Drosophila melanogaster*. Three homologous genes represent *CHCHD10* and *CHCHD2*: *Dmel/CG3100*, *Dmel/CG31008*, and *CG5010* (Baek, Choe et al. 2021). Of those, *CG5010* has the highest homology to human *CHCHD10* and *CHCHD2* and has been characterized in three separate studies (Meng, Yamashita et al. 2017, Liu, Duan et al. 2020, Baek, Choe et al. 2021). Loss of CG5010 leads to lower survival, mitochondrial dysfunction, muscle atrophy, reduced ATP production as well as reduced basal and maximal oxygen consumption rates (Meng, Yamashita et al. 2017, Liu, Duan et al. 2020). Transgenic expression of wild type CHCHD2, but not the Parkinson's disease-associated CHCHD2 ^{R145Q} variant, rescued those defects suggesting a loss-of-function mechanism (Meng, Yamashita et al. 2017). In one study, transgenic expression of the CHCHD10 ^{S59L} variant resulted in increased TDP-43 localization to mitochondria and TDP-43 aggregation, leading to chronic activation of the PINK-1 pathway (Baek, Choe et al. 2021). CHCHD2 transgenic models of the CHCHD2 ^{T61I} and CHCHD2 ^{R145Q} variants have also been studied and both confer locomotor dysfunction, dopaminergic neuron degeneration, mitochondrial dysfunction, oxidative

stress and reduction dopaminergic neurons synaptic transmission in adult flies (Tio, Wen et al. 2017).

In addition to the invertebrate models described above, a zebrafish (*Danio rerio*) model has also been used to study CHCHD10. Both genes are represented by one homologue each, *Chchd2* and *Chchd10* with 65% and 67% identity at the protein level, respectively. Following knockdown of *Chchd10* using a transient morpholino strategy, zebrafish displayed reduced ventral root motor axon length, reduced swimming behaviour and abnormal myofibrillar structure (Brockmann, Freischmidt et al. 2018). However, this study only focused on the first two days of fish embryo development.

Taken together, these studies show that the use of non-murine models can complement mouse and cellular studies when investigating potential loss- and gain-of-function pathogenic mechanisms. Of the models noted above, the zebrafish offers the opportunity to manipulate both genes in isolation or in combination permitting investigations into their relative contribution in disease (**Table 1.1**). As both CHCHD10 and CHCHD2 might have some overlapping roles, this model offers the opportunity to examine the relative contribution of either protein and various physiological processes conserved among vertebrates. Zebrafish are a simple vertebrate model with well-developed cell physiology and genetics relevant to studying diseases such as ALS (Babin, Goizet et al. 2014). Numerous studies have successfully modeled various ALS genes in zebrafish such as *SOD1* (Sakowski, Lunn et al. 2012), *C9ORF72* (Shaw, Higginbottom et al. 2018, Butti, Pan et al. 2021), *FUS* (Armstrong and Drapeau 2013, Bourefis, Campanari et al. 2020) and *TARDBP* (Schmid, Hruscha et al. 2013, Bose, Armstrong et al. 2019). Key developmental and physiological processes are conserved in the spinal cord and trunk

musculature, including the NMJ, a site that is particularly impaired in ALS. Finally, the large number of offspring, which are optically translucent at early stages of development, allows for *in vivo* imaging and drug screening.

Animal Model	Number of orthologues/ pseudogenes	Closest to orthologue to human CHCHD2	Closest to orthologue to human CHCHD10
Mus musculus	9	CHCHD2 (86 % identity)	CHCHD10 (84 % identity)
Danio rerio	2	Chchd2 (65% identity)	Chchd10 (67% identity)
Drosophila melanogaster	3	CG5010 (45 % identity)	CG5010 (45 % identity)
Caenorhabditis elegans	1	har-1(51% identity)	har-1 (54 % identity)

Table 1.1 Percentage identity of amino acid sequences between human CHCHD2 and CHCHD10 and animal models used for study.

In summary, the biological role of both CHCHD10 and CHCHD2 still remain to be fully explored as little is known about their exact functions. Variants of CHCHD10 might confer pathology in many ways, and may differ among variants, but both loss- and gain-of-function mechanisms seem to be involved. *In vivo* studies using stable models are necessary to understand the relative contribution of both proteins to disease progression. Determining their mode of action could unravel therapeutic targets, not only for patients carrying CHCHD10 variants, but might also be relevant for mitochondrial dysfunction in sporadic ALS patients. As such, in my thesis I present research that utilized both KOs and a KI zebrafish model.

Rationale and Objectives

Rationale for the study.

Variants of CHCHD10 have been shown to be associated with degenerative diseases including amyotrophic lateral sclerosis (ALS). CHCHD2, which is a paralogue of CHCHD10, has also been shown to have variants involved in degenerative diseases, more specifically in Parkinson's disease (PD). Both proteins form a complex of unknown function in the mitochondria. Understanding how the expression of disease-associated variants leads to pathology is critical for the development of therapeutic targets and strategies, as both ALS and PD have limited therapeutic tools for clinicians to slow or halt disease progression. Due to the potential overlapping and compensatory roles of both proteins, the research presented in this thesis aimed to understand the contribution of both CHCHD2 and CHCHD10 to disease pathogenesis, as well as the impact of the CHCHD10 ^{P80L} variant using zebrafish as a model organism.

Hypothesis 1: Loss of Chchd10, Chchd2 or both, can lead to ALS defects through mitochondrial dysfunction *in vivo*.

Objective 1. Create a *chchd2*, *chchd10* and double *chchd2* & *chchd10* knockout (KO) models to investigate the cellular consequences arising from the loss of the Chchd10, Chchd2 and well as the complex they form in mitochondria.

Objective 2. Characterization of Chchd10 and Chchd2 expression, as well as Chchd2/Chchd10 complex in the zebrafish model.

Objective 3. Characterization of survival, locomotor function, NMJ structural defects and impact on mitochondrial respiratory chain complex in ALS-associated Chchd10 and PD-associated Chchd2 loss-of-function models.

Objective 4. Determining relative contribution of the activation of the mt-ISR in *chchd10* and *chchd2* zebrafish models.

Hypothesis 2: While most CHCHD10 variants studied *in vivo* seem to present gain-of-function mechanisms, other CHCHD10 variants might lead to different pathogenic mechanisms.

Objective 5. Generate a zebrafish *chchd10* knock-in (KI) model analogous to an ALS/FTD mutation and determine whether they display a similar phenotype as a KO fish model.

Hypothesis 3: CHCHD10 and CHCHD2 are differentially implicated in various tissues, and their loss or variant expression might lead to varying pathology across tissues.

Objective 6. Characterization of an adult KI model to determine potential contributors to disease as well as the tissue-specific impact of variant expression.

Preface to Chapter 2

In this first chapter, we aimed to determine the pathological consequences resulting from the loss of either or both Chchd10 and Chchd2 in zebrafish larvae. Following the creation of these models, we determined whether ALS-like phenotypes were present and examined whether mitochondrial dysfunction could underlie those defects.

Chapter 2: Loss of mitochondrial Chchd10 or Chchd2 in zebrafish leads to an ALS-like phenotype and Complex I deficiency independent of the mt-ISR

Virginie Petel Légaré [1], Christian J. Rampal [1], Mari J. Aaltonen [3], Alexandre Janer [3], Lorne Zinman [2], Eric A. Shoubridge [3] and Gary A.B. Armstrong [1]

[1] Department of Neurology and Neurosurgery
Montreal Neurological Institute
Faculty of Medicine
McGill University

[3] Department of Human Genetics
McGill University
Montreal, QC H3A 2B4, Canada.

[2] Sunnybrook Health Sciences Centre
Toronto, Ontario, M4N 3M5, Canada

Corresponding author (gary.armstrong@mcgill.ca)

Published in Bioarchives May 2nd, 2022.
In Review, Developmental Neurobiology – DNEU-00056-2022

Abstract

Mutations in *CHCHD10* and *CHCHD2*, coding for two paralogous mitochondrial proteins, have been identified in amyotrophic lateral sclerosis (ALS), frontotemporal lobar degeneration (FTD), and Parkinson's disease (PD). Here we investigated the biological roles of these proteins during vertebrate development using knockout (KO) models in zebrafish. We demonstrate that loss of either or both proteins leads to motor impairment, reduced survival, and compromised neuromuscular junction (NMJ) integrity in larval zebrafish. Compensation by Chchd10 was observed in the *chchd2*$^{-/-}$ model, but not by Chchd2 in the *chchd10*$^{-/-}$ model. The assembly of mitochondrial respiratory chain Complex I was impaired in *chchd10*$^{-/-}$ and *chchd2*$^{-/-}$ zebrafish larvae, but unexpectedly not in the double *chchd10*$^{-/-}$ & *chchd2*$^{-/-}$ model, suggesting that reduced mitochondrial Complex I cannot be solely responsible for the observed phenotypes, which are generally more severe in the double KO. Activation of the mitochondrial integrated stress response (mt-ISR) was only observed in the double KO model, possibly implicating this pathway in the recovery of the Complex I defect, and suggesting that Complex I assembly defect in our single KO is independent of the mt-ISR. Our results demonstrate that both proteins are required for normal vertebrate development, but their precise molecular function in the mitochondrial biology of motoneurons remains to be discovered.

Keywords: Amyotrophic lateral sclerosis; CHCHD10; CHCHD2; mitochondria; mitochondrial integrated stress response; zebrafish; neurodegeneration

Introduction

ALS is a devastating neurodegenerative disease characterized by the progressive degeneration of lower and upper motor neurons in the spinal cord and motor cortex, that in some cases extends to the frontal and temporal cortexes where it manifests as FTD (Taylor et al., 2016). While most forms of the disease occur sporadically (sALS), a small subset of patients (~10%) have a familial history (fALS). Among the many defects observed in ALS, mitochondrial abnormalities have long been documented as pathological features, with patients presenting with mitochondrial structural defects, altered mitochondrial respiration, and increased oxidative stress (Chung and Suh, 2002; Dupuis et al., 2004; Smith et al., 2017). Yet, whether mitochondrial dysfunction plays a central role in the disease or arises as a downstream consequence of other cellular abnormalities remains to be fully elucidated. In 2014, the first dominantly inherited variants of the nuclear encoded mitochondrial protein coiled-coil-helix-coiled-coil-helix domain containing 10 (CHCHD10) were reported in a small proportion of both fALS, sALS and FTD cases (Bannwarth et al., 2014) suggesting that mitochondrial protein abnormalities could play a direct role in the disease. Since these original findings, over twenty mutations in *CHCHD10* have been associated with a spectrum of diseases, including ALS, FTD, cerebellar ataxia and mitochondrial myopathy (Bannwarth et al., 2014), Charcot–Marie–Tooth disease (Auranen et al., 2015), PD (Perrone et al., 2017), and Alzheimer's disease (AD) (Zhang et al., 2015).

In mitochondria, CHCHD10 localizes mostly near the cristae junctions of the mitochondrial intermembrane space (IMS) (Bannwarth et al., 2014; Huang et al., 2018), where it can form a complex of unknown function with its paralogue CHCHD2 (Huang et al., 2018; Straub et al., 2018). CHCHD2 has also been linked to neurodegenerative diseases with rare

autosomal dominant mutations in *CHCHD2* segregating with PD (Funayama et al., 2015; Shi et al., 2016), FTD (Che et al., 2018) AD (Che et al., 2018), and Lewy body dementia (Ogaki et al., 2015).

CHCHD2 and CHCHD10 share 58% sequence identity and have a common ancestor in yeast, suggesting that these proteins might have partially overlapping function (Cavallaro, 2010). *In vitro* studies have reported that loss of either CHCHD2, CHCHD10 or both, impacts mitochondrial respiration (Mao et al., 2019; Straub et al., 2018), survival/growth following exposure to various cellular stressors (Huang et al., 2018; Lehmer et al., 2018; Mao et al., 2019; Straub et al., 2018), the mitochondrial integrated stress response (mt-ISR) (Anderson et al., 2019; Liu et al., 2020b; Ruan et al., 2022; Sayles et al., 2022; Straub et al., 2021), apoptosis (Genin et al., 2016; Liu et al., 2014), as well as the transcription of the oxygen responsive gene *COX4I2* (Aras et al., 2020; Grossman et al., 2017; Purandare et al., 2018).

Conversely, *in vivo* studies employing mouse knockout (KO) models reported only minor defects following loss of either protein (Anderson et al., 2019; Meng et al., 2017; Xia et al., 2022), though when aged, Chchd2 KO mice did develop Parkinsonian-like symptoms (Sato et al., 2021). More recently, a double KO mouse model was created, which presented with mitochondrial structural defects, cardiomyopathy, as well as activation of the mt-ISR (Liu et al., 2020b). Other loss-of-function models, including hypomorphic and KO models of CHCHD10 and the CHCHD2 orthologue DmeI\CG5010 in *Drosophila melanogaster* (Liu et al., 2020a; Meng et al., 2017), a KO model of the CHCHD10 and CHCHD2 orthologue *har-1* in *Caenorhabditis elegans* (Woo et al., 2017), and a knockdown model (KD) of *chchd10* in *Danio rerio* (Brockmann et al., 2018), reported reduced survival and impaired motor activity, suggesting that mouse models might have a broader capacity to compensate for loss of

CHCHD10 and/or CHCHD2. Animal model studies have largely focused on either protein in isolation or used models in which CHCHD10 and CHCHD2 are represented by only one orthologue leading to disparate conclusions concerning their biological function. The zebrafish model system offers the opportunity to manipulate both genes in isolation or in combination, as both *chchd2* and *chchd10* are well-conserved, with 65% and 67% identity to human, and 60% and 72% identity at the amino acid level, respectively. As zebrafish have already been successfully used to model mitochondrial pathology (Anichtchik et al., 2008; Byrnes et al., 2018; Flinn et al., 2009; Sabharwal et al., 2020; Steele et al., 2014), we generated zebrafish CHCHD10 and CHCHD2 single and double KO models and explored the biological ramifications during development, enabling us to gain insight into their roles during vertebrate development.

Materials and methods

Zebrafish Housing and Maintenance

Adult zebrafish (*D. rerio*) of the Tübingen long fin (TL) strain were maintained according to standard procedures (Westerfield, 1995) at 28.5 °C under a 14/10 light/dark cycle at the animal research facility of the Montreal Neurological Institute (MNI) at McGill University located in Montréal Québec, Canada. All experiments were performed in compliance with the guidelines of the Canadian Council for Animal Care and approved by the Animal Care Committee of the MNI.

Cas9 mRNA and guide RNAs Synthesis

Synthesis of Cas9 mRNA and guide RNA (gRNA) was performed as previously described (Jao et al., 2013; Vejnar et al., 2016). Briefly, a zebrafish codon optimized Cas9 (pT3TS-nCas9n, Addgene plasmid # 46757) was linearized with XbaI overnight and 1 μg of linear template DNA was used for *in vitro* transcription of mRNA using the T3 mMESSAGE mMACHINE® Kit (Invitrogen) followed by phenol-chloroform extraction and precipitation with ethanol. Selected gRNA target sites were identified using CRISPRscan (Moreno-Mateos et al., 2015) synthesized using the T7 MEGAscript kit (Invitrogen) and purified by phenol-chloroform extraction and ethanol precipitation. The following gRNA target sites were used (PAM site is underlined): Chchd10 gRNA target site: TGGCCGTTGGTTCAGCTGTTGGG; Chchd2 gRNA target site: GGTGACGACGTCCGCAACGACAG.

CRISPR Mutagenesis and Screening of Founder Lines

Generation of a *chchd10* and a *chchd2* KO zebrafish models was performed using previously described methods (Armstrong et al., 2016). Briefly, Cas9 mRNA (100 ng/µl) and gRNA (100 ng/µl) were co-injected into embryos, using a volume of 1.5 nl, at the one cell stage of development. Founder zebrafish were identified at adult stages by screening their progeny for germline transmission of indels. From the offspring of candidate founders, DNA was extracted from 24 embryos, aged 24 hrs post fertilization (hpf), and polymerase chain reaction (PCR) amplification of the target site of interest was carried out followed by restriction fragment length polymorphism (PvuII and Pst1 for *chchd10* and *chchd2* respectively). Sanger sequencing (Genome Québec) was performed on amplicons to determine the exact mutation of each founder line. Primer sequences for verification of *chchd10* KO line: forward primer: GGGGGAAAAAAACAGTTCTTGGC; reverse primer: AAGAGTTGTTGGTTACACTCCAT. Primer sequences for verification of *chchd2* KO line: forward primer: AAAGGACAGGTAATTGATTGTGC; reverse primer: GCCATAACGTTTACCTGATAGGT.

Larval Morphology, Motor Function and Survival Assays

To determine whether the mutants had any visible morphological defects, dechorionated 56 hpf larvae were examined. Heart defects, including asystole, bleeding, or edema (swelling in heart region) were quantified as previously described (Pinho et al., 2013). Reduced yolk sack size was counted when the larvae's yolk sack diameter was smaller than the diameter from embryo head (10 µm).

Touch-evoked motor response was evaluated between 54–56 hpf as previously described (Armstrong and Drapeau, 2013b). Briefly, larvae were placed in the middle of a circular arena

(150 mm diameter petri dish) containing fresh system water maintained at a temperature between 27-28.5 °C. A single touch to the tail was applied to larvae to initiate burst swimming behaviour and movements were recorded from above (recorded at 30 Hz; Grasshopper 2 camera, Point Grey Research). Swim distance, mean and maximum swim velocities were quantified using the manual tracking plugin in ImageJ.

Free swimming velocity (mm/s) was examined using motion tracking software (DanioVision, Noldus) in larvae aged 5 days post fertilization (dpf) placed in 24-well plates. Following a 5 min habituation period, motor activity was recorded for a total of 30 min. System water temperature was maintained at 28.5 ºC. For survival assays, forty recently hatched 5 dpf larvae from each genotype were placed in a temperature-controlled container (28.5 ºC) and monitored from 6 to 30 dpf. Water changes were made once every 2 days.

RNA Extraction and Reverse Transcription–qPCR (RT-qPCR)

RNA was extracted from 5 pooled larvae aged 5 dpf using the PicoPure RNA Isolation Kit (Applied Biosystems). After quality control, 1 μg was used to create a cDNA library by reverse transcription using SuperScript VILO cDNA Synthesis Kit (Invitrogen). Quantitative Real time PCR was performed using SYBR Green Supermix (Bio-Rad laboratories). Relative quantification was performed using the delta-delta Ct method (Livak and Schmittgen, 2001) with *actin* and *sdha* as internal controls (see supplementary material for primer sequences).

Neuromuscular Junction Co-Localization

To investigate whether neuromuscular junction (NMJ) integrity was affected, double-labelling was performed using synaptotagmin 2 (Syt2, presynaptic marker) and alpha-bungarotoxin (αBtx, post-synaptic marker) as described before (Armstrong and Drapeau, 2013b). Briefly, 2 dpf larvae were fixed with 4 % paraformaldehyde in Phosphate-buffered saline (PBS) overnight at 4°C with gentle rotation. Larvae were rinsed with PBS (4 times 15 min), followed by a 45-min incubation at room temperature (RT) with gentle rotation in PBS containing 1 mg/ml collagenase to remove skin. Larvae were then rinsed with PBS (4 times 10 min) and incubated for 30 min in PBST (PBS;Triton X-100) at RT with gentle rotation. Larvae were then incubated in 10 mg/ml sulforhodamine conjugated αBtx in PBST for 30 min at RT with gentle rotation. Larvae were then rinsed (4 times 10 min, PBST) and incubated in blocking solution (2% Goat Serum, 1% BSA, 0.1% TritonX-100, 1% DMSO in PBS) for 1 hour (hr) at RT. Primary antibody Syt2 (1:100, DSHB in blocking solution) was applied overnight at 4°C and gentle rotation. The samples were washed (4 times 30 min, PBST) and then incubated with the secondary antibody (Alexa fluor 647, 1: 1200 ThermoFisher in blocking solution) overnight at 4°C with gentle rotation. Larvae were rinsed (4 times 20 min PBST) and mounted on a glass slide in 70% glycerol. The NMJs were visualized with 60x/1.42 oil immersion objective. Images were acquired using the Volocity software (Improvision). Co-localization analysis was performed by determining the number of orphaned receptors, both pre- and post- synaptic, present in individual ventral roots.

Immunoblot, Blue Native PAGE, and Second Dimension PAGE

For Immunoblots, larvae aged 5 dpf were deyolked using modified Ca^{2+} free Ginsburg Fish Ringer (55 mM NaCl, 1.8 mM KCl, 1.25 mM $NaHCO_3$) solution. For each condition, 10

larvae were homogenized at 4 °C using RIPA buffer (50 mM Tris-HCl, pH 7.4, 100 mM NaCl, 1% NP40, 0.1 % SDS, 0.5 % sodium deoxycholate) and a protease inhibitor cocktail (cOmplete ULTRA Tablets Mini EDTA-free Protease Inhibitor Cocktail, Roche). Lysates were recovered following centrifugation (20 min at 12,000 rpm). Protein concentrations were quantified using a Bradford assay and 30 µg of lysate was separated on a 12.5% SDS polyacrylamide gel or a 4-16% gradient gel. Proteins were transferred to a nitrocellulose membrane and blocked in 5% milk (TSBT) for 1 hr at RT. Membranes were then incubated with primary antibodies in blocking buffer at 4 °C overnight followed by respective secondary antibody labelling (Jackson Immuno Research Laboratories, 1:10 000) for 1 hr at RT. Enhanced chemiluminescence (Clarity™ Western ECL Substrate, Bio-Rad) was used to visualize immunolabelled proteins. The following antibodies were used: Ndufa9 (ab14713, Abcam), Sdhb (ab14714, Abcam), Uqcrc2 (ab14711, Abcam), Mt- co1 (ab14705, Abcam), Atp5a (ab14748, Abcam), Vinculin (V4505, Sigma), Actin (LLC 691001, MP Biomedicals), Chchd10 (ab121196, Abcam), and a custom Chchd2 antibody (MédiMabs) targeting the following epitope sequence: PDVTYQEPYQGQAM. For blue native PAGE, one 5 dpf larvae was placed in MB2 buffer (0.5 ml of 3XGB (1.5 m aminocaproic acid, 150 mM Bis-Tris, pH: 7.0), 0.5 ml of 2M aminocaproic acid, 4 µl of 500 mM EDT) and homogenized at 4 °C. Lauryl maltoside was then added to a final concentration of 1% and incubated for 15 min at 4 °C. Following centrifugation, the supernatant was recovered and ran on a non-denaturing polyacrylamide 6-13% gradient gel. Separated complexes were transferred to a PVDF membrane. Membranes were blocked and probed as described above. Sdhb or Complex II (blue native PAGE) were used as a mitochondrial loading controls and actin was used as a cytoplasmic loading control. For the two-dimensions PAGE, strips were cut off from a first-

dimension native gel that contained 30 μg of protein from 5 larvae of respective genotypes. Strips were then incubated for 45 min in 1 % SDS and 1% β-mercaptoethanol and run individually on a 10% SDS-PAGE to separate proteins, as described before. Quantifications of protein bands were performed using ImageJ.

Pharmacology

Dechorionated 24 hpf larvae were treated with 100 mM 2-deoxy-d-glucose (2-DG, sigma D8375-5G diluted in E3 buffer (5 mM NaCl 0.17 mM KCl 0.33 mM $CaCl_2$ 0.33 mM MgSO4, pH. 7.2) to inhibit glucose metabolism for 24 hr. Five treated and untreated larvae were then pooled and submitted to quantitative PCR or Immunoblot analysis as described above.

Statistical Analysis

All statistical analyses were performed using Prism 7 (GraphPad Software Inc.). Two samples were compared using unpaired students' t tests. Shapiro-Wilks test was used to test for normality. Kruskal-Wallis tests were used to compare more than 2 samples that were not normally distributed, followed by Dunn's post hoc multiple comparisons test. One-way ANOVA and Tuckey's multiple comparison were used when data was normally distributed. Survival curves were compared using the log rank test, and chi-square tests were used to compare proportions. Significance was assessed at $p < 0.05$.

Results

Generation of *chchd10* $^{-/-}$, *chchd2* $^{-/-}$, and double *chchd10* $^{-/-}$ & *chchd2* $^{-/-}$ zebrafish lines

A previous study investigating the role of Chchd10 in zebrafish using a morpholino to knockdown expression of the *chchd10* transcript showed that loss of *chchd10* resulted in reduced motor activity and survival, as well as altered myofibrillar structure and ventral root length (Brockmann et al., 2018). To avoid the variability and off-target effects associated with morpholino injections we generated genetic KO models of both *chchd10* and *chchd2* using CRISPR/Cas9 editing. We hypothesized that KO models would permit investigations further into development, as dependence on mitochondrial oxygen consumption for survival has been documented to increase with development in zebrafish (Mendelsohn et al., 2008; Strecker et al., 2011).

In zebrafish, Chchd10 and Chchd2 are encoded by genes containing 4 exons (**Fig. 1 A**, **B**). We selected guide RNAs that targeted the coding region of exon 2 in each gene and identified a single nucleotide insertion in *chchd10* and a seven base pair deletion in *chchd2* (**Fig. 1 C**, **D**). Both indels were transmitted to the next generation of offspring and could be identified by loss of PvuII and PstI restrictions sites respectively (**Fig. 1 E**, **F**, **G**, **H**). To investigate whether our mutations disrupted gene function in each fish line, we quantified expression of each transcript by RT-qPCR from 5 dpf larvae and observed a significant reduction in *chchd10* and *chchd2* expression levels in homozygous mutant carriers, suggesting that the transcripts were subjected to nonsense-mediated decay (**Fig 1 Ii**, **Ji**). Immunoblot analysis confirmed the complete loss of Chchd10 and Chchd2 protein expression in homozygous carriers (**Fig. 1 Iii**, **Jii**). A double *chchd10*$^{-/-}$ & *chchd2*$^{-/-}$ model was then generated by in-crossing the two single mutant lines.

Larval *chchd10*$^{-/-}$, *chchd2*$^{-/-}$, and double *chchd10*$^{-/-}$& *chchd2*$^{-/-}$ display morphological defects, motor impairment, reduced survival, and altered neuromuscular integrity

Morphological observations of larvae at 56 hpf showed ~64% of *chchd10*$^{-/-}$ larvae had a reduced yolk sac size compared to wild type larvae, while *chchd2*$^{-/-}$ and double *chchd10*$^{-/-}$ & *chchd2*$^{-/-}$ did not (**Fig**. **2 A**, **B)**. Cardiac defects were present in 37% of *chchd2*$^{-/-}$ larvae and 30% of double *chchd10*$^{-/-}$ & *chchd2*$^{-/-}$ larvae, with most larvae displaying a cardiac edema (Supp. video 1); however, this phenotype was not observed in *chchd10*$^{-/-}$ larvae (**Fig**. **2 A**, **C**).

As ALS impairs motor function, we next examined locomotor function in our zebrafish models by examaning touch response behaviour at 2 dpf. Touch-evoked motor responses were recorded and changes in swimming behaviour were observed in some of our measures of motor function (see 10 representative traces per genotype, **Fig**. **2 D**). Specifically, mean swimming distance was significantly reduced in *chchd10*$^{-/-}$, and double *chchd10*$^{-/-}$ & *chchd2*$^{-/-}$ larvae when compared to wild type zebrafish. The *chchd10*$^{-/-}$ larvae swam half of the distance of wild type larvae, while the double *chchd10*$^{-/-}$ & *chchd2*$^{-/-}$ larvae only swam a third of the distance swam by wild type larvae (**Fig**. **2 E**). A significant difference was also observed in the maximum velocity measure; double *chchd10*$^{-/-}$ & *chchd2*$^{-/-}$ larvae swam at a lower maximum velocity compared to wild type (**Fig**. **2 F**), while no significant differences were observed in mean velocity (**Fig**. **2 G**).

To determine whether the early motor defect could be due to reduced neuromuscular junction (NMJ) integrity as has been described in other ALS models (Armstrong and Drapeau, 2013a; Armstrong and Drapeau, 2013b; Bose et al., 2019), we explored co-localization of pre-synaptic and post-synaptic markers at 2 dpf. While few orphaned post- and pre- synaptic markers were observed in wild type larvae, the mutant models showed significant orphaned clusters of both pre-synaptic (syt2) and post-synaptic markers (αBtx). All mutants showed increased

orphaned pre-synaptic markers compared to wild type (**Fig**. **2 H**, **I**), while only *chchd10*$^{-/-}$ and double *chchd10*$^{-/-}$ & *chchd2*$^{-/-}$ had increased orphaned post-synaptic markers compared to wild type larvae (**Fig**. **2 H**, **J**).

Measures of locomotor function were then performed on 5 dpf larvae to see whether defects worsened during development due to increased reliance on oxygen consumption. Larvae were individually placed in 24-well plates filled with fish-system water and traces were recorded to measure mean swim velocity over a 30-min period from animals in all four genetic groupings (**Fig**. **3 A**). At that age, mean swim velocity was significantly reduced in all our models, with the double *chchd10*$^{-/-}$ & *chchd2*$^{-/-}$ showing the greatest deficit (**Fig**. **3 A**, **B**).

We next examined larval survival and observed reduced survival for *chchd10*$^{-/-}$ (median survival 18 days) and *chchd2*$^{-/-}$ (did not reach median survival) models when compared to wild type larvae. Under these rearing conditions, no double *chchd10*$^{-/-}$ & *chchd2*$^{-/-}$ fish survived past 15 dpf (median survival 11 days) (**Fig**. **3 C**).

Chchd10 compensates for loss of Chchd2 but not *vice versa,* and forms both a low and high molecular weight complex at 5 dpf

We next explored whether the KOs of Chchd10 and Chchd2 elicited compensatory changes in expression of either protein or the formation of higher molecular weight complexes (Huang et al., 2018; Straub et al., 2018). Using lysates from 5 dpf larvae, we performed immunoblots and observed an increase (1.9 fold) in Chchd10 protein levels in our *chchd2*$^{-/-}$ zebrafish line compared to wild- type (**Fig**. **4 Ai**, **Aii**). Unexpectedly, Chchd2 protein levels in

chchd10$^{-/-}$ lysates were 80% lower compared to wild type lysate (**Fig**. **4 Bi**, **Bii**). We next examined whether there were changes in their transcript levels in the KO models. No significant differences in the *chchd10* transcript levels in the *chchd2*$^{-/-}$ model, nor any change in the *chchd2* transcript levels in the *chchd10* $^{-/-}$ model were observed when compared to wild type larvae (**Fig**. **4 Aiii**, **Biii**), suggesting that the changes in protein levels likely occur post-transcriptionally.

To investigate whether Chchd10 and Chchd2 formed a stable high molecular weight complex as previously described in cellular models (Straub et al., 2018), a two-dimensional gel (2D-gel) analysis was performed on lysates collected from our genetic groupings aged 5 dpf. In this analysis, protein complexes are first separated on a blue native gel, and then a gel strip containing the separated complexes is run on a denaturing gel to detect proteins within complexes of various molecular weights. While our Chchd2 antibody was not able to detect the protein on the 2D-gel, our Chchd10 antibody revealed that Chchd10 is present mostly as a low molecular weight species (monomer or dimer), as in cellular models (Straub et al., 2018) (**Fig**. **4 C**). The presence of a higher molecular weight complex in wild type and *chchd2*$^{-/-}$ lysate was also observed consistent with observations in cellular models (**Fig**. **4 C**), though the complex was ~140 kDa in our model *vs* ~170 and 230 kDa in human fibroblasts (Straub et al., 2018). Finally, elevated levels of both the low and higher molecular weight Chchd10 complex were observed in the *chchd2*$^{-/-}$ lysate (**Fig**. **4 C**).

Chchd10 and Chchd2 protein levels increase in response to forced reliance on mitochondrial energy production in wild type larvae

We next examined whether Chchd10 and Chchd2 levels were responsive to mitochondrial stressors as described previously (Meng et al., 2017). Wild type larvae aged 24

hpf were exposed to the glycolytic inhibitor 2-DG for 24 hr, permitting us to test whether Chchd10 and Chchd2 expression is affected when fish are forced to rely on mitochondria for energy production (**Fig. 5 A**). Immunoblot analysis revealed that exposure to 2-DG led to increased expression of Chchd10 and Chchd2 (**Fig. 5 B**, **Ci**, **Cii**). Exposure to 2-DG did not result in a significant change of *chchd10* or *chchd2* transcript levels showing that the increase in both proteins was regulated post-transcriptionally (**Fig. 5 Cii**, **Civ**). Interestingly, touch-evoked motor behaviour analysis in 2 dpf larvae revealed a concomitant motor deficit following exposure to 2-DG. More specifically, we observed reduced swim distance in wild type larvae exposed to 2-DG while maximum swim velocity was unchanged when compared to wild type larvae not treated with 2-DG (**Fig. 5 Di**, **Dii**, **Diii**).

Reduced assembly of mitochondrial Complex I in *chchd10*$^{-/-}$ and *chchd2*$^{-/-}$ zebrafish larvae, but not in double *chchd10*$^{-/-}$ & *chchd2*$^{-/-}$ larvae at 5 dpf

As all our knockout lines displayed a significant defect in motor function at 5 dpf compared to 2 dpf, we next investigated whether mitochondrial respiratory chain integrity was compromised at that stage of development. Immunoblots revealed a significant reduction of the Ndufa9 subunit (Complex I) in *chchd10*$^{-/-}$ whole lysate but not in *chchd2*$^{-/-}$ or double *chchd10*$^{-/-}$ & *chchd2*$^{-/-}$ lysate at 5 dpf. Subunits of other respiratory chain complexes did not show differences between wild type, *chchd10*$^{-/-}$, *chchd2*$^{-/-}$ or double *chchd10*$^{-/-}$ & *chchd2*$^{-/-}$ lysates (**Fig. 6 A**, **B**). As Ndufa9 was reduced in the *chchd10*$^{-/-}$ model, we explored whether Complex I assembly was affected by blue native PAGE analysis of single zebrafish larvae aged 5 dpf (**Fig. 6 C**). We observed a significant reduction of Complex I assembly, particularly in *chchd10*$^{-/-}$, as well as in our *chchd2*$^{-/-}$ larvae at 5 dpf. Surprisingly, this defect was not observed our double

chchd10$^{-/-}$ & *chchd2*$^{-/-}$ model (**Fig**. **6 D**), suggesting that the Complex I assembly deficit is not solely responsible for the observed changes in motor behaviour at 5 dpf.

Markers of the mitochondrial integrated stress response are upregulated in *chchd10*$^{-/-}$ & *chchd2* $^{-/-}$ larvae at 5 dpf

Since no defect in mitochondrial respiratory chain complex assembly was observed in the double *chchd10*$^{-/-}$ & *chchd2*$^{-/-}$ model, we investigated whether other mechanisms could be underlying the observed deficits. As the mt-ISR has been documented in CHCHD10/2 models (Anderson et al., 2019; Ruan et al., 2022; Sayles et al., 2022; Straub et al., 2021), we explored whether the RNA levels of ISR markers were increased in the KO models at 5 dpf. While this pathway was not activated in the single gene KO models, a number of markers were increased in the double *chchd10*$^{-/-}$ & *chchd2*$^{-/-}$ model compared to wild type larvae. Transcripts orthologous to *ATF4* (*atf4a*, *atf4b*), *ATF5* (*atf5a*, *atf5b*) and CHOP (*chop*) were significantly increased in double *chchd10*$^{-/-}$ & *chchd2* $^{-/-}$larvae, but not the single KOs **(Fig**. **7 A**). *FGF21* and *HTRA2* orthologous genes (*fgf21*, *htra2*) were also significantly upregulated in the double *chchd10*$^{-/-}$ & *chchd2* $^{-/-}$ model (**Fig**. **7 B**) as was the previously described oxygen responsive transcript, *cox4i2* (Aras et al., 2020; Grossman et al., 2017; Purandare et al., 2018) (**Fig**. **7 C**).

Discussion

In this study, we demonstrate that loss of either or both Chchd10 and Chchd2 in zebrafish larvae leads to several ALS-like phenotypes including motor deficits, altered NMJ pre- and post-synaptic marker co-localization and reduced survival. As single gene KO mice generally express a very mild phenotype (Burstein et al., 2018; Meng et al., 2017; Sato et al., 2021; Xia et al., 2022), this suggests that zebrafish might be better suited for *in vivo* Chchd10 and Chchd2 loss of function studies. This study replicates *in vitro* findings in which CHCHD10 expression levels increase following loss of CHCHD2 (Harjuhaahto et al., 2020; Huang et al., 2018; Straub et al., 2018); however, loss of Chchd10 led to reduced Chchd2 levels at 5 dpf. These data suggest that while the proteins are to some degree interdependent, they likely share only partially overlapping functions. Consistent with this, the double KO larvae displayed the most severe phenotypes.

A morphological heart defect, though not fully penetrant, was only observed in larvae that did not express Chchd2. Mitochondrial dysfunction is often linked to cardiomyopathies due to the dependence of cardiac function on OXPHOS (El-Hattab and Scaglia, 2016), and heart defects result from exposure to various mitochondrial inhibitors in zebrafish (Pinho et al., 2013). Interestingly, as double CHCHD10/CHCHD2 KO mice (Liu et al., 2020b), but not CHCHD10 KO mice (Anderson et al., 2019) die from a cardiac defect, it is possible that loss of Chchd2 has a greater role in conferring a cardiac defect than loss of Chchd10, as suggested by our study. Our study also highlighted that Chchd10 might be more involved in NMJ stabilization than Chchd2. While all mutants showed increased orphaned pre-synaptic NMJ markers, only *chchd10* $^{-/-}$ and double *chchd10* $^{-/-}$ & *chchd2* $^{-/-}$ displayed orphaned post-synaptic AchRs, which may account for the reduced motor function in our models at 2 dpf. A muscle conditional KO of CHCHD10 study

in mice demonstrated that CHCHD10 was important for agrin-induced AchR clustering (Xiao et al., 2020) which could lead to reduced organization and subsequently decreased post-synaptic innervation by ventral root projections as was observed in our CHCHD10 KO model.

To investigate potential mechanisms that might underlie the observed ALS-like phenotypes, we examined the integrity of the OXPHOS system in our mutant models. Motor deficits at 5 dpf were accompanied by reduced Complex I assembly in both single gene KO models. This replicates *in vitro* results where reduced Complex I assembly was described in patient fibroblasts expressing the CHCHD10 R15L variant (Straub et al., 2018). Interestingly, the Complex I assembly defect in *chchd2*$^{-/-}$ larvae was not accompanied by reduced Ndufa9 subunit expression. This suggests that compensation by Chchd10 can mitigate the subunit expression, but not the assembly defect, and highlights that Chchd2 may be more involved in OXPHOS complex assembly and/or stability, as has been previously proposed for Complex IV and to a lesser extent Complex I (Baughman et al., 2009).

The most surprising finding of this study was that although the double *chchd10* $^{-/-}$ & *chchd2* $^{-/-}$ larvae displayed the most robust ALS-like phenotype, we did not observe a Complex I assembly defect. This suggests that reduced assembly of Complex I may not be solely responsible for the ALS-like phenotypes, but that other, more deleterious, cellular pathways are altered. The mt-ISR, a conserved transcriptional response that can be a triggered by mitochondrial dysfunction (Shpilka and Haynes, 2018), has been linked to neurodegeneration (Costa-Mattioli and Walter, 2020) and has been described in CHCHD10/2 models previously (Anderson et al., 2019; Liu et al., 2020b; Ruan et al., 2022; Sayles et al., 2022; Straub et al., 2021). Transcripts for all three upstream mt-ISR activators (*atf4, atf5, chop*) (Shpilka and

Haynes, 2018), and *fgf21*, a biomarker of mitochondrial stress (Restelli et al., 2018; Tyynismaa et al., 2010) were significantly increased in our double *chchd10*$^{-/-}$ & *chchd2*$^{-/-}$ model, but not in the single KO models. This is in line with previous studies where activation of the mt-ISR was observed in both CHCHD10 S55L knock-in mice (Anderson et al., 2019), double KO mice and cells (Liu et al., 2020b; Ruan et al., 2022), but not in CHCHD10 KO mice. A recent study using CHCHD10 S55L mice suggested that mt-ISR precedes OXPHOS deficiency due to CHCHD10 protein aggregation (Sayles et al., 2022). In contrast, our single gene KO models results suggest that OXPHOS deficiency is independent of the mt-ISR.Whether the OXPHOS deficiency triggers the mt-ISR, and whether the compensation of Complex I assembly in the double *chchd10*$^{-/-}$ & *chchd2*$^{-/-}$ is a downstream consequence of the activation of the mt-ISR, as has been suggested before in *C. elegans* (Melber and Haynes, 2018), could be explored in future studies. Nevertheless, as the double *chchd10*$^{-/-}$ & *chchd2*$^{-/-}$ seem to have a worse phenotype than single gene KOs, this suggests that downstream consequences of the mt-ISR might be more detrimental than the observed Complex I deficiency in our single KO.

Conclusions

In this study, we used three knockout models and showed that loss of either protein leads to distinct, but overlapping, phenotypes during zebrafish development. This supports the hypothesis that loss-of-function of either or both proteins might be involved in the pathogenicity of various neurodegenerative diseases and highlights that the biological mechanisms that confer disease still need to be explored. Most importantly, the recovery of Complex I defect in the double *chchd10*$^{-/-}$ & *chchd2*$^{-/-}$ as well as the activation of the mt-ISR suggests that this pathway, likely activated to resolve mitochondrial dysfunction, might lead to more detrimental consequences when activated in vertebrates.

Funding

This research was supported by a Canadian Institutes of Health Research Project Grants to G.A.B.A. (420108) and E.A.S. (133530), a Natural Sciences and Engineering Research Council of Canada Discovery Grant to G.A.B.A. (RGPIN-2018-05603), an ALS Canada – Brain Canada Discovery Grant to G.A.B.A and E.A.S, and a Healthy Brain for Healthy Lives Grant (HBHL, McGill University) to V.P.L.

Literature cited

Anderson, C. J., et al., 2019. ALS/FTD mutant CHCHD10 mice reveal a tissue-specific toxic gain-of-function and mitochondrial stress response. Acta Neuropathologica.

Anichtchik, O., et al., 2008. Loss of PINK1 function affects development and results in neurodegeneration in zebrafish. J Neurosci. 28**,** 8199-207.

Aras, S., et al., 2020. Mitochondrial Nuclear Retrograde Regulator 1 (MNRR1) rescues the cellular phenotype of MELAS by inducing homeostatic mechanisms. Proceedings of the National Academy of Sciences. 117**,** 32056-32065.

Armstrong, G. A. B., Drapeau, P., 2013a. Calcium channel agonists protect against neuromuscular dysfunction in a genetic model of TDP-43 mutation in ALS. The Journal of Neuroscience. 33**,** 1741-1752.

Armstrong, G. A. B., Drapeau, P., 2013b. Loss and gain of FUS function impair neuromuscular synaptic transmission in a genetic model of ALS. Human Molecular Genetics. 22**,** 4282-4292.

Armstrong, G. A. B., et al., 2016. Homology Directed Knockin of Point Mutations in the Zebrafish tardbp and fus Genes in ALS Using the CRISPR/Cas9 System. PLOS ONE. 11**,** e0150188.

Auranen, M., et al., 2015. CHCHD10 variant p.(Gly66Val) causes axonal Charcot-Marie-Tooth disease. Neurology Genetics. 1**,** e1.

Bannwarth, S., et al., 2014. A mitochondrial origin for frontotemporal dementia and amyotrophic lateral sclerosis through CHCHD10 involvement. Brain. 137**,** 2329-2345.

Baughman, J. M., et al., 2009. A Computational Screen for Regulators of Oxidative Phosphorylation Implicates SLIRP in Mitochondrial RNA Homeostasis. PLOS Genetics. 5**,** e1000590.

Bose, P., et al., 2019. Neuromuscular junction abnormalities in a zebrafish loss-of-function model of TDP-43. J Neurophysiol. 121**,** 285-297.

Brockmann, S. J., et al., 2018. CHCHD10 mutations p.R15L and p.G66V cause motoneuron disease by haploinsufficiency. Human Molecular Genetics. 27**,** 706-715.

Burstein, S. R., et al., 2018. In vitro and in vivo studies of the ALS-FTLD protein CHCHD10 reveal novel mitochondrial topology and protein interactions. Human Molecular Genetics. 27**,** 160-177.

Byrnes, J., et al., 2018. Pharmacologic modeling of primary mitochondrial respiratory chain dysfunction in zebrafish. Neurochem Int. 117**,** 23-34.

Cavallaro, G., 2010. Genome-wide analysis of eukaryotic twin CX9C proteins. Molecular BioSystems. 6**,** 2459-2470.

Che, X. Q., et al., 2018. Mutation Screening of the CHCHD2 Gene for Alzheimer's Disease and Frontotemporal Dementia in Chinese Mainland Population. J Alzheimers Dis. 61**,** 1283-1288.

Chung, M. J., Suh, Y.-L., 2002. Ultrastructural Changes of Mitochondria in the Skeletal Muscle of Patients with Amyotrophic Lateral Sclerosis. Ultrastructural Pathology. 26**,** 3-7.

Costa-Mattioli, M., Walter, P., 2020. The integrated stress response: From mechanism to disease. Science. 368.

Dupuis, L., et al., 2004. Mitochondria in Amyotrophic Lateral Sclerosis: A Trigger and a Target. Neurodegenerative Diseases. 1**,** 245-254.

El-Hattab, A. W., Scaglia, F., 2016. Mitochondrial Cardiomyopathies. Frontiers in cardiovascular medicine. 3**,** 25-25.

Flinn, L., et al., 2009. Complex I deficiency and dopaminergic neuronal cell loss in parkin-deficient zebrafish (Danio rerio). Brain. 132**,** 1613-23.
Funayama, M., et al., 2015. CHCHD2 mutations in autosomal dominant late-onset Parkinson's disease: a genome-wide linkage and sequencing study. Lancet Neurol. 14**,** 274-82.
Genin, E. C., et al., 2016. CHCHD10 mutations promote loss of mitochondrial cristae junctions with impaired mitochondrial genome maintenance and inhibition of apoptosis. EMBO Molecular Medicine. 8**,** 58-72.
Grossman, L. I., et al., 2017. MNRR1, a Biorganellar Regulator of Mitochondria. Oxid Med Cell Longev. 2017**,** 6739236.
Harjuhaahto, S., et al., 2020. ALS and Parkinson's disease genes CHCHD10 and CHCHD2 modify synaptic transcriptomes in human iPSC-derived motor neurons. Neurobiology of Disease. 141**,** 104940.
Huang, X., et al., 2018. CHCHD2 accumulates in distressed mitochondria and facilitates oligomerization of CHCHD10Human Molecular Genetics, 2018, Vol. 00, No. 0Human Molecular Genetics, 2018, Vol. 00, No. 0. Human molecular genetics.
Jao, L.-E., et al., 2013. Efficient multiplex biallelic zebrafish genome editing using a CRISPR nuclease system. Proceedings of the National Academy of Sciences. 110**,** 13904-13909.
Lehmer, C., et al., 2018. A novel CHCHD10 mutation implicates a Mia40-dependent mitochondrial import deficit in ALS. EMBO molecular medicine. 10**,** e8558.
Liu, W., et al., 2020a. Chchd2 regulates mitochondrial morphology by modulating the levels of Opa1. Cell Death & Differentiation. 27**,** 2014-2029.
Liu, Y., et al., 2014. CHCHD2 inhibits apoptosis by interacting with Bcl-x L to regulate Bax activation. Cell Death And Differentiation. 22**,** 1035.
Liu, Y. T., et al., 2020b. Loss of CHCHD2 and CHCHD10 activates OMA1 peptidase to disrupt mitochondrial cristae phenocopying patient mutations. Hum Mol Genet. 29**,** 1547-1567.
Livak, K. J., Schmittgen, T. D., 2001. Analysis of Relative Gene Expression Data Using Real-Time Quantitative PCR and the 2−ΔΔCT Method. Methods. 25**,** 402-408.
Mao, C., et al., 2019. CHCHD10 is involved in the development of Parkinson's disease caused by CHCHD2 loss-of-function mutation p.T61I. Neurobiology of Aging. 75**,** 38-41.
Melber, A., Haynes, C. M., 2018. UPRmt regulation and output: a stress response mediated by mitochondrial-nuclear communication. Cell Research. 28**,** 281-295.
Mendelsohn, B. A., et al., 2008. The zebrafish embryo as a dynamic model of anoxia tolerance. Developmental dynamics : an official publication of the American Association of Anatomists. 237**,** 1780-1788.
Meng, H., et al., 2017. Loss of Parkinson's disease-associated protein CHCHD2 affects mitochondrial crista structure and destabilizes cytochrome c. Nature communications. 8**,** 15500-15500.
Moreno-Mateos, M. A., et al., 2015. CRISPRscan: designing highly efficient sgRNAs for CRISPR-Cas9 targeting in vivo. Nature Methods. 12**,** 982-988.
Ogaki, K., et al., 2015. Mitochondrial targeting sequence variants of the CHCHD2 gene are a risk for Lewy body disorders. Neurology. 85**,** 2016-25.
Perrone, F., et al., 2017. Investigating the role of ALS genes CHCHD10 and TUBA4A in Belgian FTD-ALS spectrum patients. Neurobiology of Aging. 51**,** 177.e9-177.e16.
Pinho, B. R., et al., 2013. How mitochondrial dysfunction affects zebrafish development and cardiovascular function: an in vivo model for testing mitochondria-targeted drugs. British journal of pharmacology. 169**,** 1072-1090.

Purandare, N., et al., 2018. The cellular stress proteins CHCHD10 and MNRR1 (CHCHD2): Partners in mitochondrial and nuclear function and dysfunction. Journal of Biological Chemistry. 293**,** 6517-6529.
Restelli, L. M., et al., 2018. Neuronal Mitochondrial Dysfunction Activates the Integrated Stress Response to Induce Fibroblast Growth Factor 21. Cell Rep. 24**,** 1407-1414.
Ruan, Y., et al., 2022. CHCHD2 and CHCHD10 regulate mitochondrial dynamics and integrated stress response. Cell Death & Disease. 13**,** 156.
Sabharwal, A., et al., 2020. A Genetic Model Therapy Proposes a Critical Role for Liver Dysfunction in Mitochondrial Biology and Disease. bioRxiv. 2020.05.08.084681.
Sato, S., et al., 2021. Homeostatic p62 levels and inclusion body formation in CHCHD2 knockout mice. Hum Mol Genet. 30**,** 443-453.
Sayles, N. M., et al., 2022. Mutant CHCHD10 causes an extensive metabolic rewiring that precedes OXPHOS dysfunction in a murine model of mitochondrial cardiomyopathy. Cell Reports. 38**,** 110475.
Shi, C.-h., et al., 2016. CHCHD2 gene mutations in familial and sporadic Parkinson's disease. Neurobiology of Aging. 38**,** 217.e9-217.e13.
Shpilka, T., Haynes, C. M., 2018. The mitochondrial UPR: mechanisms, physiological functions and implications in ageing. Nature Reviews Molecular Cell Biology. 19**,** 109-120.
Smith, E. F., et al., 2017. The role of mitochondria in amyotrophic lateral sclerosis. Neuroscience Letters.
Steele, S. L., et al., 2014. Zebrafish as a model system for mitochondrial biology and diseases. Transl Res. 163**,** 79-98.
Straub, I. R., et al., 2018. Loss of CHCHD10–CHCHD2 complexes required for respiration underlies the pathogenicity of a CHCHD10 mutation in ALS. Human Molecular Genetics. 27**,** 178-189.
Straub, I. R., et al., 2021. Multi-OMICS study of a CHCHD10 variant causing ALS demonstrates metabolic rewiring and activation of endoplasmic reticulum and mitochondrial unfolded protein responses. Hum Mol Genet. 30**,** 687-705.
Strecker, R., et al., 2011. Oxygen requirements of zebrafish (Danio rerio) embryos in embryo toxicity tests with environmental samples. Comparative Biochemistry and Physiology Part C: Toxicology & Pharmacology. 153**,** 318-327.
Taylor, J. P., et al., 2016. Decoding ALS: from genes to mechanism. Nature. 539**,** 197-206.
Tyynismaa, H., et al., 2010. Mitochondrial myopathy induces a starvation-like response. Hum Mol Genet. 19**,** 3948-58.
Vejnar, C. E., et al., 2016. Optimized CRISPR–Cas9 System for Genome Editing in Zebrafish. Cold Spring Harbor Protocols. 2016**,** pdb.prot086850.
Westerfield, M., 1995. The Zebrafish Book. A Guide for the Laboratory Use of Zebrafish (Danio rerio). University of Oregon Press, Eugene, OR.
Woo, J.-A., et al., 2017. Loss of function CHCHD10 mutations in cytoplasmic TDP-43 accumulation and synaptic integrity. Nature Communications. 8**,** 15558.
Xia, W., et al., 2022. Chchd10 is dispensable for myogenesis but critical for adipose browning. Cell Regeneration. 11**,** 14.
Xiao, Y., et al., 2020. Loss of mitochondrial protein CHCHD10 in skeletal muscle causes neuromuscular junction impairment. Hum Mol Genet. 29**,** 1784-1796.
Zhang, M., et al., 2015. Mutation analysis of CHCHD10 in different neurodegenerative diseases. Brain. 138**,** e380-e380.

Figures.

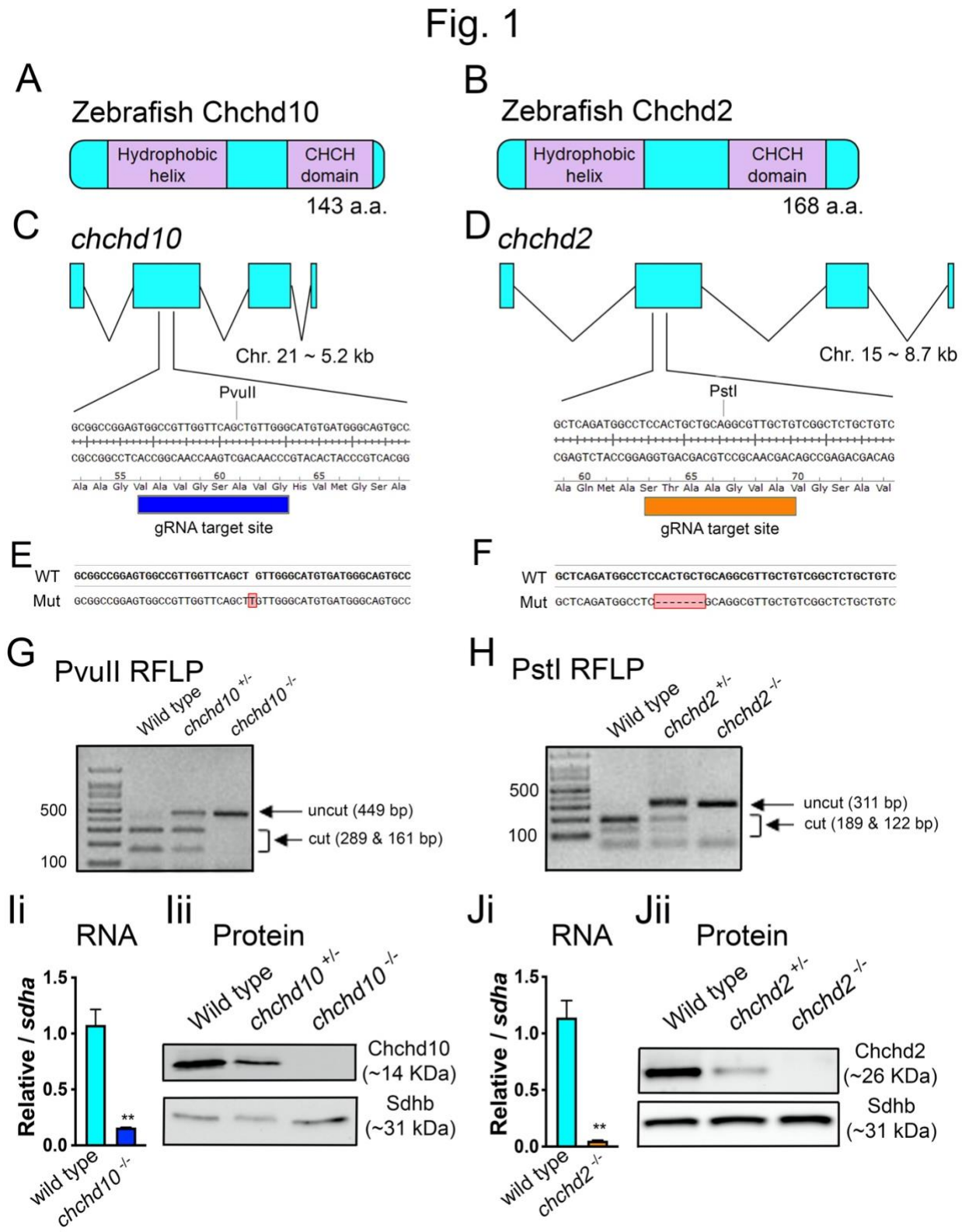
Fig. 1
A
Zebrafish Chchd10
Hydrophobic helix
CHCH domain
143 a.a.
B
Zebrafish Chchd2
Hydrophobic helix
CHCH domain
168 a.a.
C
chchd10
Chr. 21 ~ 5.2 kb
PvuII
GCGGCCGGAGTGGCCGTTGGTTCAGCTGTTGGGCATGTGATGGGCAGTGCC
CGCCGGCCTCACCGGCAACCAAGTCGACAACCCGTACACTACCCGTCACGG
55 60 65
Ala Ala Gly Val Ala Val Gly Ser Ala Val Gly His Val Met Gly Ser Ala
gRNA target site
D
chchd2
Chr. 15 ~ 8.7 kb
PstI
GCTCAGATGGCCTCCACTGCTGCAGGCGTTGCTGTCGGCTCTGCTGTC
CGAGTCTACCGGAGGTGACGACGTCCGCAACGACAGCCGAGACGACAG
60 65 70
Ala Gln Met Ala Ser Thr Ala Ala Gly Val Ala Val Gly Ser Ala Val
gRNA target site
E
WT GCGGCCGGAGTGGCCGTTGGTTCAGCT GTTGGGCATGTGATGGGCAGTGCC
Mut GCGGCCGGAGTGGCCGTTGGTTCAGCTTGTTGGGCATGTGATGGGCAGTGCC
F
WT GCTCAGATGGCCTCCACTGCTGCAGGCGTTGCTGTCGGCTCTGCTGTC
Mut GCTCAGATGGCCTC-------GCAGGCGTTGCTGTCGGCTCTGCTGTC
G
PvuII RFLP
Wild type
chchd10+/-
chchd10-/-
500
100
uncut (449 bp)
cut (289 & 161 bp)
H
PstI RFLP
Wild type
chchd2+/-
chchd2-/-
500
100
uncut (311 bp)
cut (189 & 122 bp)
Ii
RNA
Relative / sdha
1.5
1.0
0.5
0.0
**
wild type
chchd10-/-
Iii
Protein
Wild type
chchd10+/-
chchd10-/-
Chchd10
(~14 KDa)
Sdhb
(~31 kDa)
Ji
RNA
Relative / sdha
1.5
1.0
0.5
0.0
**
wild type
chchd2-/-
Jii
Protein
Wild type
chchd2+/-
chchd2-/-
Chchd2
(~26 KDa)
Sdhb
(~31 kDa)

Figure 2.1. Generation of *chchd10* $^{-/-}$ and *chchd2* $^{-/-}$ zebrafish lines.

Schematic representation of the zebrafish proteins Chchd10 (**A**) and Chchd2 (**B**). **C**, *chchd10* gene structure and gRNA target site. **D**, *chchd2* gene structure and gRNA target site. **E**, CRISPR-induced *chchd10* $^{-/-}$ mutant (mut) line. **F**, CRISPR-induced *chchd2* $^{-/-}$ mutant (mut) line. **G**, Restriction fragment length polymorphism (RFLP) screening method using PvuII which is lost in the *chchd10* $^{-/-}$ mutant. **H**, RFLP screening using PstI which is lost in the *chchd2* $^{-/-}$ mutant. **Ii**, RT-qPCR of the *chchd10* transcript using wild type and *chchd10* $^{-/-}$ cDNA. A reduction in *chchd10* ($t(4) = 6.61$, $p = 0.003$, relative to *sdha*) was observed in *chchd10* $^{-/-}$ (n= 3 per genotype, data represent mean ± S.E.M). **Iii**, Immunoblot using wild type, *chchd10* $^{+/-}$, and *chchd10* $^{-/-}$ whole brain lysate. Sdhb was used as a loading control. **Ji**, RT-qPCR of the *chchd2* transcript from wild type and *chchd2* $^{-/-}$ cDNA. A significant reduction in *chchd2* ($t(4) = 7.26$, $p = 0.002$, relative to *sdha*) was observed in *chchd2* $^{-/-}$ (n= 3 per genotype, data represent mean ± S.E.M). **Jii**, Brain lysate immunoblot from wild type, *chchd2* $^{+/-}$, *chchd2* $^{-/-}$ model. Sdhb was used as a loading control.

Fig. 2

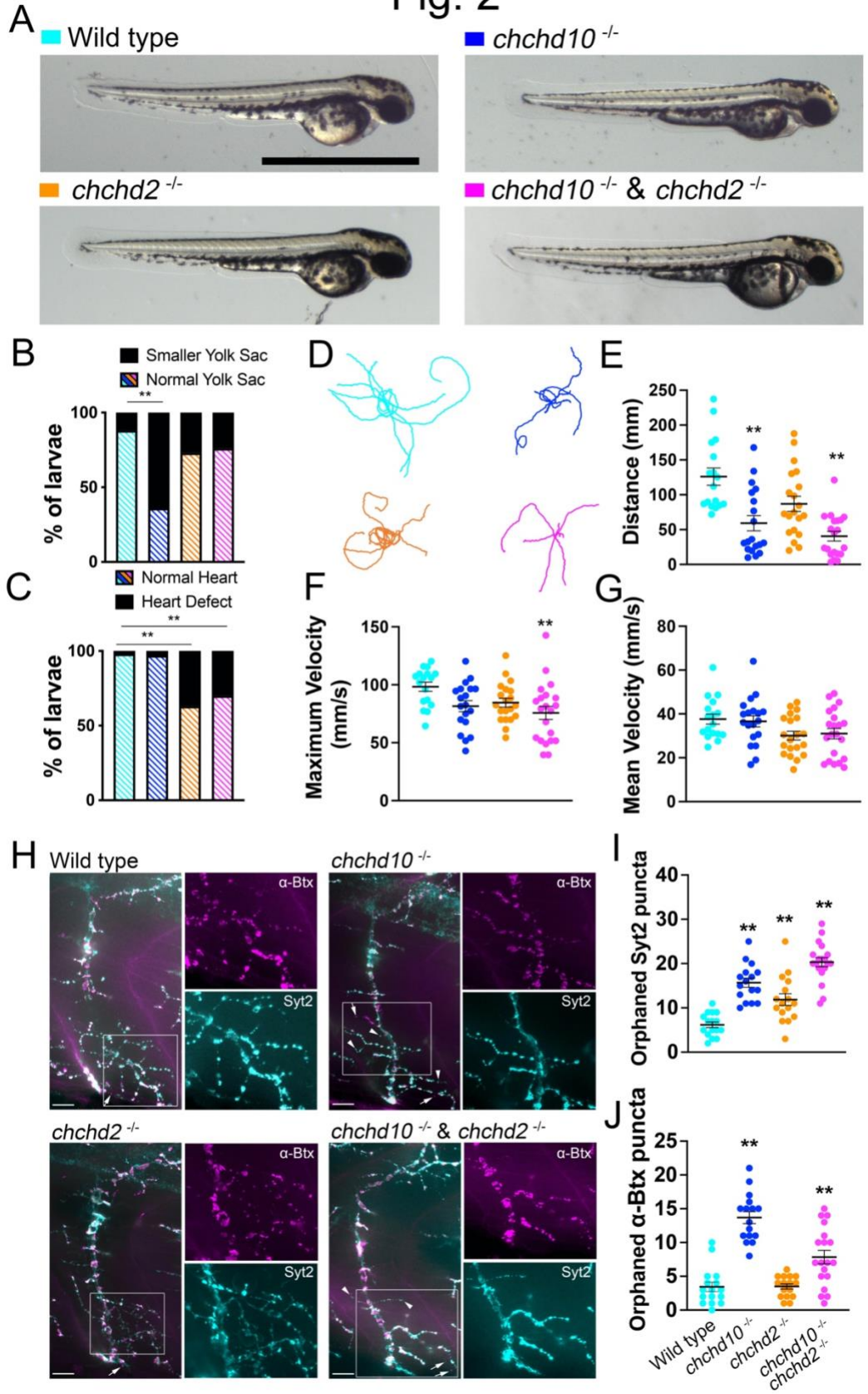
A
Wild type
chchd10 -/-
chchd2 -/-
chchd10 -/- & chchd2 -/-
B
Smaller Yolk Sac
Normal Yolk Sac
% of larvae
C
Normal Heart
Heart Defect
% of larvae
D
E
Distance (mm)
F
Maximum Velocity (mm/s)
G
Mean Velocity (mm/s)
H
Wild type
chchd10 -/-
chchd2 -/-
chchd10 -/- & chchd2 -/-
α-Btx
Syt2
I
Orphaned Syt2 puncta
J
Orphaned α-Btx puncta
Wild type
chchd10 -/-
chchd2 -/-
chchd10 -/- chchd2 -/-

Figure 2.2. Larval *chchd10*$^{-/-}$, *chchd2*$^{-/-}$ and double *chchd10*$^{-/-}$ & *chchd2*$^{-/-}$ display morphological defects, motor impairment and altered neuromuscular junction integrity.

A, Representative images of 56 hpf larvae. **B**, Quantification of yolk sacs defects. Larval *chchd10*$^{-/-}$ showing reduced yolk sack size compared to wild type larvae (χ^2= 18.5, $p < 0.0001$). Sample sizes were as follows: wild type, n = 34; *chchd10*$^{-/-}$, n = 28; *chchd2*$^{-/-}$, n = 30, and double *chchd10*$^{-/-}$ & *chchd2*$^{-/-}$, n = 37. **C**, Quantification of heart defects. Both *chchd2*$^{-/-}$ (χ^2= 23.43, $p < 0.0001$) and double *chchd10*$^{-/-}$ & *chchd2*$^{-/-}$ (χ^2= 16.05, $p < 0.0001$) larvae display cardiac abnormalities. Sample sizes are as follows: wild type, n = 58; *chchd10*$^{-/-}$, n = 35; *chchd2*$^{-/-}$, n = 62, and double *chchd10*$^{-/-}$ & *chchd2*$^{-/-}$, n = 37. **D**, Representative traces of touch-evoked motor response 2 dpf larvae (n =10 per genotype). Quantification of swim distance (**E**), maximum swim velocity (**F**), and mean swim velocity (**G**). Data shown as individual data points ± S.E.M. Samples sizes were as follows: wild type, n = 17; *chchd10*$^{-/-}$, n = 19; *chchd2*$^{-/-}$, n = 20, and double *chchd10*$^{-/-}$ & *chchd2*$^{-/-}$, n = 20. Significance was assed using Kruskal-Wallis followed by Dunn's post hoc test for swimming distance and by one-way ANOVA and Tuckey's multiple comparison test for maximum velocity and mean distance measures. **H**, Representative images of NMJs in the ventral trunk musculature of larvae aged 2 dpf. Markers are Syt2 (cyan) and αBtx (magenta). Arrow and arrowheads in example NMJ images represent orphaned αBtx and Syt2 puncta, respectively. Scale bars represent 100 µm. **I**, Tabulation of orphaned pre-synaptic (Syt2) puncta. All genetic groups were significantly different than wild type NMJs ($F (3, 63) = 34.33$, $p < 0.01$). Data shown as mean ± S.E.M. **J**, Tabulation of orphaned post-synaptic (αBtx) puncta. Both *chchd10* $^{-/-}$ and double *chchd10* $^{-/-}$ *& chchd2* $^{-/-}$ showed increased orphaned AChR clusters when compared to wild type larvae ($F (3, 63) = 34.80$, $p < 0.01$). Data shown as mean ± S.E.M Sample sizes are as follows for both presynaptic and post-synaptic quantification: wild type,

n=16 ventral roots, 6 larvae; *chchd10* $^{-/-}$, n=16 ventral roots, 6 larvae; *chchd2* $^{-/-}$, n=16 ventral roots, 6 larvae, and double *chchd10* $^{-/-}$ & *chchd2* $^{-/-}$, n=19 ventral roots, 7 larvae. Significant difference with wild type larvae is represented by a single asterisk ($p < 0.05$) or double asterisk ($p < 0.01$).

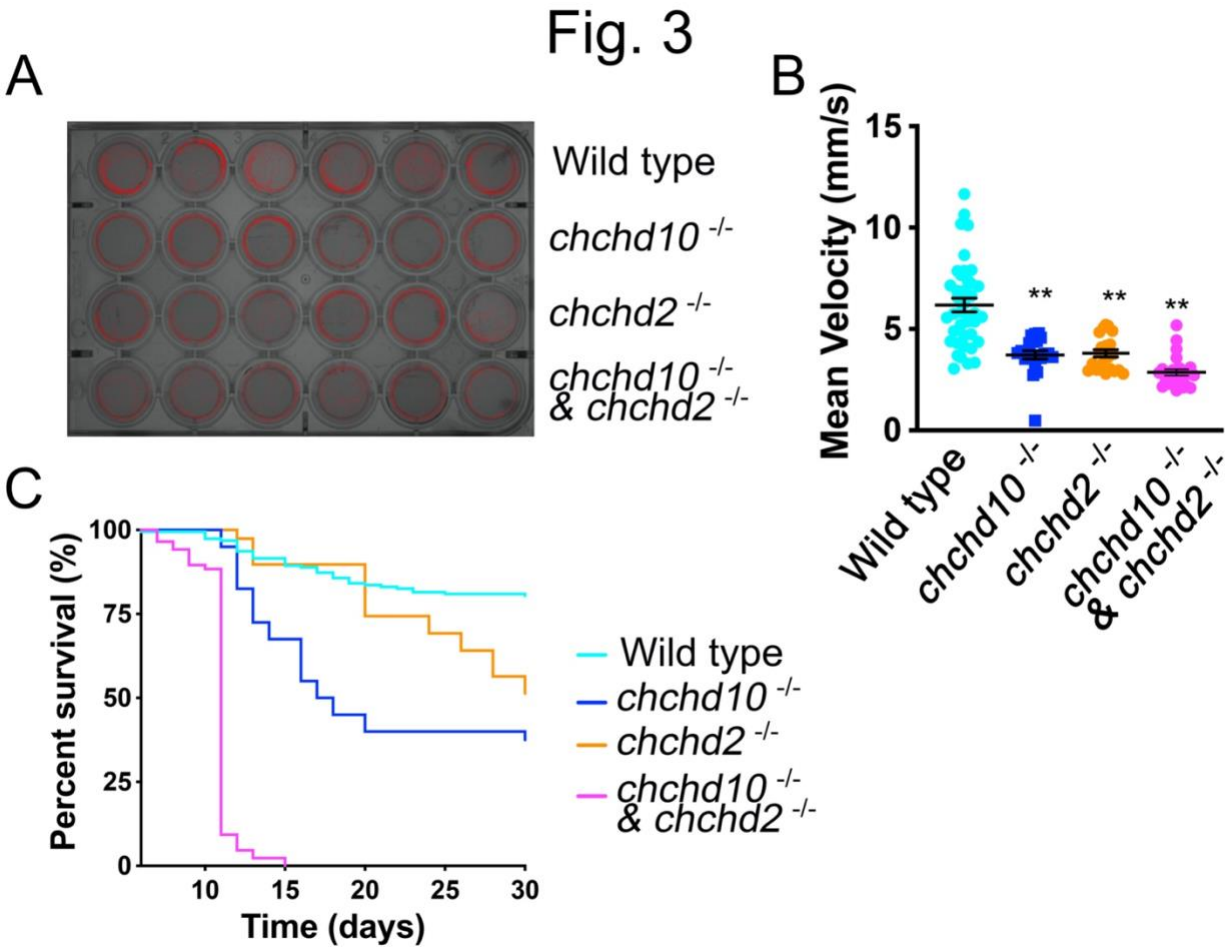

Figure 2.3. All mutant larvae present a motor deficit at 5 dpf and reduced survival**.**

A, Representative image of a 24-well plate free swim arena and movement paths (6 per genonytpe) of larvae aged 5 dpf. **B**, Quantification of mean velocity. Specific mean swim velocities are as follows: wild type, 6.2 mm/s , n = 40; *chchd10*$^{-/-}$, 3.72 mm/s, n = 21; *chchd2*$^{-/-}$, 3.80 mm/s, n = 21, and double *chchd10*$^{-/-}$ & *chchd2*$^{-/-}$, 2.87 mm/s, n = 36. Data represented as individual data points ± S.E.M. Kruskal-Wallis test was used to assess significance. Double asterisks represent $p < 0.01$, Dunn's Post hoc test. **C**, Survival rates were significantly reduced in all mutants, with no double *chchd10* $^{-/-}$ & *chchd2* $^{-/-}$ surviving past 15 days. Sample sizes are as

follows: wild type, n =189; *chchd10*$^{-/-}$, n = 40; *chchd2*$^{-/-}$, n = 39, and double *chchd10*$^{-/-}$ & *chchd2*$^{-/-}$, n = 86. Significance was assessed using Mantel-Cox test, all p <0.01 compared to wild type.

Fig. 4

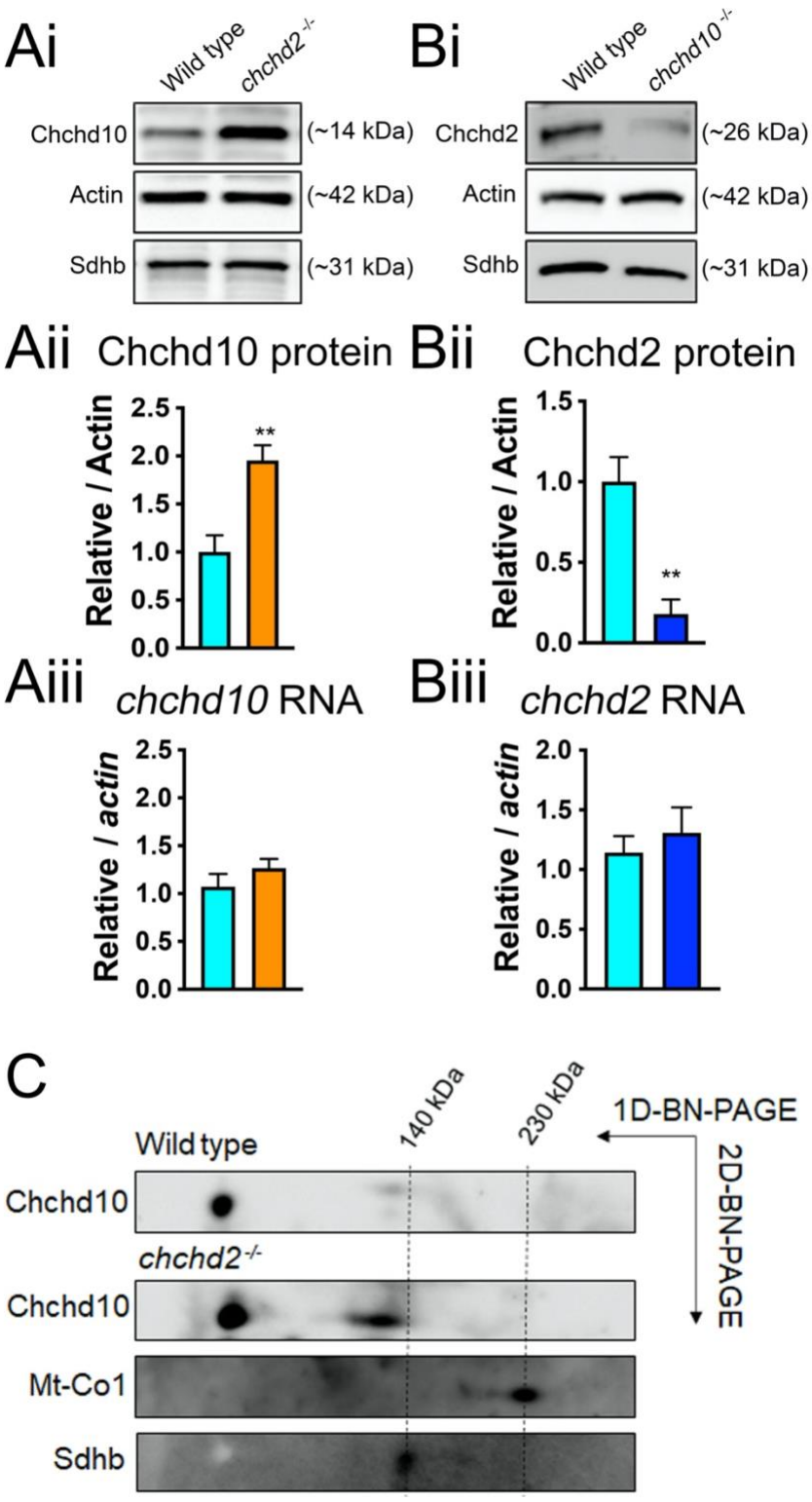
Ai
Wild type
chchd2-/-
Chchd10
(~14 kDa)
Actin
(~42 kDa)
Sdhb
(~31 kDa)
Bi
Wild type
chchd10-/-
Chchd2
(~26 kDa)
Actin
(~42 kDa)
Sdhb
(~31 kDa)
Aii Chchd10 protein
Relative / Actin
2.5
2.0
1.5
1.0
0.5
0.0
**
Bii Chchd2 protein
Relative / Actin
1.5
1.0
0.5
0.0
**
Aiii chchd10 RNA
Relative / actin
2.5
2.0
1.5
1.0
0.5
0.0
Biii chchd2 RNA
Relative / actin
2.0
1.5
1.0
0.5
0.0
C
140 kDa
230 kDa
1D-BN-PAGE
2D-BN-PAGE
Wild type
Chchd10
chchd2-/-
Chchd10
Mt-Co1
Sdhb

Figure 2.4. Larval Chchd10 compensates for loss of Chchd2 expression but not *vice versa* and is present in both a lower and higher molecular weight complex in zebrafish at 5 dpf.

Ai, Representative immunoblot of Chchd10 protein level in *chchd2*$^{-/-}$ larvae aged 5 dpf. **Aii**, Immunoblot quantification (n=3 per genotype, 5 dpf) showing increased Chchd10 expression compared to wild type in *chchd2*$^{-/-}$ larvae (t (4) = 4.04, p=0.011). Actin was used as loading control. **Aiii**, Unchanged transcript levels of *chchd10 in* 5 dpf *chchd2*$^{-/-}$ larvae (t (4) = 0.30, p = 0.30 relative to *actin*). **Bi**, Representative immunoblot of Chchd2 protein expression in *chchd10*$^{-/-}$ larvae aged 5 dpf. **Bii,** Immunoblot quantification (n=3 per genotype, 5 dpf) showing reduced Chchd2 expression levels in *chchd10*$^{-/-}$ larvae compared to wild type larvae (t (4) = 4.62, p=0.0099). Actin was used as loading control. **Biii**, Unchanged transcript levels of *chchd2* in 5dpf *chchd10*$^{-/-}$ larvae (t (4) = 0.55, p = 0.55, relative to *actin*). **C**, Second dimensional PAGE analysis using a Chchd10 antibody revealed a high molecular weight complex, close to 140 kDa, in both wild type and *chchd2*$^{-/-}$ larvae. Mt-Co1 and Sdhb are used as molecular weight markers.

Fig. 5

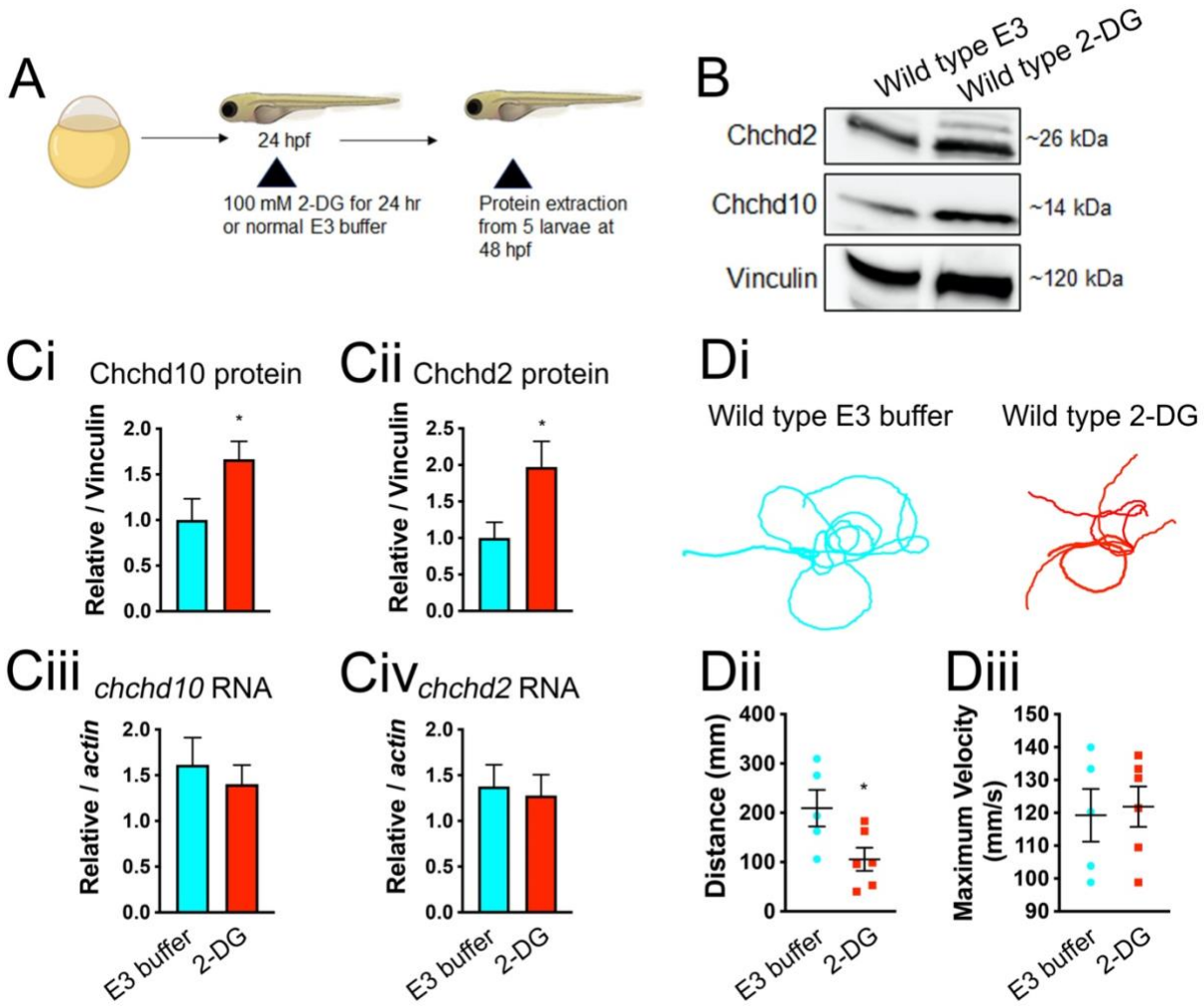

Figure 2.5. Both Chchd10 and Chchd2 proteins display elevated expression levels in response increased mitochondrial reliance in wild type larvae.

A, Experimental timeline for 2-DG treatment (Images were created using BioRender). **B**, Example immunoblot showing Chchd10 and Chchd2 expression change following treatment with to 2-DG. **Ci, Cii**, Quantification of immunoblot data. Significant difference in both Chchd10 (t (10) = 2.184, p = 0.053), and Chchd2 (t (10) = 2.348, p = 0.04) protein levels following 2-DG treatment was observed. Sample sizes are as follows: 2-DG, n = 6; E3 Buffer, n

= 6. Vinculin was used as loading control. **Ciii, Civ**, Unchanged expression levels following 2-DG exposure in both transcripts: *chchd10* (t (4) = 0.59, p = 0.59, relative to *actin*) and *chchd2*: (t (4) = 0.78, p = 0.78 relative to *actin*). Sample sizes are as follows: 2-DG, n = 3; E3 buffer, n = 3. Single asterisks represent significant differences from E3-treated wild type ($p < 0.05$). **Di**, Representative touch-evoked larval motor responses following exposure to 2-DG or E3 buffer treatment for 24 hrs. Motor responses were evaluated at 56 hpf. **Dii**, Larvae exposed to 2-DG show significantly reduced swim distance (t (9) = 2.45, p = 0.04), though maximum swim velocity. **Diii**, was not found to be significantly different (t (9) = 0.26, p = 0.80). Sample sizes as follows E3 Buffer, n =5; 2-DG, n = 6.

Fig. 6

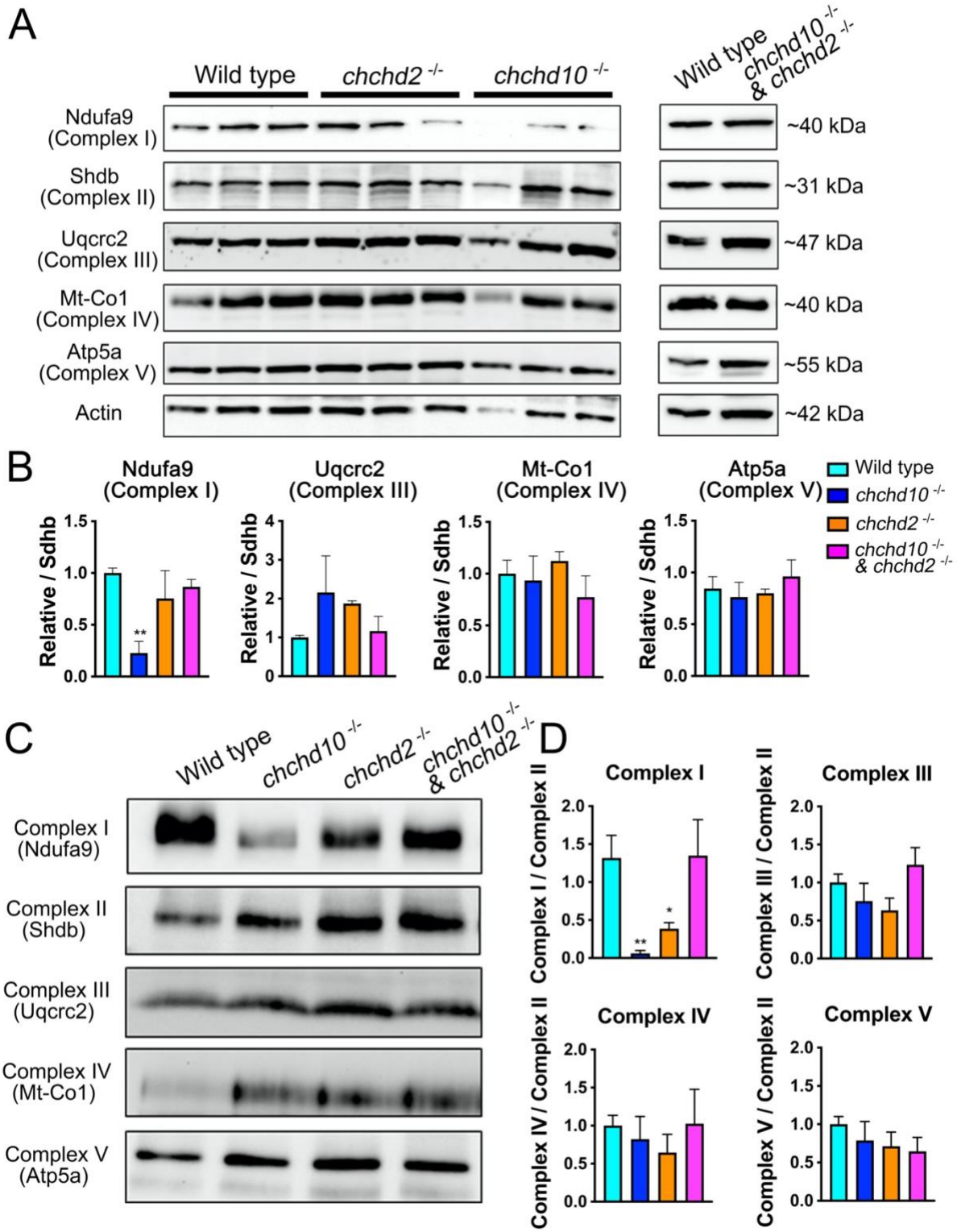
A
Wild type
chchd2 -/-
chchd10 -/-
Wild type
chchd10 -/- & chchd2 -/-
Ndufa9 (Complex I)
Shdb (Complex II)
Uqcrc2 (Complex III)
Mt-Co1 (Complex IV)
Atp5a (Complex V)
Actin
~40 kDa
~31 kDa
~47 kDa
~40 kDa
~55 kDa
~42 kDa
B
Ndufa9 (Complex I)
Uqcrc2 (Complex III)
Mt-Co1 (Complex IV)
Atp5a (Complex V)
Relative / Sdhb
Wild type
chchd10 -/-
chchd2 -/-
chchd10 -/- & chchd2 -/-
C
Wild type
chchd10 -/-
chchd2 -/-
chchd10 -/- & chchd2 -/-
Complex I (Ndufa9)
Complex II (Shdb)
Complex III (Uqcrc2)
Complex IV (Mt-Co1)
Complex V (Atp5a)
D
Complex I
Complex III
Complex IV
Complex V
Complex I / Complex II
Complex III / Complex II
Complex IV / Complex II
Complex V / Complex II

Figure 2.6. Reduced assembly of mitochondrial Complex I in *chchd10*$^{-/-}$ and *chchd2*$^{-/-}$ zebrafish larvae, but not in double *chchd10*$^{-/-}$ & *chchd2*$^{-/-}$ larvae at 5 dpf.

A, Immunoblot analysis of mitochondrial respiratory chain subunits in larvae aged 5 dpf and quantification (**B**). Ndufa9 is significantly reduced in *chchd10* $^{-/-}$ larvae ($F(3, 11) = 7.40$, $p = 0.006$, $p = 0.003$ Tuckey's, n = 3 per genotype). Data is represented as mean ± S.E.M. **C**, Representative blue native PAGE with each lane constituted of an individual 5 dpf larvae of respective genotype and quantification (**D**). Significant reduction of Complex I assembly was observed ($F(3, 25) = 7.42$, $p < 0.01$) in *chchd10*$^{-/-}$ larvae ($p < 0.01$, Tuckey's), and *chchd2*$^{-/-}$ larvae ($p < 0.05$ Tuckey's), but not in double *chchd10*$^{-/-}$ & *chchd2*$^{-/-}$ model. Sample size are as follows, wild type, n= 8; *chchd2*$^{-/-}$, n = 7; *chchd10*$^{-/-}$, n = 8, and *chchd10*$^{-/-}$ & *chchd2*$^{-/-}$ n=5. Data is represented as mean ± S.E.M. Significant difference with wild type larvae is represented by a single asterisk ($p < 0.05$) or double asterisk ($p < 0.01$).

Fig. 7

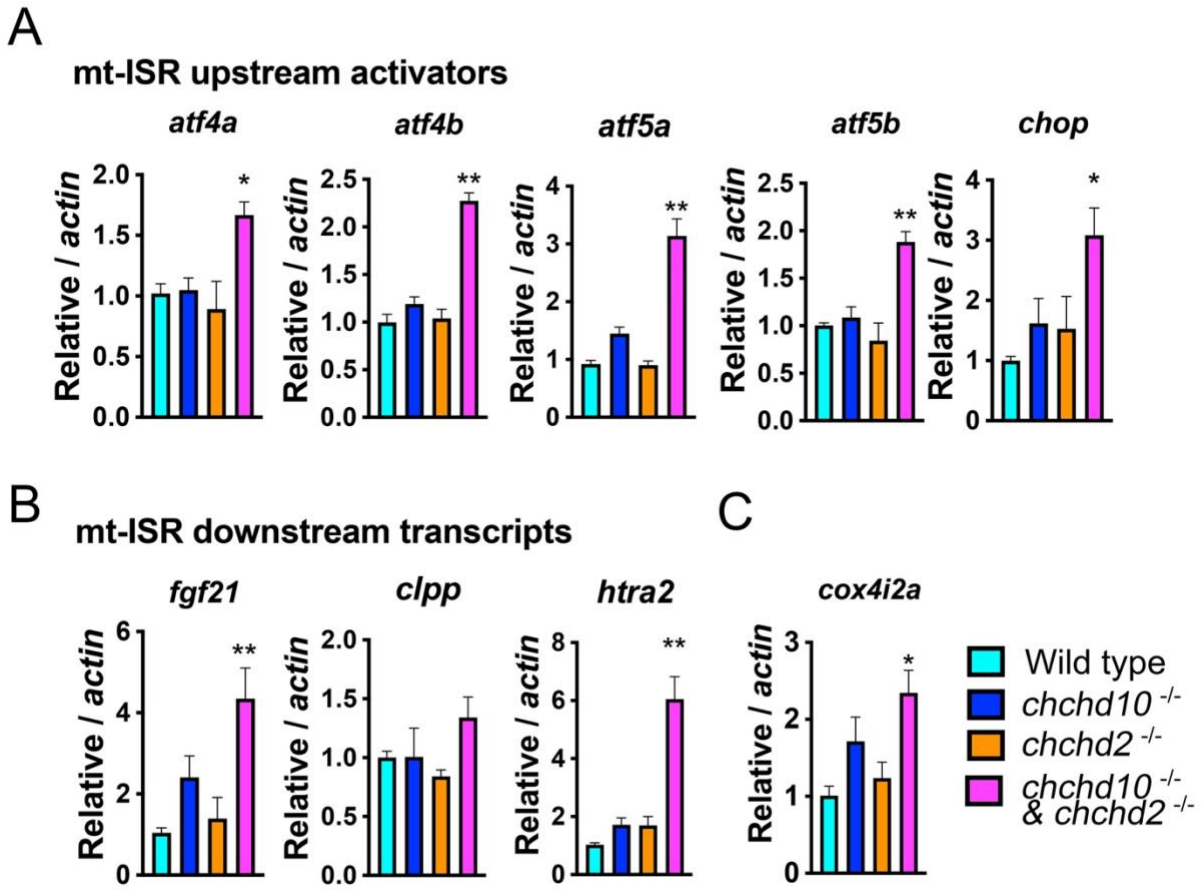

Figure 2.7. Several markers of the mitochondrial stress response are upregulated in our double *chchd10*$^{-/-}$ & *chchd2* $^{-/-}$ model at 5 dpf.

A, All mt-ISR upstream activators were significantly increased in the double *chchd10*$^{-/-}$ & *chchd2* $^{-/-}$ model including *atf4a* ($F(3, 8) = 5.964$, $p = 0.019$); *atf4b* ($F(3, 8) = 49.89$, $p < 0.01$); *atf5a* ($F(3, 12) = 56.65$, $p < 0.01$); *atf5b* ($F(3, 8) = 14.39$, $p < 0.01$); *chop* ($F(3, 8) = 6.669$, $p < 0.01$). **B**, Several downstream targets are upregulated in the double *chchd10*$^{-/-}$ & *chchd2* $^{-/-}$ model including *htra2* ($F(3, 8) = 28.38$, $p < 0.01$); *fgf21* ($F(3, 8) = 9.177$, $p < 0.01$), but not *clpp* ($F(3, 9) = 2.032$, $p = 0.1799$).

C, Oxygen responsive transcript *cox4i2a* was significantly increased in our double *chchd10*$^{-/-}$ & *chchd2* $^{-/-}$ model ($F(3, 7) = 6.919$, $p = 0.017$). Data is represented as mean ± S.E.M, n = 3 per genotype. Significant difference with wild type larvae is represented by a single asterisk ($p < 0.05$) or double asterisk ($p < 0.01$), Tuckey's multiple comparison test.

Preface Chapter 3

Chapter 2 demonstrated that loss of either or both Chchd10 and Chchd2 results in several ALS-like phenotype in zebrafish larvae. When considering therapeutic avenues for CHCHD10-related ALS cases, it is crucial to understand how a disease variant confers pathology, as it will aid in determining potential therapeutic targets. In the next chapter, I focused on the CHCHD10 ^{P83L} variant in zebrafish which is orthologous to the CHCHD10 ^{P80L} variant in human ALS cases. Moreover, in this chapter we took advantage of our stable KI line to examine the detrimental consequences in adult zebrafish and present tissue-specific pathologies that may be arising in patients with the mutation encoding this variant.

Chapter 3: *CHCHD10* ^{P80L} CRISPR knock-in model in zebrafish displays a pre-symptomatic adult muscle phenotype

Virginie Petel Légaré [1], Christian J. Rampal [1], Hana Antonicka [2], Ziyaan A. Harji [1], Esteban C. Rodríguez [1], E.A. Shoubridge [2] and Gary A.B. Armstrong [1*]

[1] Department of Neurology and Neurosurgery
Montreal Neurological Institute
Faculty of Medicine
McGill University

[2] Department of Human Genetics
McGill University
Montreal, QC H3A 2B4, Canada.

* Corresponding author (gary.armstrong@mcgill.ca)

Manuscript to be submitted

Abstract

While several mutations in *CHCHD10* have been documented in a spectrum of diseases including amyotrophic lateral sclerosis (ALS), most of these mutations have not been modelled in animals. Using the CRISPR/Cas9 system and homology directed repair, we generated a novel zebrafish knock-in (KI) model expressing the orthologous ALS-associated CHCHD10 ^{P80L} variant (Chchd10 ^{P83L}). This model displayed reduced Chchd10 expression levels, motor impairment, reduced survival, and altered neuromuscular junction (NMJ) integrity in larval zebrafish. These deficits were not accompanied by changes in transcripts involved in the mitochondrial integrated stress response (mt-ISR), phenocopying previous findings in our knockout (*chchd10* $^{-/-}$) larvae and suggesting that this variant partly acts through a loss-of-function mechanism. To further explore disease mechanisms arising from our model, we investigated phenotypes in adult zebrafish. We performed bulk RNA sequencing on whole spinal cords and confirmed that our *chchd10* $^{P83L/P83L}$ model does not display altered transcript levels associated with activation of the mt-ISR. We did, however, observe significant increases in transcripts levels associated with inflammation. Furthermore, we provide evidence that our zebrafish model develops muscle pathology characterized by significant reduction in size and number of muscle fibers while motoneuron cell bodies were mostly spared. The findings presented here suggest that a muscle-specific defect as well as inflammation may be the main contributor to disease in CHCHD10 ^{P80L} patients and we propose that future therapeutic strategies that consider muscle pathology and immune responses may result in better clinical outcomes.

Introduction

A direct genetic link between mitochondrial dysfunction and ALS was established with the discovery of rare mutations in the nuclear-encoded mitochondrial protein termed coiled-coil-helix–coiled-coil-helix domain containing 10 (CHCHD10) in 2014 (Bannwarth et al. 2014). CHCHD10 is a protein that localizes mostly in the intermembrane space of the mitochondria (Bannwarth et al. 2014; Huang et al. 2018), where it forms a complex with its paralogue CHCHD2 (Straub et al. 2018; Huang et al. 2018), a protein that has also been linked to neurodegenerative diseases, mainly Parkinson's disease (PD) (Funayama et al. 2015; Shi et al. 2016). The biological function of CHCHD10 and CHCHD2, as well as the cellular consequences resulting from the expression of disease-associated CHCHD10 variants remains to be fully explored. While research efforts are currently underway, CHCHD10, CHCHD2, and the complex they form have been proposed to be involved in mitochondrial respiration (Straub et al. 2018; Mao et al. 2019) and in the response to cellular stressors including increased mitochondrial respiration demand, loss of mitochondrial membrane potential, and starvation (Straub et al. 2018; Lehmer et al. 2018; Huang et al. 2018; Mao et al. 2019; Meng et al. 2017). Both proteins have also been linked to the mitochondrial integrated stress response (mt-ISR) (Straub, Weraarpachai, and Shoubridge 2021; Anderson et al. 2019; Ruan et al. 2022; Liu et al. 2020; Sayles et al. 2022; Petel Légaré et al. 2022).

Though most studies have focused on ALS-related pathological mechanisms of CHCHD10, there are several dozen *CHCHD10* mutations that have been documented to lead to a spectrum of degenerative diseases including not only ALS (Dols-Icardo et al. 2015; Zhang et al. 2015; Perrone et al. 2017; Ronchi, Riboldi, et al. 2015; Lehmer et al. 2018; Zhou et al. 2017), but

also frontotemporal dementia (FTD) (Dols-Icardo et al. 2015; Perrone et al. 2017), FTD-ALS (Bannwarth et al. 2014; Chaussenot et al. 2014), Charcot–Marie–Tooth type 2 disease (CMT2) (Auranen et al. 2015), PD (Perrone et al. 2017), Alzheimer's disease (AD) (Zhang et al. 2015; Xiao et al. 2017), spinal motor neuropathy Jokela type (SMAJ) (Penttilä et al. 2015) and mitochondrial myopathy (Ajroud-Driss et al. 2015; Shammas et al. 2022). Mutations encoding variants CHCHD10 ^{S59L} (Bannwarth et al. 2014; Chaussenot et al. 2014), CHCHD10 ^{R15L} (Müller et al. 2014; Traynor et al. 2014; Kurzwelly et al. 2015) as well as CHCHD10 ^{P80L} (Zhang et al. 2015; Perrone et al. 2017; Ronchi, Comi, et al. 2015; Consortium 2018) have been identified in both familial (fALS) and sporadic ALS (sALS) cases (Consortium 2018). Other variants such as CHCHD10 ^{G66V} have been associated with fALS (Müller et al. 2014), SMAJ (Penttilä et al. 2015), and CMT2 (Auranen et al. 2015), while CHCHD10 ^{G58R} has been associated with mitochondrial myopathy (Ajroud-Driss et al. 2015; Shammas et al. 2022). This suggests that the location and nature of the mutation might have an impact on disease type and severity.

In addition to distinctive CHCHD10 variants being associated with various diseases, both gain- and loss-of-function disease mechanisms have been described. *In vivo* KI studies offer an opportunity to study more accurately specific variants without confounding issues that may arise as a result of transgene over-expression or differing expression patterns resulting from the use of a non-endogenous promoter. To date, all reported *in vivo* CHCHD10 KI models have used mice and most of them focused on the disease-associated CHCHD10 ^{S55L} variant (orthologous to the human CHCHD10 ^{S59L} ALS variant) (Anderson et al. 2019; Sayles et al. 2022; Genin et al. 2019). Heterozygous expression of the CHCHD10 ^{S55L} variant leads to severe phenotype, specifically in the heart, including activation of the mt-ISR, cardiomyopathy, and premature death (Anderson et al. 2019; Sayles et al. 2022; Genin et al. 2019). This contrasts with results

from CHCHD10 knockout (KO) mice which only display a mild phenotype (Burstein et al. 2018; Anderson et al. 2019). It is unknown whether *in vivo* expression of other variants might lead to pathologies resembling ALS or display a disease-like states similar to one of the spectrum of conditions CHCHD10 is associated with. We have previously shown that zebrafish can serve as a model system to study the consequences arising following the loss of either or both Chchd10 and Chchd2 proteins (Petel Légaré et al. 2022) and propose that the fish is also an attractive model to study other disease variants. In this study, we investigated whether endogenous expression of orthologous CHCHD10 ^{P80L} variant could recapitulate the disease in patients. We show that this variant leads to reduced Chchd10 protein levels and to motor deficits that resemble our previously published *chchd10* $^{-/-}$ model at the larval stage (Petel Légaré et al. 2022). Adult zebrafish harbouring the orthologous P80L variant also display an up-regulation of spinal cord pro-inflammatory transcripts and muscle pathology. We propose that this model could be used to further our understanding of diseases associated with CHCHD10.

Methods

Zebrafish housing and maintenance

Adult zebrafish (*Danio rerio*) of the Tübingen long fin (TL) strain were maintained according to standard procedures (Westerfield 1995) at 28.5°C under a 14/10 light/dark cycle in the animal research facility of the Montreal Neurological Institute (MNI) at McGill University (Montréal, Québec, Canada). All experiments were approved by the Animal Care Committee of the MNI and followed the Canadian Council for Animal Care guidelines.

Cas9 mRNA and guide RNAs synthesis

Synthesis of Cas9 mRNA and guide RNA (gRNA) were performed as previously described (Vejnar et al. 2016; Jao, Wente, and Chen 2013). Briefly, a zebrafish codon optimized Cas9 (pT3TS-nCas9n, Addgene plasmid # 46757) was linearized with XbaI overnight and 1 μg of linear template DNA was used for *in vitro* transcription of mRNA using the T3 mMESSAGE mMACHINE® Kit (Invitrogen) followed by phenol-chloroform extraction and precipitation with ethanol. The gRNA target site AAACCAGCACCCACATATCA was identified using CRISPRscan (Moreno-Mateos et al. 2015). To generate a *chchd10* $^{P83L/P83L}$ KI fish line, both gRNA and donor RNA were synthesized using the T7 MEGAscript kit (Invitrogen) and purified by phenol-chloroform extraction and ethanol precipitation. Chchd10 ^{P83L} donor template was as follows: AGCAGTTCAGAGGCACTCAAACCAGCACCAACATATCAGGTCATACCCAA. Underlined is the ALS-associated mutation (T), as well as a silent mutation (A) added to prevent re-cutting by the Cas9 following homologous recombination.

CRISPR mutagenesis and screening of founder lines

Both *chchd10* $^{-/-}$ and *chchd2* $^{-/-}$ models have been described previously (Petel Légaré et al. 2022). Generation of orthologous CHCHD10 $^{P80L/P80L}$ KI line, *chchd10* $^{P83L/P83L}$, was performed as previously described (Armstrong et al. 2016; Petel Légaré et al. 2022). Briefly, Cas9 mRNA, gRNA and donor RNA were co-injected into embryos, using a volume of 1.5 nl, at the one cell stage of development. Founder zebrafish were identified at adult stages by screening their progeny for germline transmission of indels. DNA was extracted from 24 embryos from the offspring of candidate founders aged 24 hours post fertilization (hpf). Polymerase chain reaction (PCR) amplification of the target site was carried out followed by High Resolution Melting (HRM). Sanger sequencing (Genome Québec) was performed on amplicons to determine the exact mutation of each founder line. The following primers were used, resulting in a 55 base pair length PCR product: forward primer: GCAGCAGTTCAGAGGCAC, reverse primer: TATTTTGGGTATGACCTGATATG.

Larval morphology, motor function, survival assays, and neuromuscular junction examination

Free swimming, at 5 dpf, as well as burst swimming touch response, at 2 dpf, were assessed in system water at a maintained temperature of 28.5 ºC ± 3 °C. A survival curve was performed from 6 dpf to 30 dpf and neuromuscular junction integrity was also examined as described (Petel Légaré et al. 2022; Armstrong and Drapeau 2013).

Adult locomotion

Free swim assay was performed on aged-matched adult zebrafish which were placed in a square 30 cm ^{2} arena filled with water at a temperature between 28.5 ± 3 °C. Following a 5-minute habituation period, a 5-minute recording was performed and subsequently analyzed using

motion tracking software (DanioVision, Noldus). Forced swim measures were also performed to determine whether exercise would lead to increased deficiency. To do so, adult fish were placed in a swim tunnel (Loligo® Systems), in which water flow was increased every minute until failure to swim. Maximum sprint swimming speed was used as an output measure using the formula $U_{MAX} = U_f + U_s * (t_f / t_s)$, where U_{MAX} = Maximum sprint swimming speed, U_f = water velocity of last completed step, U_s = increase in water velocity of each step, t_f = length of time the fish swam in its final interval t_s = duration of the interval (Gilbert, Zerulla, and Tierney 2014).

RNA extraction and reverse transcription–qPCR (RT-qPCR)

RNA was extracted from 5 pooled larvae aged 5 dpf using the PicoPure RNA Isolation Kit (Applied Biosystems) and 1 μg was used to create a cDNA library by reverse transcription using the SuperScript VILO cDNA Synthesis Kit (Invitrogen). Quantitative Real time PCR (qPCR) was performed using SYBR Green Supermix (Bio-Rad Laboratories). Relative quantification was performed using the delta-delta Ct method (Livak and Schmittgen 2001) with *actin* and *sdha* transcripts as internal controls.

Western blot

For Western Blot, 5 larvae aged 5 dpf were homogenized and 30 μg at equal concentration was loaded on a 4-16% gradient gel and separated by gel electrophoresis. Separated proteins were transferred to a nitrocellulose membrane and blocked in 5% milk (TSBT) for 1 hour at room temperature (RT). Membranes were incubated overnight with primary antibodies (**Supplementary Table 1**) in blocking buffer at 4 °C followed by respective secondary antibody labelling (Jackson Immuno Research Laboratories, 1:10 000)

for 1 hour at RT. Enhanced chemiluminescence (Clarity™ Western ECL Substrate, Bio-Rad) was used to visualize immunolabelled proteins. Quantification of protein bands was performed using ImageJ. Sdhb were used as mitochondrial loading controls and actin or vinculin were used as cytoplasmic loading controls.

Adult tissue collection

Adult zebrafish were euthanized and dissected into five segments (Benedetti et al. 2016). Following dissection, segments 2 and 3 were fixed in 4% paraformaldehyde (PFA) for 3-4 hours, and then rinsed several times with phosphate-buffered saline (PBS) (137 mM NaCl, 2.7 mM KCl, 10 mM Na_2HPO_4, 2 mM KH_2PO_4). Segments were then incubated in a 30% sucrose solution (Fisher Scientific) at 4 °C overnight. Segments 4 and 5 were mounted in tragacanth gum (Sigma-Aldrich) and snap frozen in 2-methylbutane (Sigma-Aldrich). After incubation in 30 % sucrose, spinal cords were dissected from segments 2 and 3, frozen using dry ice and then stored at -80 °C.

Hematoxylin and eosin (H&E) staining and quantification

Slides containing cryostat muscle cross-sections (10 µm) from segment 5 were warmed to RT for 30 minutes prior to staining. Tissues were fixed with 4% phosphate buffered PFA (FD Neurotechnologies, Inc.) for 10 minutes, then stained with Harris modified hematoxylin solution (Fisher Scientific) for 1 minute and then rinsed with water. Sections were then differentiated in 1% HCl (Fisher Scientific), dissolved in 10 % ethanol (EtOH) (Commercial Alcohols, 10 seconds), washed again in water, dipped 10 times in 80% EtOH, and stained in 0.25% Eosin Y (Fisher Chemical, 10 minutes). Eosin was rinsed off with water (5 minutes) and the tissue was dehydrated through a gradient of EtOH (30% - 50% - 70% - 95% - 95%) and then treated with

Xylene (Fisher Health Care). Following this, tissue was mounted with Xylene-based mounting medium (Fisher Health Care) and allowed to cure overnight. Muscle sections were imaged using a brightfield microscope (Zeiss Axio Imager.M2, 10X objective) and stitched together using Photoshop CS4 (Adobe).

Analysis was performed using ImageJ. Total area of the entire trunk cross-section was first measured for all our models. Both slow and fast twitch individual muscle cell areas were then measured. To do so, a vertical line was drawn across the more laterally located slow twitch fibers, and the area of each fiber touching it was measured. A more central line was drawn for fast twitch muscle fibers and quantified a similar way. Lastly, centrally located nuclei were counted in one quarter of the cross-section of muscle fibers in all our models.

Spinal cord immunolabelling

Six to 12 spinal cord sections of 40 μm were cut from Segment 2 using a Microm (HM500M) cryostat at -17 °C. Sections were then mounted on glass slides coated with 0.5% gelatine (BDH Chemicals) and 0.05% CrK(SO4)2·12H2O (Sigma-Aldrich). Sections were then allowed to return to RT, rinsed with PBS, and permeabilized with PBST for 30 minutes. Sections were then rinsed again with PBS and incubated for 1 hour in block solution (in PBS: 5% normal donkey serum (Abcam), 100mM glycine (Sigma-Aldrich)), and incubated with their respective primary antibody overnight at 4 °C. The following primary antibodies were used: (in PBS + 5% donkey serum: goat polyclonal anti-ChAT (EMD millipore), 1:500; rabbit polyclonal anti-Tdp-43 (MédiMabs), 1:2000) After rinsing with PBS, the secondary antibody was applied (in PBS + 5% donkey serum: AlexaFluor 555 anti-goat IgG (Thermofisher), 1:2000; AlexaFluor 647 anti-rabbit IgG (Thermofisher), 1:2000) at RT for 1 hour. Tissue was mounted with ProLong™ Gold

Antifade Mountant with DAPI (Thermo Fisher, P36931) and images were acquired using a confocal microscope (Leica TCS SP-8, Leica Microsystems), and analyzed with Fiji.

RNA sequencing

Spinal cords were dissected from two 7-month-old adult fish and pooled followed by total RNA extraction using PicoPure RNA Isolation Kit (Applied Biosystems). RNA samples were then sent to Genome Quebec for Illumina Sequencing (NovaSeq 6000 PE100, 25M read). The MUGQIC RNA-Seq pipeline was used to reconstruct RNA raw reads. Illumina sequencing adapters were first removed from the reads, with a threshold of at least 32 base pairs to survive using Trimmomatic (Bolger, Lohse, and Usadel 2014). STAR (Dobin et al. 2013) was then used to align reads to the zebrafish reference genome (Danio_rerio.GRCz11), creating a BAM file. Readsets from the same sample were then merged into one BAM file using Picard (http://broadinstitute.github.io/picard/). Differentially expressed genes were selected using pairwise comparisons with DeSeq (Robinson, McCarthy, and Smyth 2010; McCarthy, Chen, and Smyth 2012): with a cut-off of $p < 0.05$ following multiple testing corrections. Database for Annotation, Visualization and Integrated Discovery (DAVID) (Huang da, Sherman, and Lempicki 2009b, 2009a) was used to explore gene ontology.

Examination of degenerative phenotype

When KI fish started to show a gross degenerative phenotype, they were transferred to an individual tank with one of their non-phenotypic siblings. Weight and free-swimming behavior were examined as previously described, every 3 to 4 days following disease onset. When

possible, fish muscle and spinal cord tissue were collected and H&E and immunolabeling stainings were respectively performed.

Statistical analysis

All statistical analyses and graphs were performed using Prism 7 (GraphPad Software Inc). Shapiro-Wilks tests were used to test for normality. One-way ANOVA and Tuckey's multiple comparison, or unpaired students' t tests were used when data were normally distributed. Kruskal-Wallis test followed by Dunn's post hoc multiple comparisons test or Mann-Whitney test were used when data were not normally distributed. Survival curves were compared using the log rank test, and chi-square tests were used to compare proportions. Significance was assessed at $p < 0.05$.

Results

Creation of a zebrafish *chchd10* $^{P83L/P83L}$ CRISPR KI model

The CHCHD10 ^{P80L} variant, which has been identified in individuals with both sALS (Zhang et al. 2015; Ronchi, Comi, et al. 2015; Consortium 2018) and fALS (Zhang et al. 2015), is conserved in zebrafish. Using the CRISPR/Cas9 mutagenic system, we designed a gRNA that targets exon 2 to create a KI model in which the proline amino acid at position 83, orthologous to position 80 in humans, was replaced by a leucine (**Fig. 1 A**). Injection of both the gRNA and donor RNA was performed in wild type eggs at the one cell stage which were subsequently raised for screening. Screening was performed by high resolution melting (HRM) on PCR amplified genomic DNA and sequencing was performed to confirm the KI mutation (**Fig. 1 C**). A heterozygous adult founder with a fully integrated template was identified by sequencing (**Fig. 1 B**). Homozygous carriers of the P83L variant were used throughout this study as this would allow the examination of the consequences resulting from the variant, without the contribution of wild type Chchd10.

Previous research has noted that different variants lead to altered protein expression levels of CHCHD10 and CHCHD2 (Straub et al. 2018; Lehmer et al. 2018), while other variants, including the CHCHD10 ^{P80L} variant, were reported to have no impact on the level of protein in HeLa cells transfected with HA-tagged CHCHD10 ^{P80L} compared to wild type (Lehmer et al. 2018). To investigate if a similar phenomenon was occurring following the expression of CHCHD10 ^{P83L} in the fish, we examined levels of both Chchd10 and Chchd2. Measurements using whole larvae lysate by immunoblot revealed that at 5 dpf, homozygous expression of the Chchd10 ^{P83L} variant led to a reduction of Chchd10 protein concentrations by around half (46%) that of wild type zebrafish, contrary to previous cell model findings noted above (**Fig. 1 Di, Dii**).

Expression of the Chchd10 ^{P83L} variant also led to a trend of reduced Chchd2, with Chchd2 concentrations in *chchd10* $^{P83L/P83L}$ larvae expressed only at 28% of wild type levels, though this did not reach significance ($p = 0.1$) (**Fig. 1 Di, Diii**). To confirm whether the change occurred post-transcriptionally, we next investigated whether expression levels of either transcript were altered. Neither *chchd10* nor *chchd2* transcript levels were changed compared to wild type larvae suggesting that the reduction of Chchd10 protein concentrations is regulated post-transcriptionally (**Fig. 1 Ei, Eii**).

Zebrafish *chchd10* $^{P83L/P83L}$ larvae display motor deficits, reduced survival, and impaired neuromuscular junctions, independent of the mt-ISR

While no obvious morphological defects were observed in *chchd10* $^{P83L/P83L}$ compared to wild type (**Fig. 2 A**), we investigated touch response behaviour at 2 dpf as motor function is known to be impaired in ALS. Motor deficit was present, as *chchd10* $^{P83L/P83L}$ larvae swam about half of the mean distance swam by wild type larvae at about half the velocity (**Fig. 2 Bi, Bii, Biii**). This deficit was concomitant with altered neuromuscular junction integrity (NMJ), as *chchd10* $^{P83L/P83L}$ larvae presented increased orphaned markers of both pre- and post-synaptic markers (synaptotagmin-2, Syt2, and alpha bungarotoxin, αBtx; respectively) (**Fig. 2 Ci, Cii, Ciii**), replicating previous findings in a *chchd10* $^{-/-}$ larval model (Petel Légaré et al. 2022). We also observed reduced survival in zebrafish expressing the Chchd10 ^{P83L} variant resulting in 46% of *chchd10* $^{P83L/P83L}$ larvae dying before day 30 as compared to 19 % for wild type larvae (**Fig. 2 D**).

As dependence on oxygen increases with development in zebrafish (Mendelsohn, Kassebaum, and Gitlin 2008; Strecker et al. 2011), we next investigated whether our KI model maintained its

motor deficit behaviour at 5 dpf. Individual larvae were placed in a 24-well petri dish and free swim behaviour was recorded for 30 minutes (**Fig. 3 A**). The *chchd10* $^{P83L/P83L}$ larvae swam at a significantly lower mean velocity than wild type larvae, with *chchd10* $^{P83L/P83L}$ swimming at about half the velocity compared to the mutants (**Fig. 3 B**). As we suspected that mitochondrial defects would be more relevant at these later stages, we performed the rest of our larval experiment at 5 dpf. We next investigated whether mitochondrial subunit expression levels were affected by expression of the P83L variant. No significant differences in any of the respiratory chain subunits were observed in *chchd10* $^{P83L/P83L}$ larvae (**Fig 3. Ci, Cii**).

As we previously reported that double *chchd10* $^{-/-}$ & *chchd2* $^{-/-}$, but not single *chchd10* $^{-/-}$ or *chchd2* $^{-/-}$ KO presented mt-ISR activation (Petel Légaré et al. 2022), we investigated whether the upstream transcription factors *CHOP* (*chop*), *ATF4* (*atf4a*, *atf4b*) and *ATF5* (*atf5a*, *atf5b*) (Shpilka and Haynes 2018) were increased in our KI model. No upregulation of these transcriptional activators was observed in *chchd10* $^{P83L/P83L}$ larvae compared to wild type larvae (**Fig. 3 D**).

Muscle pathology is not accompanied by motor defects or loss of motoneurons in *chchd10* $^{P83L/P83L}$ adult zebrafish

We previously investigated the biological consequences following loss of either or both Chchd10 and Chchd2 in zebrafish larvae (Petel Légaré et al. 2022). As ALS is an adult-onset disease, we took advantage of our mutant lines to explore whether adult models had degenerative phenotypes. In addition, we wanted to investigate if there would be different phenotypes between our Chchd10 ^{P83L} and single KO models. To explore this, we first examined adult swimming behaviour in both a free and a forced swim test. Timepoints of 6 months to 1 and a half year

were chosen to determine whether there were any deficits that would worsen with age. Surprisingly, no locomotion deficits compared to wild type, across all genotypes, in swimming behaviour measures were observed at both timepoints, suggesting that the observed larval motor phenotype resolved itself during development, possibly due to compensatory mechanisms in larvae surviving until adulthood (**Fig 4 Ai, Aii, Aiii, Aiv, Bi, Bii, Biii)**. Of note, we did observe a significant difference between *chchd10* $^{-/-}$ and *chchd2* $^{-/-}$ in the forced swim measure at 6 months of age.

While our measures of motor function in adult fish yielded largely no difference in performance, we focused our attention on fish between the age of 6 months to 12 months for the remaining experiments, in the hopes of capturing any relevant changes that would occur pre-symptomatically and could lead to development of symptoms at later stages.

Muscle degeneration has been described as a potential contributing factor in CHCHD10 mice models (Genin et al. 2019; Xiao et al. 2020; Xia et al. 2022). We therefore explored whether mutants showed signs of degeneration in muscle around 1 year of age, even though no gross motor phenotype was observed. Several muscle abnormalities in both our single gene KOs and KI models were observed. First, we investigated whether our models had altered slow- and fast-twitch muscle fiber cross-sectional area, as these fiber types have differing mitochondrial content which may be preferentially impacted in our models. Adult fish, in all our genetic groupings, showed a significant lower mean cross-sectional area of fast-twitch fibers when compared to muscle fibers in wild type fish even though their mitochondrial content is lower (Jackson and Ingham 2013) (**Fig. 5 Ai, Aii**). Slow-twitch mean cross-sectional areas were also found to be significantly reduced in our genetic models compared to wild type (**Fig. 5 Ai, Bii**). In both measures, *chchd2* $^{-/-}$ and *chchd10* $^{P83L/P83L}$ showed the greatest fiber size area reduction compared to wild type. Second, mean trunk

circumference was also reduced compared to wild type among all our groupings except in the *chchd2* $^{-/-}$ model which was not found to be significantly altered ($p = 0.06$) (**Fig. 5 C**). Third, we assessed whether there was an increase in centrally located nuclei, which is observed when muscle cells are regenerating in response to denervation and degeneration. Though no significant difference were found, there was a tendency for more centrally located nuclei in both *chchd2* $^{-/-}$ and *chchd10* $^{P83L/P83L}$ models (**Fig. 5 Di, Dii**). We next explored whether muscle pathology was accompanied by motoneuron loss in our models (**Fig. 5 Ei**). Examination of adult spinal cord cross-sections using confocal immunofluorescent imaging revealed no reduction in motoneuron count (**Fig. 5 Eii**) or area (**Fig. 5 Eiii**) in both our *chchd10* $^{-/-}$ and *chchd2* $^{-/-}$ models as well as in our *chchd10* $^{P83L/P83L}$ model, suggesting that muscle pathology arises independently of motoneuron cell body loss in our models at 1 year of age.

Spinal cord RNA sequencing revealed elevated inflammatory transcriptional profile and mitochondrial dysfunction markers in *chchd10* $^{P83L/P83L}$ fish.

Though predominant muscle degeneration was observed in our models, we decided to perform bulk RNA sequencing on whole spinal cord RNA extracts as this might identify relevant transcriptional changes arising preclinically in motoneurons which are usually highly affected in ALS. While only a small fraction of the cells within the zebrafish spinal cord are motor neurons, bulk RNA approach allowed the examination of a broader status of transcriptional changes arising throughout the spinal cord while still capturing some motor neurons. Using 7-month-old fish, we hoped to capture early contributing factors involved in possible denervation of muscle which could lead to subsequent muscle degeneration which we observed in our fish observed around 1 year of age. We identified several significantly altered transcripts in our genetic groups with *chchd10*

P83L/P83L having the greatest number of altered transcripts (1540 transcripts), followed by *chchd10* $^{-/-}$ (1222 transcripts), and *chchd2* $^{-/-}$ (222 transcripts) compared to wild type zebrafish (**Fig. 6 A, B**). Using this dataset of differentially regulated transcripts and MitoCarta (Calvo, Clauser, and Mootha 2016), we investigated whether mitochondrial pathways were specifically affected in our mutants. Several noteworthy transcripts were significantly different in our models including *slc25a10*, which encodes a mitochondrial dicarboxylate carrier for the Krebs cycle, which was three times higher in all models compared to wild type fish. The transcript *ucp1*, which encodes a protein that dissipates mitochondrial membrane potential, was also significantly increased in both in *chchd10* $^{-/-}$ and *chchd2* $^{-/-}$ spinal cords. Other transcripts of note include *pklr*, encoding the last enzyme in glycolysis, which was upregulated in both *chchd10* $^{-/-}$ and *chchd10* $^{P83L/P83L}$, and *acadsb*, encoding an enzyme involved in the metabolism of fatty acids, which was downregulated in both *chchd2* $^{-/-}$ and *chchd10* $^{P83L/P83L}$. In total, 23 transcripts levels were commonly altered across all our models compared to our wild type group. Gene ontology revealed that a number of those transcripts encode proteins involved in amino acid biosynthesis and metabolism (**Fig 6 A, C**). Commonly downregulated transcripts included *fah* and *tat*, both encoding proteins involved in tyrosine breakdown, while commonly upregulated transcripts include *pycr1a*, which encode a protein that is part of the proline biosynthesis and localizes to the mitochondria, and *trim63a* which encodes a protein that regulates proteasomal degradation following starvation to provide amino acids as an energy source.

We also identified the upregulation of several transcriptional markers that encode proteins involved with immune response activity as well as apoptosis, especially in *chchd10* $^{P83L/P83L}$ spinal cords (**Fig. 6 D**). Inflammatory markers of pathogenic T cells, which have been linked to the chronic inflammation of the central nervous system and neurodegeneration (Fu et

al. 2022), were significantly increased in *chchd10* $^{P83L/P83L}$ spinal cords. These include the transcripts *il17a/f3* and *il17ra1a* associated with Th17, as well as Th1 markers including *il12rb2* and *il12rb2l* transcripts. Furthermore, transcripts involved with regulatory T cell markers were also increased in our *chchd10* $^{P83L/P83L}$ RNA dataset including *il10*, *il10ra*, *il2rb*, *il2rga*, *tgfbr2a* and *tgfb1b*. Numerous transcripts related to apoptosis and autophagy were also altered (**Fig. 6 E**). Finally, we also explored whether the mt-ISR was transcriptionally activated in our adult models, as has been described in other CHCHD10/2 KO models (Anderson et al. 2019; Sayles et al. 2022) but did not find any changes in transcripts involved with mt-ISR (**Fig. 6 F**), replicating our findings in our KO larvae (Petel Légaré et al. 2022), and our KI larvae.

Motor defects are accompanied by muscle pathology, but not loss of motoneurons in symptomatic *chchd10* $^{P83L/P83L}$ zebrafish

Following the lack of motoneuron deficits at 1 year of age in all our genetic groupings, we examined the tissue-specific pathology in symptomatic *chchd10* $^{P83L/P83L}$ adults, as we speculated that motor neuron loss could occur at that stage. Symptomatic fish showed both a lower starting weight and reduced motor behaviour, which is how they were selected as symptomatic. Both measures decreased rapidly over the course of days, while no obvious changes were observed in asymptomatic fish (**Fig. 7 A, B, C**). Mean age of symptom onset was around 709 days, but we did observe symptomatic fish as early as 371 days. Muscle pathology was observed in symptomatic fish, such as reduced fiber size and whole circumference of muscle cross-sections compared to asymptomatic fish (Representative image, **Fig 7 D.**). However, symptomatic fish did not present any obvious reduction in motoneuron count or area (**Figure 7 Ei, Eii, Eiii**). Finally, as our symptomatic phenotype did resemble some aspects of

microsporidiosis (Ramsay et al. 2009), we performed a LUNA stain (Peterson et al. 2011), and though microsprodia were present in our zebrafish colony, we did not find increased prevalence in our symptomatic fish (**Supplementary Methods, Supplementary Figure 1**).

Discussion

This study explored the pathogenic nature of the orthologous ALS- and FTD-associated CHCHD10 ^{P80L} variant using a novel zebrafish CRISPR KI model. We have previously demonstrated that loss of either or both Chchd10 and Chchd2 leads to a detrimental phenotype in larvae (Petel Légaré et al. 2022). Here, we show that homozygous expression of the orthologous Chchd10 ^{P80L} variant leads to reduced Chchd10 levels, as well as a tendency of reduced Chchd2 levels at 5 dpf. Reduced motor function, survival, as well as altered pre-synaptic and post-synaptic markers at the NMJ without activation of the mt-ISR were also observed, partly phenocopying our previous findings in *chchd10* $^{-/-}$ larvae (Petel Légaré et al. 2022). Interestingly, mitochondrial respiratory chain deficits were not present in our KI model as our KO models, suggesting that residual Chchd10 protein might confer some function, thereby partially preserving mitochondrial respiratory chain integrity. These results also suggest that this variant acts in a partial loss-of-function manner at larval stages of development and might lead to a milder pathology when compared to other CHCHD10 variants, and that other, yet to be described mechanisms, could underlie the observed defects (Anderson et al. 2019; Sayles et al. 2022; Genin et al. 2019; Shammas et al. 2022). This may also be underscored in some of the patient data, as this variant has been documented to lead to heterogenous ALS clinical presentations, including a wide range of clinical age of onset (between 27 and 78 years old), and in onset location (limb and bulbar) (Zhang et al. 2015; Ronchi, Riboldi, et al. 2015; Perrone et al. 2017). Of note, this variant was also identified in a 57-year-old control patient (Perrone et al. 2017), suggesting that this variant might be incompletely penetrant.

We next examined the pathological consequences resulting from the loss of either Chchd2 or Chchd10 as well as the homozygous expression of Chchd10 ^{P83L} in adult zebrafish. Though no motor deficits were observed up to 16 months, closer histological examination revealed that muscle pathology was present as early as one year in all examined mutants without loss of spinal cord motoneurons. Muscle pathology has been documented to precede NMJ degeneration in KI mice carrying orthologous CHCHD10 ^{S59L} variant (Genin et al. 2019), while muscle conditional CHCHD10 KO leads to NMJ degeneration (Xiao et al. 2019). This is further supported by patient data, as muscle respiratory chain deficiencies were documented in biopsied skeletal muscle of patients carrying the CHCHD10 ^{P80L} variant (Ronchi, Riboldi, et al. 2015). Though contribution of the NMJ denervation is not ruled out in this study, these previous studies, as well as our own, suggest that muscle pathology is present before symptom onset and might contribute more prominently to the degenerative process in CHCHD10-associated ALS cases. Our study also highlights that Chchd2, though mostly linked to PD, has an important physiological role in adult muscle cell biology.

While evidence from larvae suggests that the main disease mechanism occurs through loss-of-function in Chchd10 ^{P83L} fish, our RNA sequencing data suggests that there could also be a partial gain-of-function disease mechanism. These fish showed the greatest number of significantly altered transcripts compared to wild type, including several markers indicating mitochondrial dysfunction that were not observed in either of our KO models. RNA sequencing results also suggest that the pathological mechanism of this variant may differ from others, such as the CHCHD10 ^{S59L} variant, as we did not observe altered expression levels of transcripts involved with the activation of the mt-ISR. As orthologous CHCHD10 ^{S59L} variant in mice was

reported to sequester and aggregate with CHCHD2 (Anderson et al. 2019), aberrant aggregation of the CHCHD10^{S59L}/CHCHD2 complex might lead to a toxic-gain-of function and activation of the mt-ISR, this variant might also confer disease in a dominant negative manner, which is supported by the fact that double CHCHD10/2 mice partially phenocopy the activation of the mt-ISR (Liu et al. 2020). However, contrary to CHCHD10 ^{S59L}, cellular models indicate that the CHCHD10 ^{P80L} variant loses its association with CHCHD2 (Purandare et al. 2018). This suggests both CHCHD10 ^{P80L} and CHCHD2 might retain some independent partial function and that loss of the complex might play a larger role following the expression of CHCHD10 ^{P80L}, which is not sufficient to trigger the mt-ISR.

Inflammation has been identified as a significant contributor to neurodegeneration in diseases including in ALS (McCauley and Baloh 2019; Liu and Wang 2017; Fu et al. 2022; Correia et al. 2015; Béland et al. 2020) and several inflammatory markers were upregulated in our pre-symptomatic KI model. A shift toward pro-inflammatory markers such as Il-17 has been observed in ALS patients (Rentzos et al. 2010) and increased Th1/Th17 cells compared to anti-inflammatory profile has been linked to ALS severity (Jin et al. 2020). While the exact mechanism remains to be fully explored in CHCHD10-associated ALS, mitochondrial dysfunction could trigger neuroinflammation through the release of mitochondrial DNA (mt-DNA), reactive oxygen species, ATP, or through the activation of the mt-ISR, though the latter was not activated in either our KOs or our KI model (Lin et al. 2022). Interestingly, several markers related to mt-DNA release in the cytoplasm were upregulated in our models (Matsui et al. 2021; Lin et al. 2022) (**Supplementary Figure 2**). Mt-DNA release has been previously observed in ALS models and could lead to activation of the cGAS-STING immune sensor pathway, triggering inflammation (Kumar and Julien 2021; Motwani, Pesiridis, and Fitzgerald

2019; Fryer et al. 2021; Yu et al. 2020). Further studies should focus on the mechanisms leading to inflammation, particularly in the Chchd10 $^{P83L/P83L}$ model, as it might be an important contributor to disease.

Finally, examining our KI model at symptom onset revealed that *chchd10* $^{P83L/P83L}$ zebrafish developed ALS-like symptoms, with loss of motor function and weight. We examined whether reduction of motor function could be due to loss of motoneurons, as our 1-year-old fish did not show any motor deficits. At symptomatic stages, while muscle pathology was still obvious, motoneuron cell bodies were not significantly altered in size or lost. This suggests that muscle pathology might be a predominant contributor to degeneration during the late stages of disease, or that CHCHD10 patients might present with a muscle myopathy rather than ALS.

In conclusion, this study highlights the importance of considering variant-specific disease mechanisms when investigating genes involved with ALS as this is likely to be important for the design and creation of precision therapeutics that act on specific cellular targets. Moreover, we suggest that muscle pathology should be explored when examining CHCHD10-related ALS cases as this tissue may be the primary site of degeneration.

Literature cited

Ajroud-Driss, S., F. Fecto, K. Ajroud, I. Lalani, S. E. Calvo, V. K. Mootha, H. X. Deng, N. Siddique, A. J. Tahmoush, T. D. Heiman-Patterson, and T. Siddique. 2015. 'Mutation in the novel nuclear-encoded mitochondrial protein CHCHD10 in a family with autosomal dominant mitochondrial myopathy', *Neurogenetics*, 16: 1-9.

Anderson, Corey J., Kirsten Bredvik, Suzanne R. Burstein, Crystal Davis, Samantha M. Meadows, Jalia Dash, Laure Case, Teresa A. Milner, Hibiki Kawamata, Aamir Zuberi, Alessandra Piersigilli, Cathleen Lutz, and Giovanni Manfredi. 2019. 'ALS/FTD mutant CHCHD10 mice reveal a tissue-specific toxic gain-of-function and mitochondrial stress response', *Acta Neuropathol*.

Armstrong, Gary A.B., and Pierre Drapeau. 2013. 'Loss and gain of FUS function impair neuromuscular synaptic transmission in a genetic model of ALS', *Human Molecular Genetics*, 22: 4282-92.

Armstrong, Gary Alan Barclay, Meijiang Liao, Zhipeng You, Alexandra Lissouba, Brian Edwin Chen, and Pierre Drapeau. 2016. 'Homology Directed Knockin of Point Mutations in the Zebrafish tardbp and fus Genes in ALS Using the CRISPR/Cas9 System', *PLoS ONE*, 11: e0150188.

Auranen, Mari, Emil Ylikallio, Maria Shcherbii, Anders Paetau, Sari Kiuru-Enari, Jussi P Toppila, and Henna Tyynismaa. 2015. 'CHCHD10 variant p.(Gly66Val) causes axonal Charcot-Marie-Tooth disease', *Neurology Genetics*, 1: e1.

Bannwarth, Sylvie, Samira Ait-El-Mkadem, Annabelle Chaussenot, Emmanuelle C Genin, Sandra Lacas-Gervais, Konstantina Fragaki, Laetitia Berg-Alonso, Yusuke Kageyama, Valérie Serre, and David G Moore. 2014. 'A mitochondrial origin for frontotemporal dementia and amyotrophic lateral sclerosis through CHCHD10 involvement', *Brain*, 137: 2329-45.

Béland, L. C., A. Markovinovic, H. Jakovac, F. De Marchi, E. Bilic, L. Mazzini, J. Kriz, and I. Munitic. 2020. 'Immunity in amyotrophic lateral sclerosis: blurred lines between excessive inflammation and inefficient immune responses', *Brain Commun*, 2: fcaa124.

Benedetti, L., A. Ghilardi, E. Rottoli, M. De Maglie, L. Prosperi, C. Perego, M. Baruscotti, A. Bucchi, L. Del Giacco, and M. Francolini. 2016. 'INaP selective inhibition reverts precocious inter- and motorneurons hyperexcitability in the Sod1-G93R zebrafish ALS model', *Sci Rep*, 6: 24515.

Bolger, Anthony M, Marc Lohse, and Bjoern Usadel. 2014. 'Trimmomatic: a flexible trimmer for Illumina sequence data', *Bioinformatics*, 30: 2114-20.

Burstein, S. R., F. Valsecchi, H. Kawamata, M. Bourens, R. Zeng, A. Zuberi, T. A. Milner, S. M. Cloonan, C. Lutz, A. Barrientos, and G. Manfredi. 2018. 'In vitro and in vivo studies of the ALS-FTLD protein CHCHD10 reveal novel mitochondrial topology and protein interactions', *Human Molecular Genetics*, 27: 160-77.

Calvo, S. E., K. R. Clauser, and V. K. Mootha. 2016. 'MitoCarta2.0: an updated inventory of mammalian mitochondrial proteins', *Nucleic Acids Res*, 44: D1251-7.

Chaussenot, Annabelle, Isabelle Le Ber, Samira Ait-El-Mkadem, Agnès Camuzat, Anne de Septenville, Sylvie Bannwarth, Emmanuelle C. Genin, Valérie Serre, Gaëlle Augé, Alexis Brice, Jean Pouget, and Véronique Paquis-Flucklinger. 2014. 'Screening of CHCHD10 in a French cohort confirms the involvement of this gene in frontotemporal

dementia with amyotrophic lateral sclerosis patients', *Neurobiology of Aging*, 35: 2884.e1-84.e4.
Consortium, Project MinE ALS Sequencing. 2018. 'CHCHD10 variants in amyotrophic lateral sclerosis: Where is the evidence?', 84: 110-16.
Correia, Ana Sofia, Priyanka Patel, Kallol Dutta, and Jean-Pierre Julien. 2015. 'Inflammation Induces TDP-43 Mislocalization and Aggregation', *PLoS ONE*, 10: e0140248.
Dobin, Alexander, Carrie A Davis, Felix Schlesinger, Jorg Drenkow, Chris Zaleski, Sonali Jha, Philippe Batut, Mark Chaisson, and Thomas R Gingeras. 2013. 'STAR: ultrafast universal RNA-seq aligner', *Bioinformatics*, 29: 15-21.
Dols-Icardo, Oriol, Irene Nebot, Ana Gorostidi, Sara Ortega-Cubero, Isabel Hernández, Ricard Rojas-García, Alberto García-Redondo, Monica Povedano, Albert Lladó, Victoria Álvarez, Pascual Sánchez-Juan, Julio Pardo, Ivonne Jericó, Juan Vázquez-Costa, Teresa Sevilla, Fernando Cardona, Begoña Indakoechea, Fermín Moreno, Roberto Fernández-Torrón, Laia Muñoz-Llahuna, Sonia Moreno-Grau, Maiteé Rosende-Roca, Álvaro Vela, José Luís Muñoz-Blanco, Onofre Combarros, Eliecer Coto, Daniel Alcolea, Juan Fortea, Alberto Lleó, Raquel Sánchez-Valle, Jesús Esteban-Pérez, Agustín Ruiz, Pau Pastor, Adolfo López De Munain, Jordi Pérez-Tur, Jordi Clarimón, and on behalf of the Dementia Genetics Spanish Consortium. 2015. 'Analysis of the CHCHD10 gene in patients with frontotemporal dementia and amyotrophic lateral sclerosis from Spain', *Brain*, 138: e400-e00.
Fryer, Amelia L., Amar Abdullah, Juliet M. Taylor, and Peter J. Crack. 2021. 'The Complexity of the cGAS-STING Pathway in CNS Pathologies', *Frontiers in Neuroscience*, 15.
Fu, Jiajia, Yan Huang, Ting Bao, Chengcheng Liu, Xi Liu, and Xueping Chen. 2022. 'The role of Th17 cells/IL-17A in AD, PD, ALS and the strategic therapy targeting on IL-17A', *Journal of Neuroinflammation*, 19: 98.
Funayama, M., K. Ohe, T. Amo, N. Furuya, J. Yamaguchi, S. Saiki, Y. Li, K. Ogaki, M. Ando, H. Yoshino, H. Tomiyama, K. Nishioka, K. Hasegawa, H. Saiki, W. Satake, K. Mogushi, R. Sasaki, Y. Kokubo, S. Kuzuhara, T. Toda, Y. Mizuno, Y. Uchiyama, K. Ohno, and N. Hattori. 2015. 'CHCHD2 mutations in autosomal dominant late-onset Parkinson's disease: a genome-wide linkage and sequencing study', *Lancet Neurol*, 14: 274-82.
Genin, Emmanuelle C., Blandine Madji Hounoum, Sylvie Bannwarth, Konstantina Fragaki, Sandra Lacas-Gervais, Alessandra Mauri-Crouzet, Françoise Lespinasse, Julien Neveu, Baptiste Ropert, Gaelle Augé, Charlotte Cochaud, Cynthia Lefebvre-Omar, Stéphanie Bigou, Aude Chiot, Fanny Mochel, Séverine Boillée, Christian S. Lobsiger, Delphine Bohl, Jean-Ehrland Ricci, and Véronique Paquis-Flucklinger. 2019. 'Mitochondrial defect in muscle precedes neuromuscular junction degeneration and motor neuron death in CHCHD10S59L/+ mouse', *Acta Neuropathol*.
Gilbert, Matthew J. H., Tanja C. Zerulla, and Keith B. Tierney. 2014. 'Zebrafish (Danio rerio) as a model for the study of aging and exercise: Physical ability and trainability decrease with age', *Experimental Gerontology*, 50: 106-13.
Huang da, W., B. T. Sherman, and R. A. Lempicki. 2009a. 'Bioinformatics enrichment tools: paths toward the comprehensive functional analysis of large gene lists', *Nucleic Acids Res*, 37: 1-13.
———. 2009b. 'Systematic and integrative analysis of large gene lists using DAVID bioinformatics resources', *Nat Protoc*, 4: 44-57.

Huang, Xiaoping, Beverly P Wu, Diana Nguyen, Yi-Ting Liu, Melika Marani, Jürgen Hench, Paule Bénit, Vera Kozjak-Pavlovic, Pierre Rustin, and Stephan Frank. 2018. 'CHCHD2 accumulates in distressed mitochondria and facilitates oligomerization of CHCHD10Human Molecular Genetics, 2018, Vol. 00, No. 0Human Molecular Genetics, 2018, Vol. 00, No. 0', *Human Molecular Genetics*.

Jackson, Harriet E., and Philip W. Ingham. 2013. 'Control of muscle fibre-type diversity during embryonic development: The zebrafish paradigm', *Mechanisms of Development*, 130: 447-57.

Jao, Li-En, Susan R. Wente, and Wenbiao Chen. 2013. 'Efficient multiplex biallelic zebrafish genome editing using a CRISPR nuclease system', *Proceedings of the National Academy of Sciences*, 110: 13904-09.

Jin, M., R. Günther, K. Akgün, A. Hermann, and T. Ziemssen. 2020. 'Peripheral proinflammatory Th1/Th17 immune cell shift is linked to disease severity in amyotrophic lateral sclerosis', *Sci Rep*, 10: 5941.

Kumar, Sunny, and Jean-Pierre Julien. 2021. 'TDP-43 triggers immune response via mitochondrial DNA release', *Cell Research*, 31: 379-80.

Kurzwelly, Delia, Michael T. Heneka, Saskia Biskup, and Stefanie Krüger. 2015. 'A distinct clinical phenotype in a German kindred with motor neuron disease carrying a CHCHD10 mutation', *Brain*, 138: e376-e76.

Lehmer, Carina, Martin H Schludi, Linnea Ransom, Johanna Greiling, Michaela Junghänel, Nicole Exner, Henrick Riemenschneider, Julie van der Zee, Christine Van Broeckhoven, and Patrick Weydt. 2018. 'A novel CHCHD10 mutation implicates a Mia40-dependent mitochondrial import deficit in ALS', *EMBO Molecular Medicine*, 10: e8558.

Lin, Miao-miao, Na Liu, Zheng-hong Qin, and Yan Wang. 2022. 'Mitochondrial-derived damage-associated molecular patterns amplify neuroinflammation in neurodegenerative diseases', *Acta Pharmacologica Sinica*.

Liu, J., and F. Wang. 2017. 'Role of Neuroinflammation in Amyotrophic Lateral Sclerosis: Cellular Mechanisms and Therapeutic Implications', *Front Immunol*, 8: 1005.

Liu, Y. T., X. Huang, D. Nguyen, M. K. Shammas, B. P. Wu, E. Dombi, D. A. Springer, J. Poulton, S. Sekine, and D. P. Narendra. 2020. 'Loss of CHCHD2 and CHCHD10 activates OMA1 peptidase to disrupt mitochondrial cristae phenocopying patient mutations', *Hum Mol Genet*, 29: 1547-67.

Livak, Kenneth J., and Thomas D. Schmittgen. 2001. 'Analysis of Relative Gene Expression Data Using Real-Time Quantitative PCR and the $2^{-\Delta\Delta CT}$ Method', *Methods*, 25: 402-08.

Mao, Chengyuan, Herui Wang, Haiyang Luo, Shuyu Zhang, Huisha Xu, Shuo Zhang, Jared Rosenblum, Zhilei Wang, Qi Zhang, Mibo Tang, Matthew J. Shepard, Xiang Wang, Yaohe Wang, Zhengping Zhuang, Changhe Shi, and Yuming Xu. 2019. 'CHCHD10 is involved in the development of Parkinson's disease caused by CHCHD2 loss-of-function mutation p.T61I', *Neurobiology of Aging*, 75: 38-41.

Matsui, H., J. Ito, N. Matsui, T. Uechi, O. Onodera, and A. Kakita. 2021. 'Cytosolic dsDNA of mitochondrial origin induces cytotoxicity and neurodegeneration in cellular and zebrafish models of Parkinson's disease', *Nat Commun*, 12: 3101.

McCarthy, Davis J, Yunshun Chen, and Gordon K Smyth. 2012. 'Differential expression analysis of multifactor RNA-Seq experiments with respect to biological variation', *Nucleic acids research*, 40: 4288-97.

McCauley, Madelyn E., and Robert H. Baloh. 2019. 'Inflammation in ALS/FTD pathogenesis', *Acta Neuropathol*, 137: 715-30.
Mendelsohn, Bryce A., Bethany L. Kassebaum, and Jonathan D. Gitlin. 2008. 'The zebrafish embryo as a dynamic model of anoxia tolerance', *Developmental dynamics : an official publication of the American Association of Anatomists*, 237: 1780-88.
Meng, Hongrui, Chikara Yamashita, Kahori Shiba-Fukushima, Tsuyoshi Inoshita, Manabu Funayama, Shigeto Sato, Tomohisa Hatta, Tohru Natsume, Masataka Umitsu, Junichi Takagi, Yuzuru Imai, and Nobutaka Hattori. 2017. 'Loss of Parkinson's disease-associated protein CHCHD2 affects mitochondrial crista structure and destabilizes cytochrome c', *Nature Communications*, 8: 15500-00.
Moreno-Mateos, Miguel A., Charles E. Vejnar, Jean-Denis Beaudoin, Juan P. Fernandez, Emily K. Mis, Mustafa K. Khokha, and Antonio J. Giraldez. 2015. 'CRISPRscan: designing highly efficient sgRNAs for CRISPR-Cas9 targeting in vivo', *Nature Methods*, 12: 982-88.
Motwani, M., S. Pesiridis, and K. A. Fitzgerald. 2019. 'DNA sensing by the cGAS-STING pathway in health and disease', *Nat Rev Genet*, 20: 657-74.
Müller, Kathrin, Peter M. Andersen, Annemarie Hübers, Nicolai Marroquin, Alexander E. Volk, Karin M. Danzer, Thomas Meitinger, Albert C. Ludolph, Tim M. Strom, and Jochen H. Weishaupt. 2014. 'Two novel mutations in conserved codons indicate that CHCHD10 is a gene associated with motor neuron disease', *Brain*, 137: e309-e09.
Penttilä, S., M. Jokela, H. Bouquin, A. M. Saukkonen, J. Toivanen, and B. Udd. 2015. 'Late onset spinal motor neuronopathy is caused by mutation in CHCHD10', *Ann Neurol*, 77: 163-72.
Perrone, Federica, Hung Phuoc Nguyen, Sara Van Mossevelde, Matthieu Moisse, Anne Sieben, Patrick Santens, Jan De Bleecker, Mathieu Vandenbulcke, Sebastiaan Engelborghs, Jonathan Baets, Patrick Cras, Rik Vandenberghe, Peter De Jonghe, Peter P. De Deyn, Jean-Jacques Martin, Philip Van Damme, Christine Van Broeckhoven, and Julie van der Zee. 2017. 'Investigating the role of ALS genes CHCHD10 and TUBA4A in Belgian FTD-ALS spectrum patients', *Neurobiology of Aging*, 51: 177.e9-77.e16.
Petel Légaré, Virginie , Christian J. Rampal, Mari J. Aaltonen, Alexandre Janer, Lorne Zinman, Eric A. Shoubridge, and Gary A.B. Armstrong. 2022. 'Loss of mitochondrial Chchd10 or Chchd2 in zebrafish leads to an ALS-like phenotype and Complex I deficiency independent of the mt-ISR', *bioRxiv*: 2022.05.02.488746.
Peterson, T. S., J. M. Spitsbergen, S. W. Feist, and M. L. Kent. 2011. 'Luna stain, an improved selective stain for detection of microsporidian spores in histologic sections', *Dis Aquat Organ*, 95: 175-80.
Purandare, Neeraja, Mallika Somayajulu, Maik Hüttemann, Lawrence I Grossman, and Siddhesh Aras. 2018. 'The cellular stress proteins CHCHD10 and MNRR1 (CHCHD2): Partners in mitochondrial and nuclear function and dysfunction', *Journal of Biological Chemistry*, 293: 6517-29.
Ramsay, J. M., V. Watral, C. B. Schreck, and M. L. Kent. 2009. 'Pseudoloma neurophilia infections in zebrafish Danio rerio: effects of stress on survival, growth, and reproduction', *Dis Aquat Organ*, 88: 69-84.
Rentzos, M, A Rombos, C Nikolaou, M Zoga, V Zouvelou, A Dimitrakopoulos, T Alexakis, A Tsoutsou, A Samakovli, and M Michalopoulou. 2010. 'Interleukin-17 and interleukin-23

are elevated in serum and cerebrospinal fluid of patients with ALS: a reflection of Th17 cells activation?', *Acta Neurologica Scandinavica*, 122: 425-29.

Robinson, Mark D, Davis J McCarthy, and Gordon K Smyth. 2010. 'edgeR: a Bioconductor package for differential expression analysis of digital gene expression data', *Bioinformatics*, 26: 139-40.

Ronchi, Dario, Giacomo Pietro Comi, Giulietta Riboldi, Nereo Bresolin, Roberto Del Bo, Stefania Corti, Nicola Ticozzi, Vincenzo Silani, Marina Scarlato, and Daniela Galimberti. 2015. 'CHCHD10 mutations in Italian patients with sporadic amyotrophic lateral sclerosis', *Brain*, 138: e372-e72.

Ronchi, Dario, Giulietta Riboldi, Roberto Del Bo, Nicola Ticozzi, Marina Scarlato, Daniela Galimberti, Stefania Corti, Vincenzo Silani, Nereo Bresolin, and Giacomo Pietro Comi. 2015. 'CHCHD10 mutations in Italian patients with sporadic amyotrophic lateral sclerosis', *Brain*, 138: e372-e72.

Ruan, Yu, Jiaqiao Hu, Yaping Che, Yanyan Liu, Zhenhuan Luo, Jin Cheng, Qi Han, He He, and Qinghua Zhou. 2022. 'CHCHD2 and CHCHD10 regulate mitochondrial dynamics and integrated stress response', *Cell Death & Disease*, 13: 156.

Sayles, Nicole M., Nneka Southwell, Kevin McAvoy, Kihwan Kim, Alba Pesini, Corey J. Anderson, Catarina Quinzii, Suzanne Cloonan, Hibiki Kawamata, and Giovanni Manfredi. 2022. 'Mutant CHCHD10 causes an extensive metabolic rewiring that precedes OXPHOS dysfunction in a murine model of mitochondrial cardiomyopathy', *Cell Reports*, 38: 110475.

Shammas, M. K., X. Huang, B. P. Wu, E. Fessler, I. Y. Song, N. P. Randolph, Y. Li, C. K. Bleck, D. A. Springer, C. Fratter, I. A. Barbosa, A. F. Powers, P. M. Quirós, C. Lopez-Otin, L. T. Jae, J. Poulton, and D. P. Narendra. 2022. 'OMA1 mediates local and global stress responses against protein misfolding in CHCHD10 mitochondrial myopathy', *J Clin Invest*, 132.

Shi, Chang-he, Cheng-yuan Mao, Shu-yu Zhang, Jing Yang, Bo Song, Ping Wu, Chuan-tao Zuo, Yu-tao Liu, Yan Ji, Zhi-hua Yang, Jun Wu, Zheng-ping Zhuang, and Yu-ming Xu. 2016. 'CHCHD2 gene mutations in familial and sporadic Parkinson's disease', *Neurobiology of Aging*, 38: 217.e9-17.e13.

Shpilka, Tomer, and Cole M. Haynes. 2018. 'The mitochondrial UPR: mechanisms, physiological functions and implications in ageing', *Nature Reviews Molecular Cell Biology*, 19: 109-20.

Straub, I. R., W. Weraarpachai, and E. A. Shoubridge. 2021. 'Multi-OMICS study of a CHCHD10 variant causing ALS demonstrates metabolic rewiring and activation of endoplasmic reticulum and mitochondrial unfolded protein responses', *Hum Mol Genet*, 30: 687-705.

Straub, Isabella R., Alexandre Janer, Woranontee Weraarpachai, Lorne Zinman, Janice Robertson, Ekaterina Rogaeva, and Eric A. Shoubridge. 2018. 'Loss of CHCHD10–CHCHD2 complexes required for respiration underlies the pathogenicity of a CHCHD10 mutation in ALS', *Human Molecular Genetics*, 27: 178-89.

Strecker, Ruben, Thomas-Benjamin Seiler, Henner Hollert, and Thomas Braunbeck. 2011. 'Oxygen requirements of zebrafish (Danio rerio) embryos in embryo toxicity tests with environmental samples', *Comparative Biochemistry and Physiology Part C: Toxicology & Pharmacology*, 153: 318-27.

Traynor, Bryan J., Janel O. Johnson, Shannon M. Glynn, J. Raphael Gibbs, Mike A. Nalls, Mario Sabatelli, Gabriella Restagno, Vivian E. Drory, Adriano Chiò, and Ekaterina Rogaeva. 2014. 'Mutations in the CHCHD10 gene are a common cause of familial amyotrophic lateral sclerosis', *Brain*, 137: e311-e11.

Vejnar, Charles E., Miguel A. Moreno-Mateos, Daniel Cifuentes, Ariel A. Bazzini, and Antonio J. Giraldez. 2016. 'Optimized CRISPR–Cas9 System for Genome Editing in Zebrafish', *Cold Spring Harbor Protocols*, 2016: pdb.prot086850.

Westerfield, Monte. 1995. *The Zebrafish Book. A Guide for the Laboratory Use of Zebrafish (Danio rerio)* (University of Oregon Press: Eugene, OR).

Xia, Wei, Jiamin Qiu, Ying Peng, Madigan M. Snyder, Lijie Gu, Kuilong Huang, Nanjian Luo, Feng Yue, and Shihuan Kuang. 2022. 'Chchd10 is dispensable for myogenesis but critical for adipose browning', *Cell Regeneration*, 11: 14.

Xiao, Tingting, Bin Jiao, Weiwei Zhang, Chuzheng Pan, Jingya Wei, Xiaoyan Liu, Yafang Zhou, Lin Zhou, Beisha Tang, and Lu Shen. 2017. 'Identification of CHCHD10 Mutation in Chinese Patients with Alzheimer Disease', *Molecular Neurobiology*, 54: 5243-47.

Xiao, Y., J. Zhang, X. Shu, L. Bai, W. Xu, A. Wang, A. Chen, W. Y. Tu, J. Wang, K. Zhang, B. Luo, and C. Shen. 2020. 'Loss of mitochondrial protein CHCHD10 in skeletal muscle causes neuromuscular junction impairment', *Hum Mol Genet*, 29: 1784-96.

Xiao, Yatao, Jianmin Zhang, Xiaoqiu Shu, Lei Bai, Wentao Xu, Ailian Wang, Aizhong Chen, Wen-Yo Tu, Jianwen Wang, Kejing Zhang, Benyan Luo, and Chengyong Shen. 2019. 'Loss of mitochondrial protein CHCHD10 in skeletal muscle causes neuromuscular junction impairment', *Human Molecular Genetics*, 29: 1784-96.

Yu, C. H., S. Davidson, C. R. Harapas, J. B. Hilton, M. J. Mlodzianoski, P. Laohamonthonkul, C. Louis, R. R. J. Low, J. Moecking, D. De Nardo, K. R. Balka, D. J. Calleja, F. Moghaddas, E. Ni, C. A. McLean, A. L. Samson, S. Tyebji, C. J. Tonkin, C. R. Bye, B. J. Turner, G. Pepin, M. P. Gantier, K. L. Rogers, K. McArthur, P. J. Crouch, and S. L. Masters. 2020. 'TDP-43 Triggers Mitochondrial DNA Release via mPTP to Activate cGAS/STING in ALS', *Cell*, 183: 636-49.e18.

Zhang, Ming, Zhengrui Xi, Lorne Zinman, Amalia C. Bruni, Raffaele G. Maletta, Sabrina A. M. Curcio, Innocenzo Rainero, Elisa Rubino, Lorenzo Pinessi, Benedetta Nacmias, Sandro Sorbi, Daniela Galimberti, Anthony E. Lang, Susan Fox, Ezequiel I. Surace, Mahdi Ghani, Jing Guo, Christine Sato, Danielle Moreno, Yan Liang, Julia Keith, Bryan J. Traynor, Peter St George-Hyslop, and Ekaterina Rogaeva. 2015. 'Mutation analysis of CHCHD10 in different neurodegenerative diseases', *Brain*, 138: e380-e80.

Zhou, Q., Y. Chen, Q. Wei, B. Cao, Y. Wu, B. Zhao, R. Ou, J. Yang, X. Chen, S. Hadano, and H. F. Shang. 2017. 'Mutation Screening of the CHCHD10 Gene in Chinese Patients with Amyotrophic Lateral Sclerosis', *Mol Neurobiol*, 54: 3189-94.

Figures

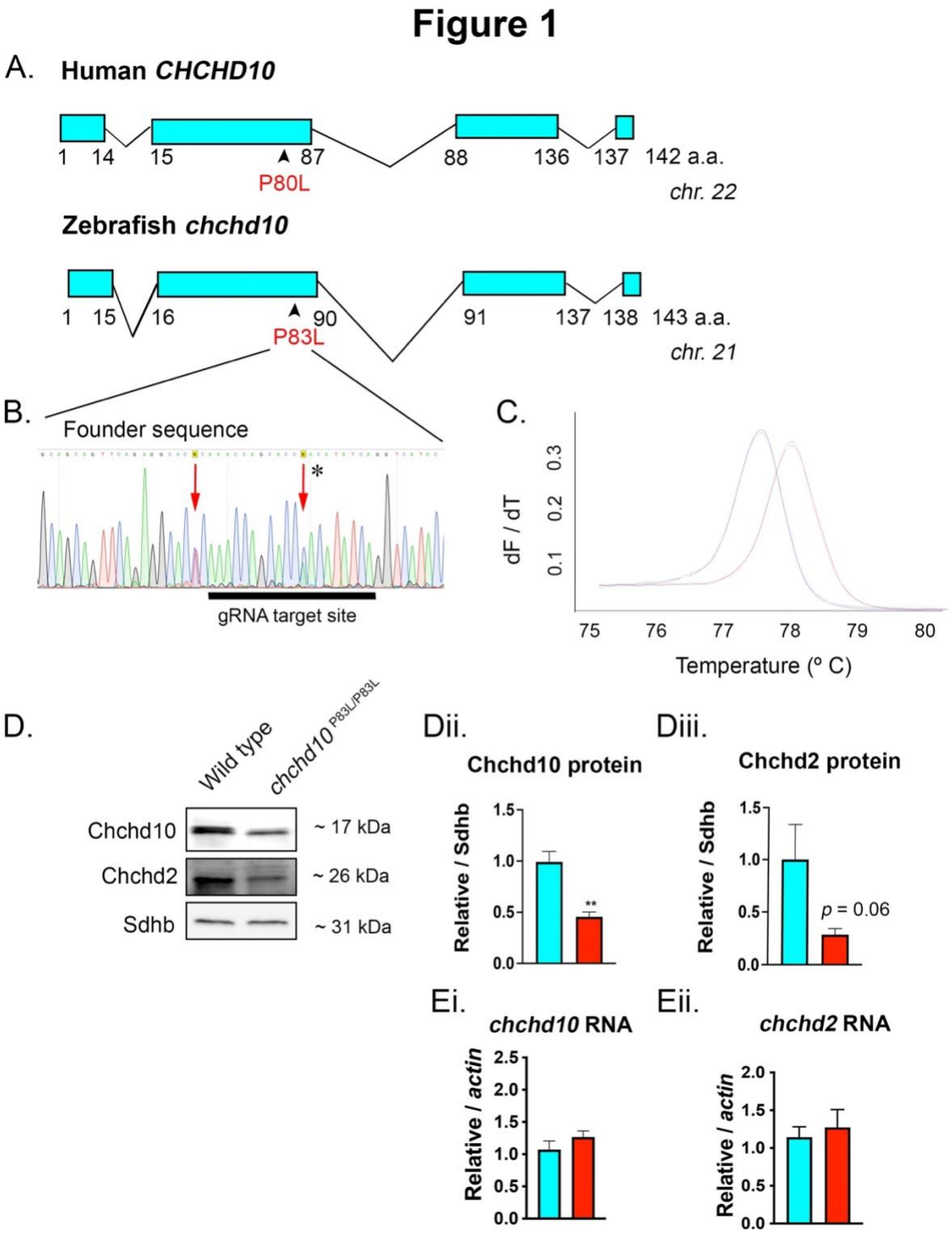
Figure 1
A.
Human CHCHD10
1 14 15 87 88 136 137 142 a.a.
P80L
chr. 22
Zebrafish chchd10
1 15 16 90 91 137 138 143 a.a.
P83L
chr. 21
B.
Founder sequence
gRNA target site
C.
dF / dT
0.1 0.2 0.3
75 76 77 78 79 80
Temperature (° C)
D.
Wild type
chchd10 P83L/P83L
Chchd10
Chchd2
Sdhb
~ 17 kDa
~ 26 kDa
~ 31 kDa
Dii.
Chchd10 protein
Relative / Sdhb
Diii.
Chchd2 protein
Relative / Sdhb
p = 0.06
Ei.
chchd10 RNA
Relative / actin
Eii.
chchd2 RNA
Relative / actin

Figure 3.1 Generation of the *chchd10* $^{P83L/P83L}$ zebrafish lines**.**

A, Human *CHCHD10* and zebrafish *chchd10* gene structure depicting the ALS-associated P80L variant location and orthologous P83L variant. **B**, Electropherogram of the heterozygous founder *chchd10* ^{P83L} sequence along with gRNA target sequence. The asterisk represent a silent mutation included in our donor template. **C**, Example HRM melting curve derivatives used for genotyping with the blue lines denoting homozygous *chchd10* $^{P83L/P83L}$ and red lines representing wild type DNA amplicons. Peaks melting points are as follows: 78.5 °C for wild type DNA and 77.25 °C for *chchd10* $^{P83L/P83L}$. **Di**, Representative immunoblot of Chchd10 and Chchd2 in whole larval lysate from both wild type and *chchd10* $^{P83L/P83L}$ models. Sdhb was used as a loading control and for quantification (**Dii**). Chchd10 protein concentrations were significantly reduced in our *chchd10* $^{P83L/P83L}$ model compared to wild type (t (4) = 4.73, $p < 0.01$) (**Diii**). A tendency for reduced Chchd2 protein concentrations was also observed in our mutant model, though this was not found to be significant (t (4) = 2.094, $p = 0.10$) (n=3 per genotype, 5 dpf data represent mean ± S.E.M.). **Fi**, **Fii**, RT-qPCR of the *chchd10* and *chchd2* transcript in *chchd10* $^{P83L/P83L}$ and wild type larvae. No difference was observed in either *chchd10* (t (4) = 1.182, $p = 0.30$) or *chchd2* (t (4) = 0.48, $p = 0.66$) transcript expression levels (n=3 per genotype, 5 dpf data represent mean ± S.E.M.).

Figure 2

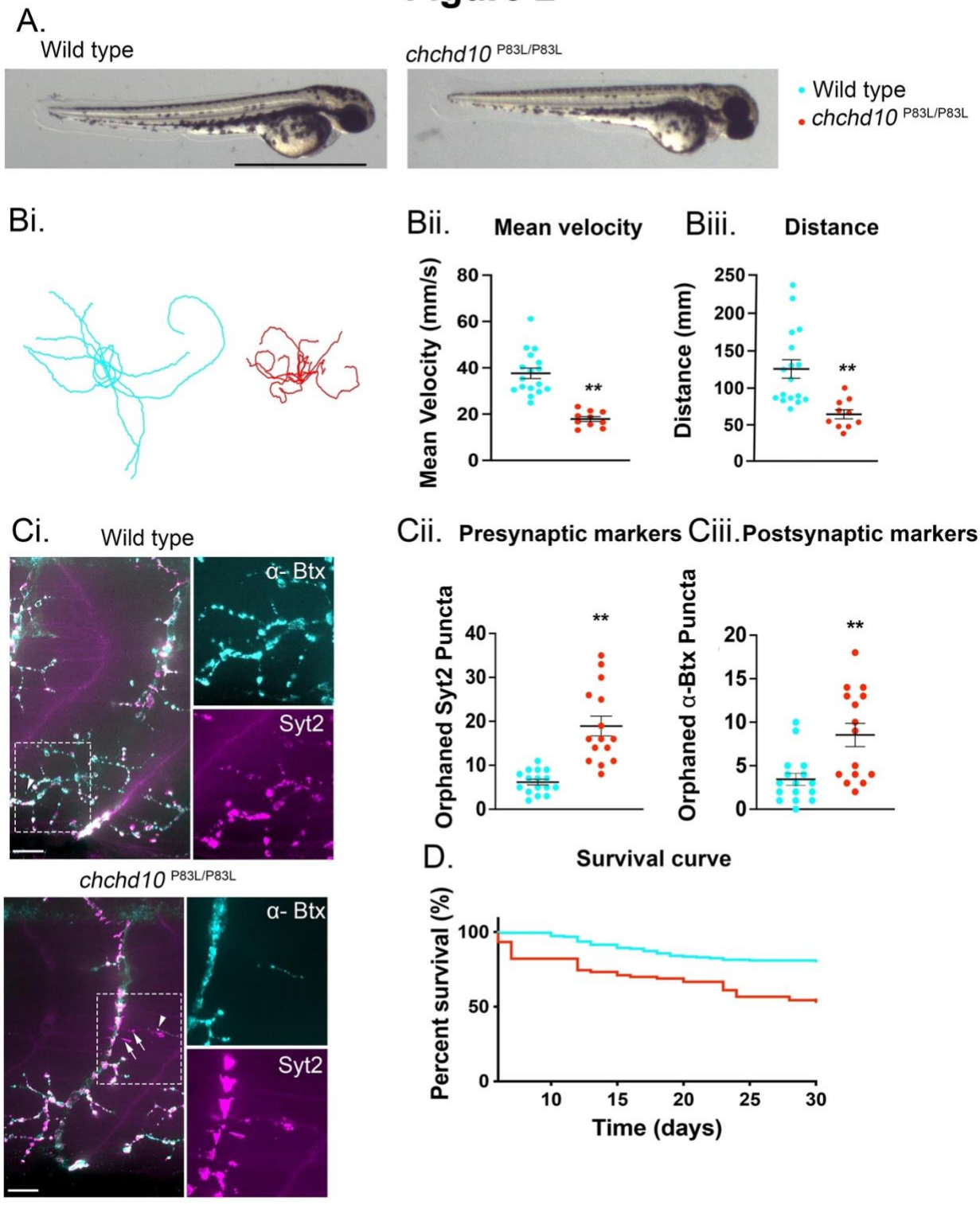
A.
Wild type
chchd10 P83L/P83L
Wild type
chchd10 P83L/P83L
Bi.
Bii. Mean velocity
Biii. Distance
Mean Velocity (mm/s)
Distance (mm)
**
**
Ci. Wild type
α- Btx
Syt2
chchd10 P83L/P83L
α- Btx
Syt2
Cii. Presynaptic markers
Ciii. Postsynaptic markers
Orphaned Syt2 Puncta
Orphaned α-Btx Puncta
**
**
D.
Survival curve
Percent survival (%)
Time (days)

Figure 3.2 Homozygous *chchd10* ^{P83L} larvae display reduced touch response behaviour, reduced NMJ pre- and post-synaptic marker colocalization and lower survival.

A, Representative images of 56 hpf larvae. Scale bar represent 1 mm. **Bi**, Ten representative touch-evoked motor response traces superimposed on each other from *chchd10* $^{P83L/P83L}$ and wild type larvae aged 2 dpf. **Bii**, *chchd10* $^{P83L/P83L}$ displayed significantly shorter mean distances compared to wild type larvae (U = 13, Mann-Whitney U-test, p <0.01). Mean swim distance and sample sizes are as follows: wild type (mean = 126.00 mm, n = 17), *chchd10* $^{P83L/P83L}$ (mean= 63.66 mm, n= 10). **Biii**, *Chchd10* $^{P83L/P83L}$ swam at a significantly lower mean velocity compared to wild type fish (t (25) = 6.36, p < 0.01). Mean swim velocity and sample sizes are as follows: wild type (mean = 37.62 mm/s, n = 17), *chchd10* $^{P83L/P83L}$ (mean= 17.90 mm/s, n= 10). **Ci**, Representative confocal images of ventral trunk NMJs in larvae aged 2 dpf. Markers are Syt2 (pre-synaptic, cyan) and αBtx (post-synaptic, magenta). Arrowheads and arrows represent orphaned αBtx and Syt2 puncta, respectively. Scale bars represent 100 µm. **Cii**, Quantification of orphaned pre-synaptic puncta. *Chchd10* $^{P83L/P83L}$ larvae have significantly more orphaned pre-synaptic terminals devoid of post-synaptic labelling when compared to wild type NMJs (t (29) =5.594, p < 0.01). Data are represented as mean ± S.E.M. **Ciii**, Quantification of orphaned post-synaptic (αBtx) puncta. C*hchd10* $^{P83L/P83L}$ display increased orphaned AChR clusters lacking pre-synaptic Syt2 puncta when compared to wild type NMJs (U = 45.50, p < 0.01). Significance is represented by a single asterisk (p < 0.05) or double asterisk (p < 0.01). Sample sizes are as follows; wild type n = 16; *chchd10* $^{P83L/P83L}$ n =15. **D**, C*hchd10* $^{P83L/P83L}$ larvae displayed reduced survival when compared to wild type zebrafish larvae (Log-rank test, Mantel-Cox : χ^2=24.36, p < 0.01).

Figure 3

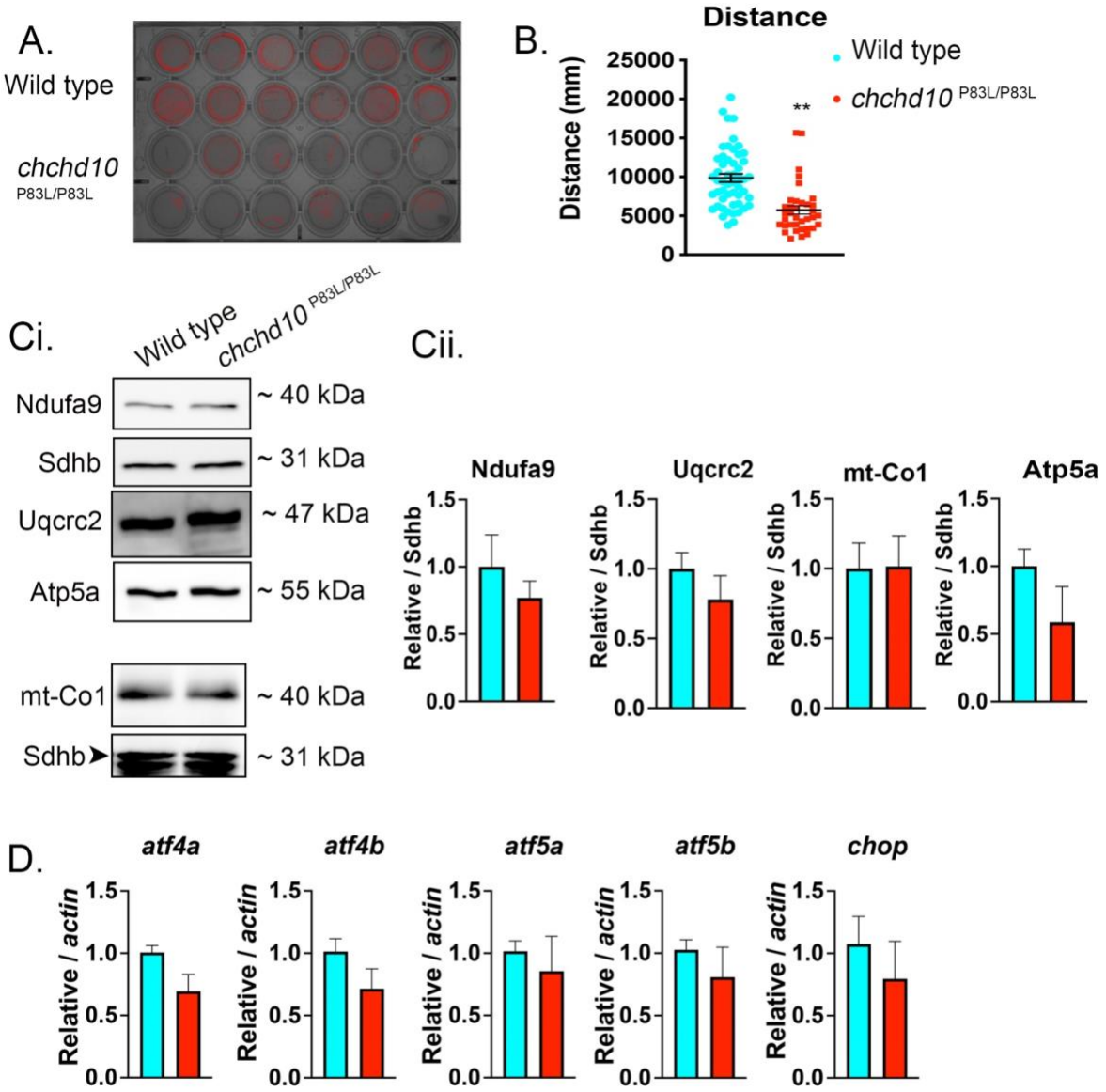
A.
Wild type
chchd10
P83L/P83L
B.
Distance
Wild type
chchd10 P83L/P83L
Distance (mm)
25000
20000
15000
10000
5000
0
**
Ci.
Wild type
chchd10 P83L/P83L
Ndufa9
~ 40 kDa
Sdhb
~ 31 kDa
Uqcrc2
~ 47 kDa
Atp5a
~ 55 kDa
mt-Co1
~ 40 kDa
Sdhb
~ 31 kDa
Cii.
Ndufa9
Uqcrc2
mt-Co1
Atp5a
Relative / Sdhb
1.5
1.0
0.5
0.0
D.
atf4a
atf4b
atf5a
atf5b
chop
Relative / actin

Figure 3.3 Homozygous *chchd10* ^{P83L} display reduced motor function, but no mitochondrial respiratory chain complex deficiency or increased mt-ISR transcripts.

A, Representative image of a 24-well plate free swim arena and movement paths (12 larvae per genotype) of fish aged 5 dpf. **B**, Quantification of free swim mean velocity: *chchd10* $^{P83L/P83L}$ = 3.26 mm/s, wild type = 6.18 mm/s ($p < 0.01$, Mann-Whitney U-test). Sample size (n) are as follows: *chchd10* $^{P83L/P83L}$ = 36, wild type = 40. Data represented as single data points and mean ± S.E.M. **Ci**, Representative immunoblot of mitochondrial respiratory chain subunits in 5 dpf wild type and *chchd10* $^{P83L/P83L}$ whole larval lysate and respective quantification (**Cii**). No significant differences were found between wild type and *chchd10* $^{P83L/P83L}$ larvae in any of the respiratory chain subunits levels: ndufa9 (t (4) = 0.89, p = 0.44); mt-Co1 (t (4) = 0.006, p = 0.95); uqcrc2 (t (4) = 1.07, p=0.35); atp5a (t (4) = 1.42, p = 0.23). Sdhb was used as loading control. **D**, Transcripts related to mt-ISR activation were not significantly increased in *chchd10* $^{P83L/P83L}$ larvae: *atf4a* (t (4) = 2.10, p = 0.10); *atf4b* (t (4) = 1.565, p = 0.19); *atf5a* (t (4) = 0.5494, p = 0.61); *atf5b* (t (4) = 0.8625, p = 0.44), and *chop* (t (4) = 0.745, p = 0.49). Significant differences from the wild type group are represented by either a single asterisk ($p < 0.05$) or double asterisk ($p < 0.01$).

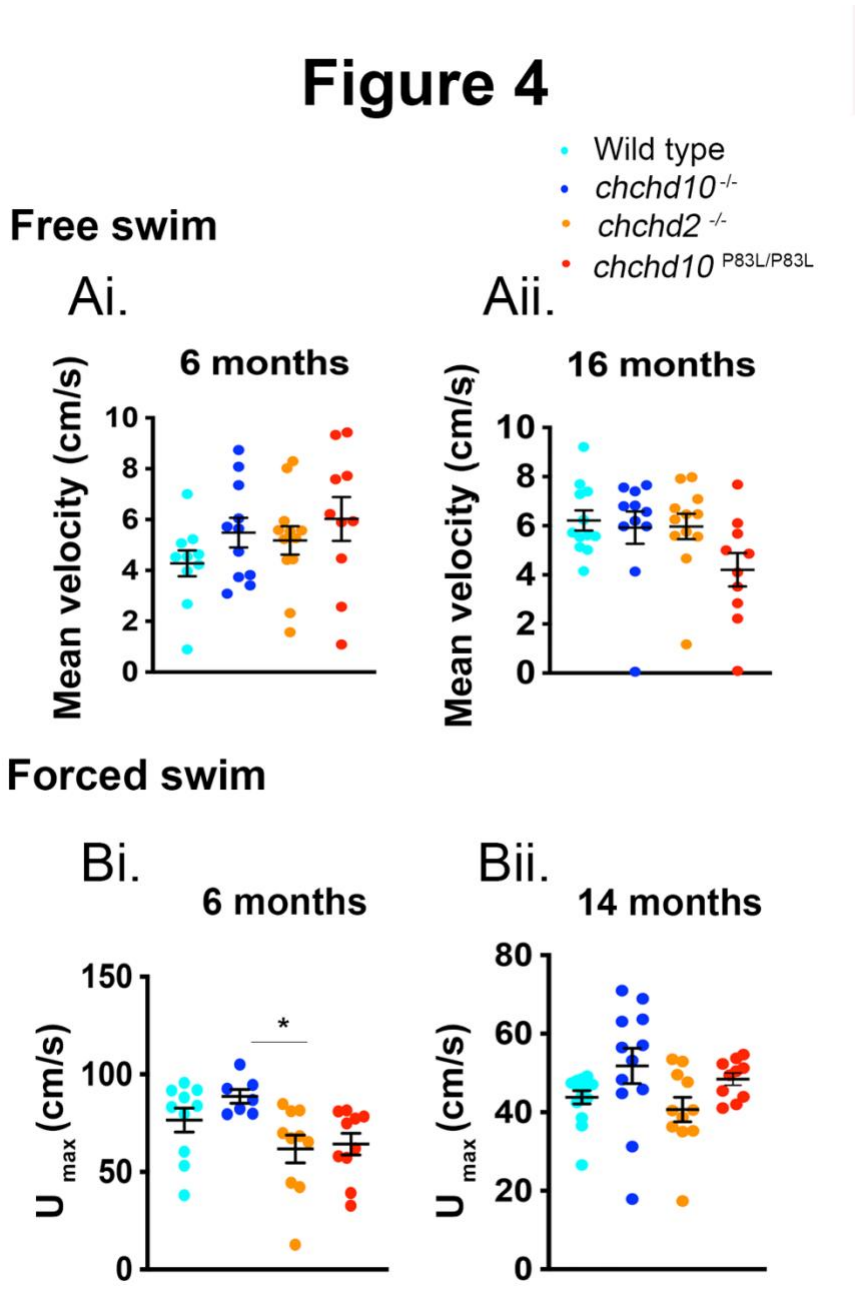

Figure 3.4 Adult single gene knock-out (*chchd10* $^{-/-}$ or *chchd2* $^{-/-}$) and *chchd10* $^{P83L/P83L}$ zebrafish do not display a motor deficit in either free or forced swim assays.

Ai, Adult zebrafish, aged 6 months, were placed into an open field arena and mean swim velocity was measured. No differences in mean free swim velocity were found across all of the

genotypes (F (3,39) = 1.24, $p > 0.05$). Mean free swim velocity and sample sizes are as follows: wild type (4.28 cm/s, n= 10); *chchd10*$^{-/-}$ (5.49 cm/s, n=11); *chchd2* $^{-/-}$ (5.18 cm/s, n= 12); *chchd10* $^{P83L/P83L}$ (6.03 cm/s, n =12). **Aii**, Free swim velocity was assessed at 16 months of age. No significant differences in mean swim velocity was observed in older fish (H (4) = 7.21, p=0.07, Kruskal-Wallis test). Measures of mean velocity and sample sizes were as follows: wild type (6.21 cm/s, n = 12); *chchd10* $^{-/-}$ (5.92 cm/s, n=11); *chchd2* $^{-/-}$ (5.97 cm/s, n=12); and *chchd10*$^{P83L/P83L}$ (4.20 cm/s, n = 10). **Bi**, Adult zebrafish were placed into a swim tunnel and a forced swim assay was performed to examine if aerobic exercises was impaired. A single significant difference was observed in our forced swim measure (F (3,33) = 3.73, p= 0.02) between *chchd10*$^{-/-}$ and *chchd2* $^{-/-}$ (p = 0.027) at 6 months of age. Mean critical swim speed (U_{max}) and sample sizes were as follows: wild type (76.58 cm/s, n = 10); *chchd10*$^{-/-}$ (88.69 cm/s, n =7); *chchd2* $^{-/-}$ (61.76 cm/s, n = 10); and *chchd10* $^{P83L/P83L}$ (64.26 cm/s, n = 10). **Bii**, The forced swim tunnel assay was re-examined at 14 months of age and no significant differences were observed across genotypes (H (4) = 8.76, p=0.03). U_{max} and sample sizes were as follows: wild type (48.81 cm/s, n = 14); *chchd10*$^{-/-}$ (51.80 cm/s, n =12); *chchd2* $^{-/-}$ (40.68 cm/s, n = 11); and *chchd10* $^{P83L/P83L}$ (48.43 cm/s, n = 10). Data is represented as individual fish measures ± S.E.M.

Figure 5

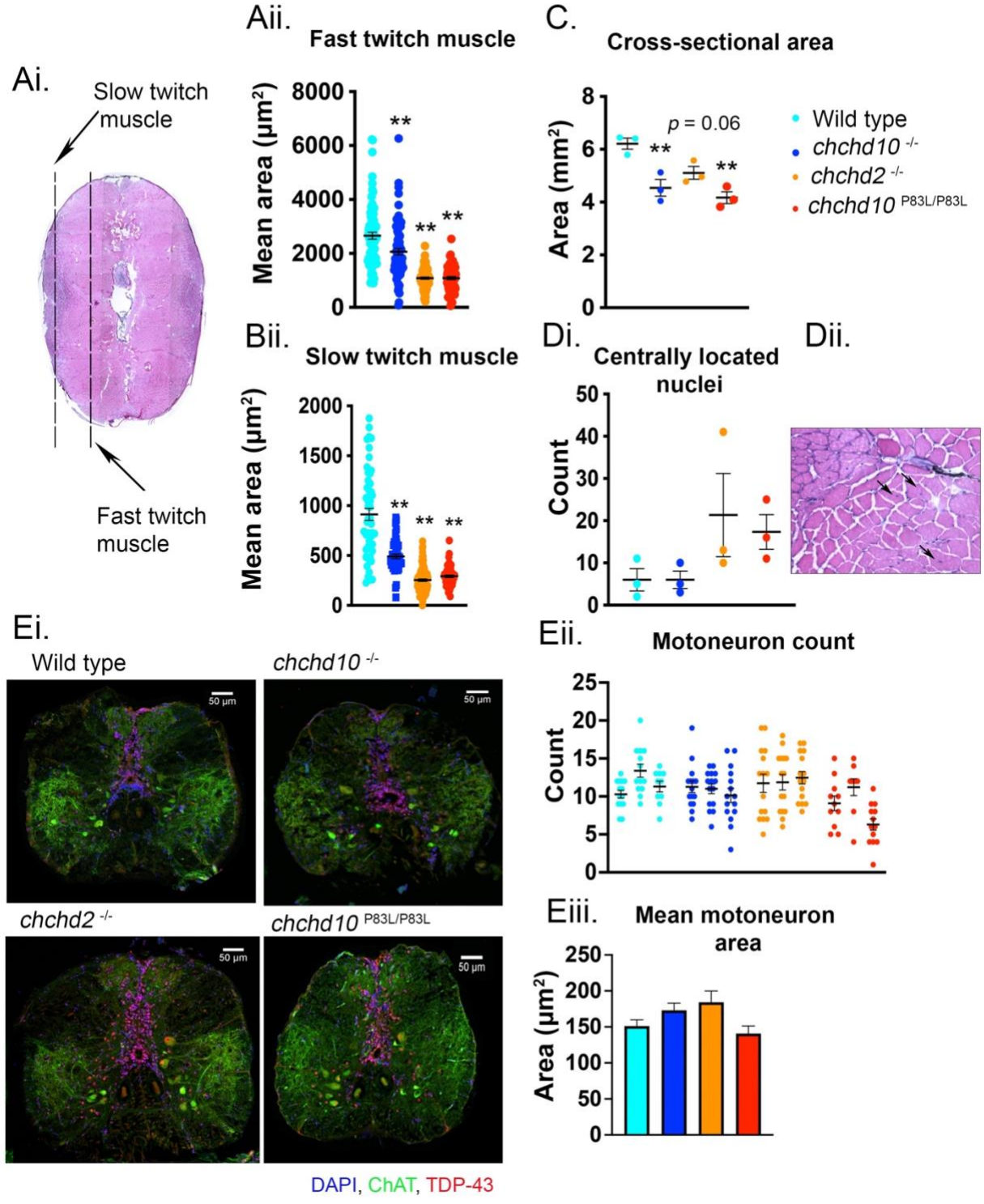
Ai.
Slow twitch muscle
Fast twitch muscle
Aii.
Fast twitch muscle
Mean area (µm²)
8000
6000
4000
2000
0
**
**
**
Bii.
Slow twitch muscle
Mean area (µm²)
2000
1500
1000
500
0
**
**
**
C.
Cross-sectional area
Area (mm²)
8
6
4
2
0
p = 0.06
**
**
Wild type
chchd10 -/-
chchd2 -/-
chchd10 P83L/P83L
Di.
Centrally located nuclei
Count
50
40
30
20
10
0
Dii.
Ei.
Wild type
chchd10 -/-
chchd2 -/-
chchd10 P83L/P83L
50 µm
DAPI, ChAT, TDP-43
Eii.
Motoneuron count
Count
25
20
15
10
5
0
Eiii.
Mean motoneuron area
Area (µm²)
250
200
150
100
50
0

Figure 3.5 Muscle defects are not accompanied by motor neuron deficits in our models at 11 months of age.

Ai, Representative whole trunk cross-section with overlayed dashed line indicating the specific fast-twitch muscle cells selected for measurement. **Aii**, Fast-twitch cross-sectional area was significantly smaller among our *chchd10* $^{-/-}$, *chchd2* $^{-/-}$, and *chchd10* $^{P83L/P83L}$ when compared muscle cell areas of wild type fish ($F(3, 313) = 71.84$, $p < 0.0001$). Mean areas and number of fibers counted were as follows: wild type, 2656 μm^2 (n= 208); *chchd10* $^{-/-}$, 2063 μm^2 (n =192, $p < 0.0001$); *chchd2* $^{-/-}$, 1085 μm^2 (n= 240, $p < 0.0001$); *chchd10*$^{P83L/P83L}$, 1086 μm^2 (n= 173, $p < 0.0001$). **Bi**, Representative line drawn across muscle cross section indicating which slow-twitch muscle cells were selected for measurement. **Bii**, Slow-twitch muscle cell cross-sectional area was significantly lower across all our genetic groups when compared to muscle cross-sectional areas from wild type zebrafish ($F(3, 255) = 107.7$, $p < 0.0001$). Mean areas and number of fibers counted are as following: wild type, 911.7 μm^2 (n= 138) *chchd10*$^{-/-}$, 490 μm^2 (n= 136, $p < 0.0001$); *chchd2* $^{-/-}$, 253 μm^2 (n= 205, $p < 0.0001$); *chchd10* $^{P83L/P83L}$, 292.2 μm^2 (n =144, $p < 0.0001$). **C**, Whole trunk cross section areas were found to be different among our genetic groupings ($F(3,8) = 12.58$, $p = 0.002$), with the following mean areas: wild type, 6.21 mm^2; *chchd10* $^{-/-}$, 4.54 mm^2 ($p = 0.007$); *chchd2* $^{-/-}$, 5.10 mm^2 ($p = 0.057$); *chchd10* $^{P83L/P83L}$, 4.17 mm^2 ($p = 0.002$). **Di**, Example muscle cell cross-sections with centrally located nuclei, here in the *chchd2* $^{-/-}$ model**. Dii**, No significant differences were found in our tabulation of centrally located nuclei across our genetic groupings ($F(3, 8) = 1.973$, $p = 0.20$.). **Ei**, Example of spinal cord immunolabeling, with DAPI (blue), ChAT (green) and TDP-43 (red). The number of spinal cord motoneurons was unchanged at this age across our genetic groups ($F(3,8) = 2,61$, $p = 0.12$) (**Eii**) nor did we observe any changes in mean motoneuron area ($F(3,8) = 2.93$, $p = 0.099$) (**Eiii**). All animals were 11 months of age, n = 3 per genotype. Data represented as single data

points and mean ± S.E.M. Significant difference with wild type is represented by a single asterisk ($p < 0.05$) or double asterisk ($p < 0.01$).

Figure 6

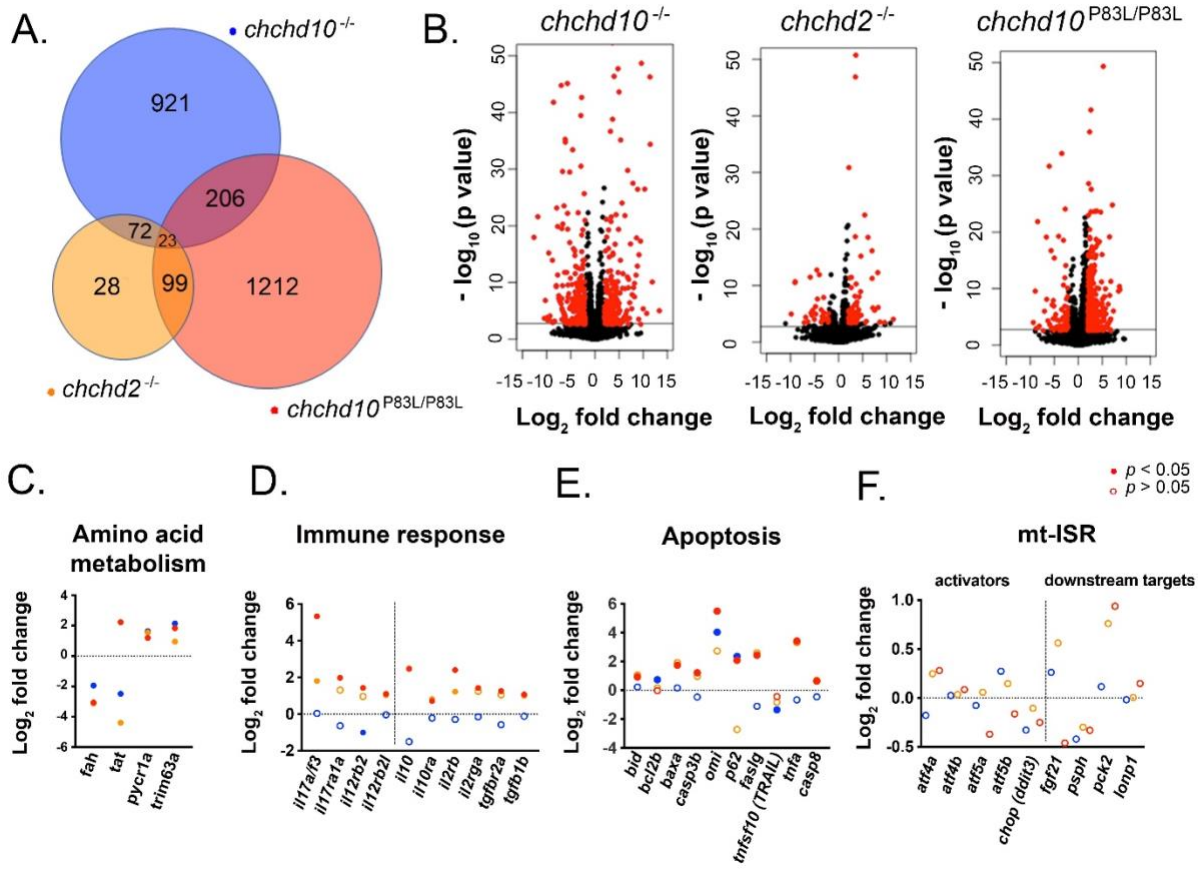

Figure 3.6 RNA sequencing results of 7-month old adult *chchd10* $^{-/-}$, *chchd2* $^{-/-}$, and *chchd10* $^{P83L/P83L}$ spinal cords compared to RNA from wild type spinal cords.

A, Number of shared and total significantly altered transcripts ($p > 0.05$) compared to transcripts in spinal cords from wild type zebrafish. **B**, Volcano plots showing significantly altered transcripts with their Log_2 fold change, significantly altered transcripts ($p > 0.05$) are represented in red. Transcripts involved with different cellular pathways were significantly altered including amino acid metabolism (**C**), immune response (**D**), apoptosis (**E**), but not transcripts related to the mt-ISR (**F**). Data presented in **C**-**F** are Log_2 fold change compared to wild type spinal cord RNA. Filled dots

represent significant changes (p <0.05), and empty dots represent transcript expression levels that are not significantly different when compared to wild type RNA (p > 0.05).

Figure 7

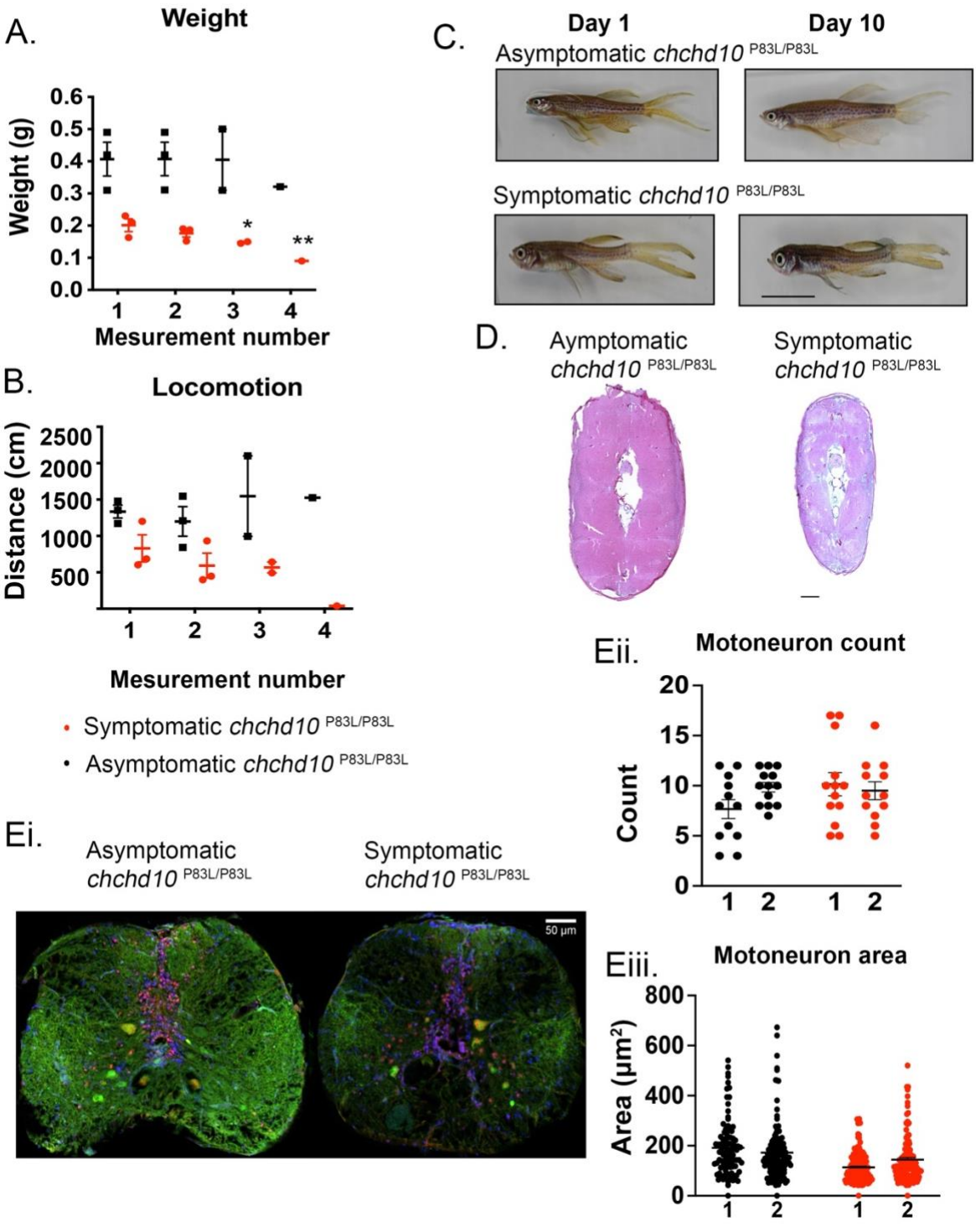
A.
Weight
Weight (g)
0.6
0.5
0.4
0.3
0.2
0.1
0.0
*
**
1
2
3
4
Mesurement number
B.
Locomotion
Distance (cm)
2500
2000
1500
1000
500
1
2
3
4
Mesurement number
Symptomatic chchd10 P83L/P83L
Asymptomatic chchd10 P83L/P83L
C.
Day 1
Day 10
Asymptomatic chchd10 P83L/P83L
Symptomatic chchd10 P83L/P83L
D.
Aymptomatic chchd10 P83L/P83L
Symptomatic chchd10 P83L/P83L
Ei.
Asymptomatic chchd10 P83L/P83L
Symptomatic chchd10 P83L/P83L
50 µm
Eii.
Motoneuron count
Count
20
15
10
5
0
1
2
1
2
Eiii.
Motoneuron area
Area (µm²)
800
600
400
200
0
1
2
1
2

Figure 3.7 Adult *chchd10* $^{P83L/P83L}$ develop ALS-like symptoms before death.

A, Symptomatic *chchd10* $^{P83L/P83L}$ fish weigh less than asymptomatic fish. Significant weight loss is seen before death (Mixed-effects analysis, Genotype x Measurement number F (3, 6) = 7.202, $p < 0.05$), with a significant reduction in weight seen in symptomatic fish between measurement 1 and measurement 3 ($p < 0.05$, Dunnett's multiple comparison), and measurement 1 and measurement 4 ($p < 0.0$, Dunnett's multiple comparison). Mean and sample size were as follows: symptomatic (n = 3 fish, mean = 0.17 g); asymptomatic (n = 3 fish, mean = 0.40 g). Measurement number represent repeated measures taken every 3 days or until death, data represented as individual values ± S.E.M. Asterisks represent significant difference of $p > 0.05$ (*) or $p > 0.01$ (**) compared to matched first measure. **B**, Symptomatic *chchd10* $^{P83L/P83L}$ fish swam, less than asymptomatic fish, and their locomotor behaviour worsened before death, though not significant Mixed-effects analysis, Genotype x Measurement number F (3, 6) = 3.948, $p = 0.07$. Mean and sample size were as follows: symptomatic (n = 3, mean = 604.7 cm); asymptomatic (n = 3, mean = 1358 cm). Measurement number represent repeated measures taken every 3 days or until death, data represented as individual values ± S.E.M. **C**, Representative images of zebrafish over 10 days showing thinning in symptomatic but not by asymptomatic *chchd10* $^{P83L/P83L}$ fish. Representative muscle H & E staining (scale bar = 300 μm) (**D**) and immunofluorescent labelling of spinal cord cross-sections (**Ei**) of symptomatic and asymptomatic *chchd10* $^{P83L/P83L}$ fish, respectively. Quantification showed no significant differences between mean count (**Eii**, t (2) = 0.94, $p > 0.05$) nor and differences in mean motoneuron area (**Eiii**, t (2) = 2.929, $p > 0.05$), n = 2 per phenotype, data represented as single points and mean ± S.E.M.

LUNA staining. To detect whether there were microsporidia present in our fish, we performed LUNA staining on muscle sections (Luna 1968, Peterson, Spitsbergen et al. 2011). After 4 % PFA fixation, slides were rinsed with PBS (2 times for 2 minutes). Staining was performed using a 9:1 mix of Weigert's iron hematoxylinand Biebrich scarlet solution (1%) for 5 minutes. Slides were then dipped in 1% acid alcohol (8 dips); rinsed in tap water (5 minutes) and dipped in a lithium carbonate solution (0.5%) until sections turned blue (approximately 5 dips). Slides were then washed in running water (2 minutes) and dehydrated through a gradient of alcohols-xylene (2 min each). Finally, a thin band of xylene-based medium was applied. Slides were allowed to cure overnight and imaged using a brightfield microscope (Zeiss Axio Imager.M2, 10X and 63X objective). Images were stitched together using Photoshop CS4 (Adobe).

Supplementary Figure 1

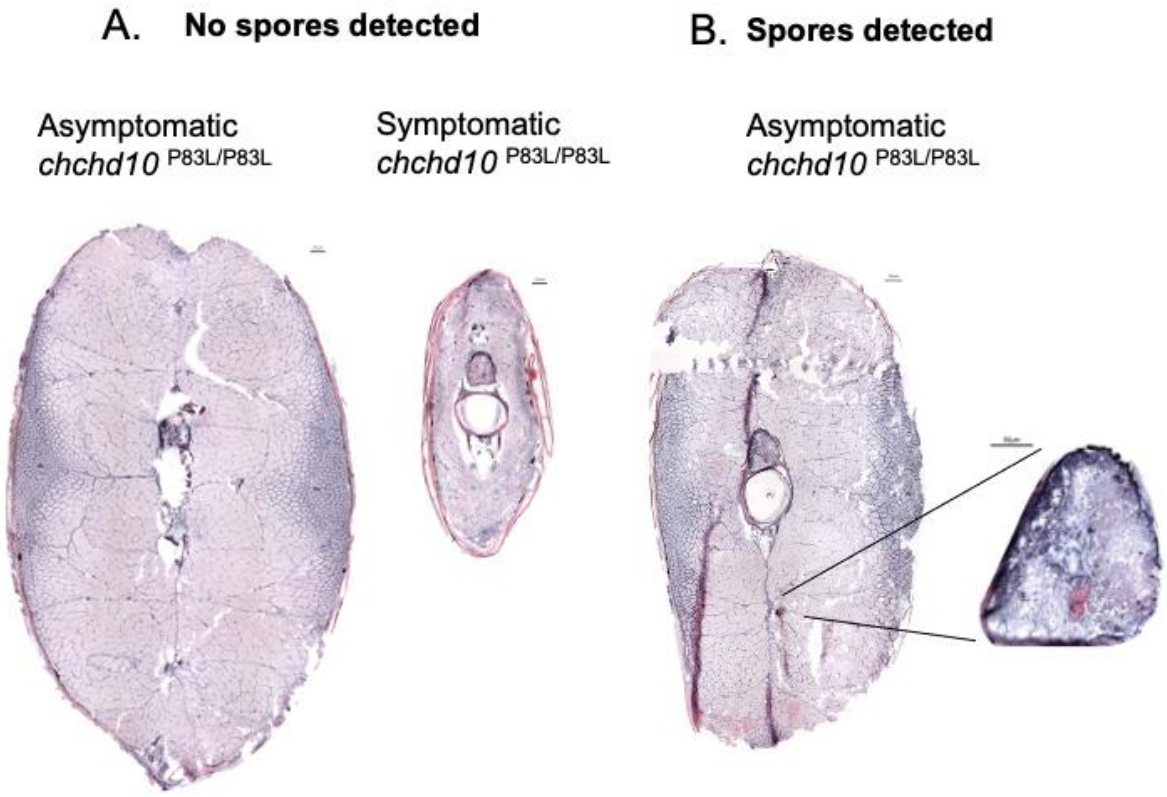

Supplementary Figure 3.1 Microsporidia presence concomitant to symptom expression. **A,** Absence of microsporidia was observed in both symptomatic and asymptomatic fish using LUNA staining (sections sampled per zebrafish n =16 symptomatic, n= 15 asymptomatic). **B**, Example of infected fish. Here, 10% of examined sections were infected with microsporidia in an asymptomatic *chchd10* $^{P83L/P83L}$ fish (sections sampled, n =10). Total number of sampled *chchd10* $^{P83L/P83L}$ fish, N=7 fish).

Supplementary Figure 2

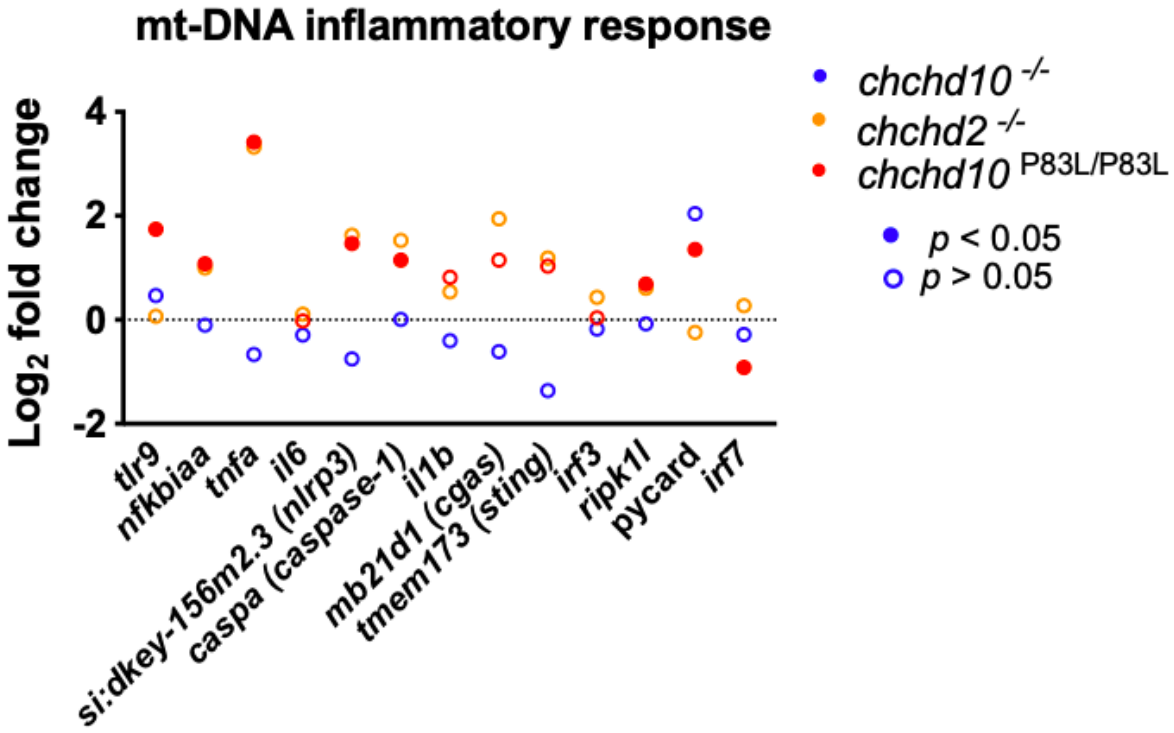

Supplementary Figure 3.2 Several mt-DNA sensor transcripts are increased in *chchd10* $^{P83L/P83L}$ zebrafish.

Data is represented as Log_2 fold change compared to wild type larvae. Filled dots represent significant changes ($p < 0.05$) and empty dots represent transcripts that were not found to be significantly altered ($p > 0.05$)

Protein	Primary Antibody
Ndufa9	ab14713, Abcam
Sdhb	ab14714, Abcam
Uqcrc2	14742-1-AP, Proteintech
Mt- co1	ab14705, Abcam
Atp5a	ab14748, Abcam
Vinculin	V4505, Sigma
Actin	LLC 691001, MP Biomedicals
Chchd10	ab121196, Abcam
Chchd2	custom epitope sequence: PDVTYQEPYQGQAM, MédiMabs

Supplementary Table 3.1 Primary antibodies used in this study.

Chapter 4: General Discussion

1. Summary of findings

The paralogues CHCHD10 and CHCHD2 are small nuclear encoded proteins mostly located in the mitochondrial IMS (Bannwarth, Ait-El-Mkadem et al. 2014, Zhou, Ma et al. 2018). Both have been linked to several neurodegenerative diseases, primarily to ALS and Parkinson's disease, respectively (Dols-Icardo, Nebot et al. 2015, Foo, Liu et al. 2015, Funayama, Ohe et al. 2015, Jansen, Bras et al. 2015, Ronchi, Riboldi et al. 2015, Zhang, Xi et al. 2015, Shi, Mao et al. 2016, Ikeda, Matsushima et al. 2017, Perrone, Nguyen et al. 2017, Zhou, Chen et al. 2017, Lehmer, Schludi et al. 2018, Yang, Zhao et al. 2019). Since their association with diseases were uncovered, several studies have attempted to understand their role in physiological and pathological conditions, and mounting evidence has shown that both proteins are involved in mitochondrial respiration, stress responses, activation of the mt-ISR, as well as mitochondrial morphology. Yet, disparate findings from *in vivo* KO models for both proteins have reduced our understanding of the specific contribution of either protein in biological and pathological pathways (Meng, Yamashita et al. 2017, Tio, Wen et al. 2017, Woo, Liu et al. 2017, Brockmann, Freischmidt et al. 2018, Burstein, Valsecchi et al. 2018, Liu, Duan et al. 2020, Liu, Huang et al. 2020, Sato, Noda et al. 2021). An aim of this thesis was to further our understanding of the relative contribution of Chchd10 and Chchd2 as well as the pathological consequences resulting from the expression of the orthologous ALS-associated CHCHD10 ^{P80L} variant in a zebrafish model. I hypothesized that these models would allow the examination of consequences arising from loss of either protein, and support loss-of-function mechanisms of disease that have been proposed using *in vitro* model systems of CHCHD10 (Huang, Wu et al. 2018, Lehmer, Schludi et al. 2018, Purandare, Somayajulu et al. 2018, Straub, Janer et al. 2018). In Chapter 2,

we confirmed the importance of both proteins in several measures, including survival, locomotion, NMJ integrity, response to stress and mitochondrial respiratory chain integrity. The data presented here provides support to a growing body of evidence that suggest CHCHD10 and CHCHD2 should be considered in tandem even when pathology is individually believed to be associated with one protein (Straub, Janer et al. 2018, Anderson, Bredvik et al. 2019, Liu, Huang et al. 2020). Our KO models did, however, differ in certain measures, most notably in their role in NMJ integrity and mitochondrial respiratory chain subunit expression. In Chapter 3, we compared our single KO results to our KI larvae which displayed similar but milder defects and suggested that this variant partly acts through a loss-of-function mechanism. Our studies suggest that zebrafish might have a broader ability to model CHCHD10 and CHCHD2 related diseases, especially for variants that act mostly through loss-of-function. As larvae present with a quantifiable phenotype, our studies also lay the foundation for high throughput drug screening. In the last part of Chapter 3, we explored adult fish as ALS is an adult-onset disease. We observed muscle pathology in both our KO and KI models, while motoneurons cell bodies were mostly spared. Then, focusing on our KI model, we uncovered a rapidly developing degenerative phenotype and neuroinflammation, supporting its use as an ALS model. Though our results shed light on potential mechanisms involved in CHCHD10-related ALS cases, several unanswered questions remain to be elucidated. In this section, I will highlight and speculate on some of these questions.

2. Chchd10 and Chchd2 regulation and complex formation

In the second research chapter of this thesis, I presented an *in vivo* study confirming that both Chchd10 and Chchd2 have an impact on each other's protein levels. While this study

replicated previous *in vitro* findings that the compensation by Chchd10 occurs following loss of Chchd2 (Huang, Wu et al. 2018, Straub, Janer et al. 2018), we observed that loss of Chchd10 led to reduced Chchd2 levels at larval stages of development. This implies that at 5 dpf, *chchd10* $^{-/-}$ larvae have lower levels of both Chchd10 and Chchd2, suggesting that those larvae could resemble double c*hchd10* $^{-/-}$ & c*hchd2* $^{-/-}$ KO more closely at that stage. Reduced levels of both proteins might explain the more severe phenotype of *chchd10* $^{-/-}$ larvae compared to *chchd2* $^{-/-}$ larvae in some of the measures presented in Chapter 2, such as reduced survival and impaired respiratory chain Complex I assembly.

The mechanisms by which each protein level influences the other remains unknown (Huang, Wu et al. 2018), but it has been suggested that CHCHD10 and CHCHD2 levels could be regulated by reducing their degradation, as both proteins have been documented to have very short half-lives of 4 hours and 1.5 hours respectively (Burstein, Valsecchi et al. 2018, Huang, Wu et al. 2018). I propose that the loss of Chchd2 triggers mechanisms that reduce Chchd10 degradation, which is supported by the lack of transcriptional changes in our models. Conversely, Chchd10 may have a role in either Chchd2 stability, or in the regulation of its degradation, leading to lower Chchd2 levels in our *chchd10* $^{-/-}$ fish model as well as a tendency for reduction in our *chchd10* $^{P83L/P83L}$ model. While our studies focused on larval stages, it would be of interest to determine whether the compensation of each protein varies at later stages, as well as whether those changes are specific to certain affected tissues such as the muscle or spinal cord. Preliminary results suggest that compensation by Chchd10 in *chchd2* $^{-/-}$ fish might reduce over time, and that reduced compensation in muscle, which is the main affected tissue in our fish, might occur at an earlier time point (**Supplementary Figure 5.1**). We thus hypothesize that

changes in compensation levels over time could lead to or contribute to the pathological manifestation in adulthood.

Our study was also the first *in vivo* study replicating findings that CHCHD10 and CHCHD2 exist either in a high molecular weight complex or as a monomer or a heterodimer. Though cellular studies have highlighted a molecular complex of around 170 and 220 kDa (Huang, Wu et al. 2018, Straub, Janer et al. 2018), we observed a complex at around 140 kDa suggesting that the complex composition might differ in zebrafish. We were not able to detect Chchd2 in our 2D gel, potentially due limitations of our antibody. Further studies should confirm whether Chchd10 and Chchd2 heterodimerize in zebrafish as well as investigate the impact that the Chchd10 ^{P83L} variant may have on heterodimerization in both the low and high molecular weight complexes. While preliminary data indicates that the Chchd10 ^{P83L} variant can form both a low and a high molecular weight complex (**Supplementary Figure 5.2**), it would still be of interest to determine the effect of this variant on the potential Chchd10 and Chchd2 complex formation. Subsequent studies could also explore the protein composition of the high molecular weight complex as this will likely shed further light into the role it plays in the cell.

Stress has also been suggested to influence the formation of CHCHD10/2 containing complexes. For example, loss of MMP led to increased CHCHD2/CHCHD10 complex formation (Huang, Wu et al. 2018), while exposure to galactose was reported to lead to the formation of a new 40 kDa complex containing both CHCHD10 and CHCHD2 and correlated with increased cell survival in both control and CHCHD10 ^{R15L} patient derived fibroblasts (Straub, Janer et al. 2018). We observe that both low and high molecular weight complexes containing Chchd10 were increased in our *chchd2*$^{-/-}$ model suggesting that compensation following loss of Chchd2

leads to increased Chchd10 in both its monomeric and dimeric form, as well as the higher molecular weight complex. As Chchd10 and Chchd2 respond to mitochondrial stresses (such as exposure to 2-DG, Chapter 2 **Figure 5**) it would be of interest for future studies to investigate the impact of stress on both the higher and the lower molecular weight complexes, and the formation of new complexes potentially involved in mitigating stress.

3. Chchd10 and Chchd2's involvement in Complex I assembly

Chapter 2 of my thesis presents data suggesting that Chchd10 and Chchd2 are both involved in Complex I assembly. While loss of Chchd10 leads to low levels of Ndufa9, as well as a reduction of Complex I assembly, loss of Chchd2 results in a milder Complex I assembly defect. A fascinating finding was made when we detected no defect in Complex I assembly in our double *chchd10* $^{-/-}$ & *chchd2* $^{-/-}$ KO fish model. In this model, while we did not observe any mitochondrial respiratory chain assembly deficits, increased mt-ISR markers were observed, which led us to theorize that activation of the mt-ISR might play a role in mitigating defects arising following loss of both proteins. This is supported by our observation that the oxygen responsive *cox4i2* transcript level was significantly increased in our double *chchd10* $^{-/-}$ & *chchd2* $^{-/-}$ model, but not in our single KO models. This could potentially underlie increased transcription of the Complex IV subunit and could be part of the compensatory response. It would be of interest to examine transcription changes of other subunits, and specially subunits of Complex I such as Ndufa9, which we hypothesize would be increased in our *chchd10* $^{-/-}$ & *chchd2* $^{-/-}$ model. In subsequent studies, it would also be interesting to determine whether impaired Complex I assembly translates into reduced mitochondrial respiration in both single KO *chchd10* $^{-/-}$ and *chchd2* $^{-/-}$ larvae. While not included in Chapter 2, we did preliminary exploration of basal

respiration in both single KO and did observe a reduction in oxygen consumption rates in *chchd10* $^{-/-}$ larvae (**Supplementary Figure 5.3**). Future studies may also consider examining whether the double *chchd10* $^{-/-}$ & *chchd2* $^{-/-}$ model, which recovers assembly of Complex I, also recovers respiration and/or whether blocking the activation of the mt-ISR impedes recovery of Complex I assembly. While our studies were focused on a single developmental time point (5 dpf) it would be of interest to determine whether maintenance of Complex I assembly in our double *chchd10* $^{-/-}$ & *chchd2* $^{-/-}$ KO model is maintained further into development.

Finally, all our measures were performed under normal rearing conditions. Future studies may consider investigating the impact of mitochondrial stress, such as exposure to 2-DG or starvation, on mitochondrial respiratory chain subunit expression and assembly *in vivo*. As *in vitro* studies on HeLa cells as well as patient's fibroblast suggest that mitochondrial stress worsen the respiratory phenotype (Huang, Wu et al. 2018, Straub, Janer et al. 2018), I hypothesize that the defect in mitochondrial respiratory chain complex assembly would increase following stress, and subsequently worsen the gross phenotype of locomotion and survival.

4. Chchd10 and Chchd2's involvement in mt-ISR activation

In Chapter 2 of this thesis, I presented findings which supported previous studies implicating both Chchd10 and Chchd2 in the mt-ISR (Anderson, Bredvik et al. 2019, Liu, Huang et al. 2020, Straub, Weraarpachai et al. 2021, Ruan, Hu et al. 2022, Sayles, Southwell et al. 2022). This response can be activated by several mitochondrial defects including misfolded proteins, OXPHOS deficiency, ROS, and mt-DNA genome deletions (Shpilka and Haynes 2018). Though single KO and *chchd10* $^{P83L/P83L}$ larvae did not display mt-ISR activation, this response was observed in our double *chchd10* $^{-/-}$ & *chchd2* $^{-/-}$ KO suggesting that the mitochondrial defects

resulting from single KO as well as Chchd10 ^{P83L} expression were not sufficient to trigger this response. As we and others documented that both Chchd10 and Chchd2 respond to mitochondrial stress, I propose that following exposition to various mitochondrial stressors, activation of the mt-ISR could be triggered in both our single KO as well as our KI models. Indeed, loss of either protein or expression of the ALS-associated Chchd10 ^{P83L} variant reduces Chchd10 and Chchd2 levels (**Chapter 2, Figure 1 Iii** and **Chapter 3 Figure 1 Dii, Diii**). This could reduce the ability to sense and respond to stress compared to wild type fish thereby leading to the activation of stress responses such as the mt-ISR following mitochondrial stress. This would be in line with previous reports where activation of the mt-ISR was observed in patient fibroblasts carrying the CHCHD10 ^{R15L} variant only when exposed to galactose which increases reliance on mitochondria for energy (Straub, Weraarpachai et al. 2021). I speculate that loss of either protein, or expression of disease-associated variants that do not confer an obvious toxic gain-of-function such as CHCHD10 ^{S59L} variant, are not individually sufficient to trigger the mt-ISR. Yet, additive exposures to various mitochondrial stressors along with loss of either CHCHD10 or CHCHD2 could trigger the mt-ISR. Furthermore, while an acute activation of the mt-ISR might mitigate the defects and resolve mitochondrial dysfunction as the observed Complex I recovery in our double *chchd10* $^{-/-}$ & *chchd2* $^{-/-}$ KO, chronic activation might lead to detrimental cellular consequences that could underlie or culminate in disease. This may entail the accumulation of mt-DNA mutations and deletions which is a known consequence of chronic mt-ISR activation and has been linked to age-related degeneration (Lehtonen, Forsström et al. 2016, Lin, Schulz et al. 2016, Tian, Merkwirth et al. 2016, Shpilka and Haynes 2018, Wang, Xu et al. 2019). As mt-DNA damage accumulates, this may lead to increased unfolded mitochondrial proteins and further the activation of the mt-ISR, but also lead to impairments in the ability to

produce mitochondrial respiratory chain proteins encoded by the mt-DNA genome in both humans (Taylor and Turnbull 2005) and zebrafish (Broughton, Milam et al. 2001). This hypothesis is partly supported by the observation of mt-DNA deletions arise following chronic activation of the mt-ISR in the heart of CHCHD10 ^{S55L} mice (Sayles, Southwell et al. 2022). I thus propose that following the loss of either protein or expression of a CHCHD10 variant, mt-DNA deletion could accumulate due to mt-ISR activation after repeated exposure to stress, resulting in mt-DNA heterogeneity and triggering disease (**Figure 4.1**). Future studies could explore whether the mt-ISR can lead to mt-DNA deletion in our models, and whether its inhibition could mitigate the defects and prevent disease onset. It would also be of interest to determine whether at later stages and at symptom onset the extent of mt-DNA deletions in symptomatic fish.

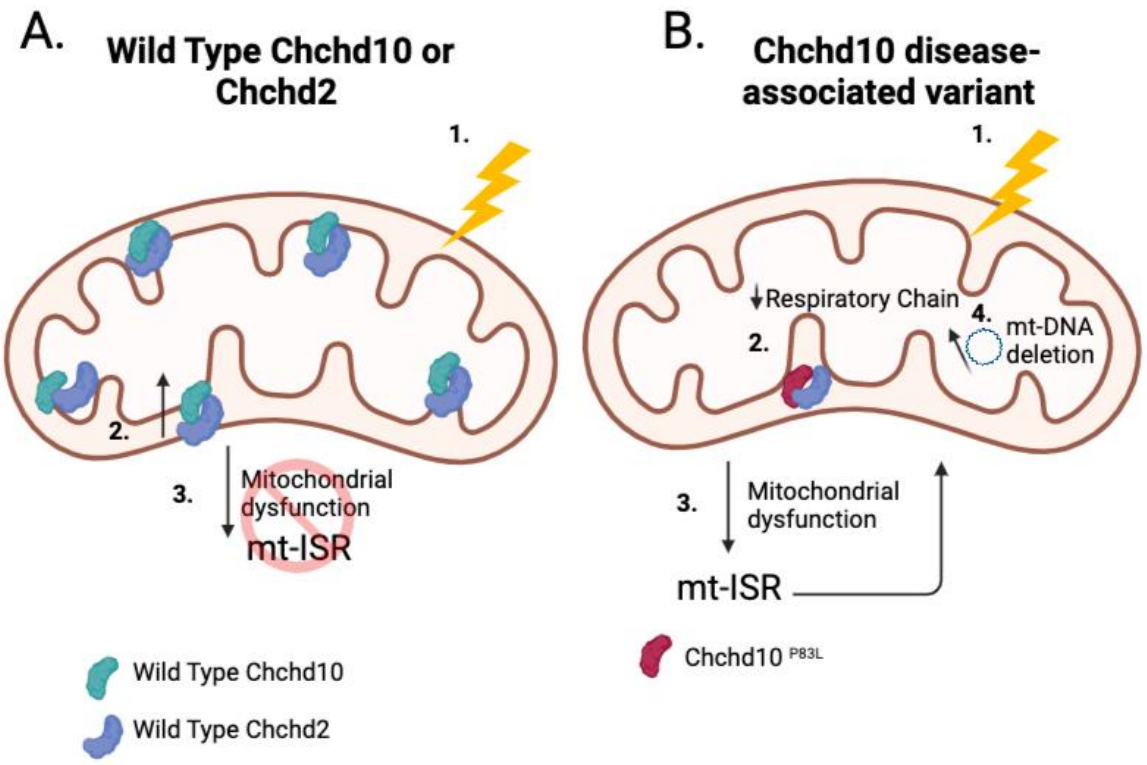

Figure 4.1 Proposed mechanism of activation of mt-ISR following loss of Chchd10 and Chchd2 or the expression of Chchd10 disease-associated variant.

A, Wild type condition. Mitochondrial stress (1) leads to increased Chchd10 and Chchd2 protein level (2). This serves to mitigate the stress and partially restore mitochondrial function without activation of the mt-ISR (3). **B**, in a situation where mitochondria harbour the Chchd10 ^{P83L} variant, mitochondrial stress (1) might overwhelm the capacity to mitigate the stress due to reduced Chchd10 and Chchd2 levels (2). This could result in mitochondrial dysfunction, which I speculate could lead to activation of the mt-ISR (3). Repeated exposure to stress may then lead to further detrimental consequences for mitochondrial function including mt-DNA deletion, which in turn could lead to further mitochondrial dysfunction.

5. The role of neuroinflammation in the *chchd10* ^{P83L} mutant zebrafish

While I propose that the mt-ISR might have a role in CHCHD10 and CHCHD2 related pathology, especially following exposure to mitochondrial stress, our study also highlighted other potential contributors to pathology, including most notably chronic inflammation in our KI model. The research findings presented in Chapter 3 of this thesis suggest that the CHCHD10 ^{P83L} variant does not act solely in a loss-of-function manor but also partially confers some toxic gain-of-function pathology, as inflammatory markers were not upregulated in our single KO. This finding has not been reported in other disease-associated variants of CHCHD10. Mitochondrial dysfunction can lead to inflammation in several ways (Lin, Liu et al. 2022). Loss of mitochondrial membrane integrity can result in the release of mitochondrial-derived damage-associated molecular patterns (DAMPs) that trigger the innate immune responses (Lin, Liu et al. 2022). Examples of DAMPs include: mt-DNA, ATP, cardiolipin, mitochondrial transcription factor A (TFAM), cytochrome c, ROS, as well calcium ions and iron ions (Nakahira, Hisata et al. 2015, Lin, Liu et al. 2022). It has also been proposed that the mt-ISR could lead to the activation of immune signalling and activation of the innate immune response (Liu, Samuel et al. 2014, Pellegrino, Nargund et al. 2014), yet, our RNA sequencing results presented in Chapter 3 suggest that activation of the mt-ISR does not occur in our single KOs or KI models. Another interesting avenue of research worth pursuing is the release of mt-DNA. As I speculated above, mt-DNA damage may form a cornerstone in the degenerative process, but its release from mitochondria could also lead to inflammation (West and Shadel 2017). During stress, mt-DNA can be released through the mitochondrial permeability transition pores; BCL-2 family BAK and BAX (McArthur, Whitehead et al. 2018, Riley, Quarato et al. 2018), and through the mitochondrial permeability transition pore (mPTP) (Patrushev, Kasymov et al. 2004, De Gaetano, Solodka et

al. 2021). More recently, some preliminary evidence also points to the possibility of mt-DNA being released through mitochondrial derived vesicles (MDVs) (Todkar, Chikhi et al. 2021) (**Figure 4.2 A**). Interestingly, *baxa* and other Bcl-2 family transcripts were significantly increased in our KI model (**Chapter 3, Fig 6 E**). Release of mt-DNA in the cytoplasm can lead to inflammation in several ways (**Figure 4.2 B**). Firstly, release of mt-DNA can trigger inflammation through the Toll-like receptor 9 (TLR9) on endosomes of glial cells which then trigger the NF-κB signaling pathway resulting in the release of IL-6 and TNF-α. Interestingly, the orthologous transcripts, including *tlr9*, *nfkbiaa*, *tfna* were significantly upregulated in our *chchd10* $^{P83L/P83L}$ fish (**Supplementary Figure 5.4 A**) (Lin, Liu et al. 2022). Secondly, it can also trigger inflammation through NLR family pyrin domain containing 3 protein (NLRP3), promoting the expression of IL-18 and IL-1β, both pro-inflammatory cytokines, through activation of caspase-1 (Lin, Liu et al. 2022). Both orthologous transcripts of NLRP3 (*si:dkey-156m2.3*) and caspase-1 (*caspa*) were also significantly upregulated in *chchd10* $^{P83L/P83L}$ fish (**Supplementary Figure 5.4 B**). Of note, this pathway may also be triggered by the release of cardiolipin, ATP and ROS (Lin, Liu et al. 2022) and could be an alternative inflammatory-evoking pathway modulated in our KI model. Lastly, mt-DNA release may activate the cyclic GMP-AMP synthase (cGAS) and the stimulator of interferon genes (STING) cellular pathway. Respective transcripts *mb21d1*, encoding orthologous cGAS, and *tmem173*, encoding orthologous STING, were not significantly altered in our KI fish model, though there was a general tendency for these transcripts to be increased (**Supplementary Figure 5.4 C**). Several transcripts involved in zebrafish cytoplasmic DNA sensing and involved in the cGAS STING pathway were also significantly altered in our mutants including *nfkbiaa*, *rsad2*, *mxc*, and *tnfa*

(Ge, Zhou et al. 2015, Hu, Zhang et al. 2018, Matsui, Ito et al. 2021) (**Supplementary Figure 5.4 C**).

As the cGAS-STING pathway has been suggested to be involved in several neurodegenerative diseases including ALS (Motwani, Pesiridis et al. 2019, Yu, Davidson et al. 2020, Fryer, Abdullah et al. 2021), I decided to explore its potential activation in our models. This pathway can be activated by foreign cytosolic DNA but can also be activated by self-DNA if it is released into the cytoplasm (Motwani, Pesiridis et al. 2019, Bai and Liu 2022). As noted in Chapter 3, pathology at 1 year of age is concentrated in the muscle. Using our *chchd10* $^{P83L/P83L}$ model, I performed preliminary experiments to determine whether cGAS-STING pathway was activated in this tissue. Through qPCR, we observed a trend towards upregulation of the *cgas* (*md21d1*) transcript (**Supplementary Figure 5.5 A**). As the cGAS-STING pathway can be activated by nuclear or mitochondrial DNA (Motwani, Pesiridis et al. 2019), I next examined whether there were any obvious muscle fibres with nuclear DNA damage by staining with gamma H2A histone family member X (H2A.X), which reveals whether histone phosphorylation of H2A.X at serine 139 occurred in response to DNA damage (**Supplementary Method**). Closer examination ruled out the contribution of nuclear DNA damage (**Supplementary Figure 5.5 Bi, Bii**). Though I did not explore nuclear DNA release, these results do not rule out the possibility that mt-DNA might be responsible for the observed activation of cGAS-STING pathway, a phenomenon that has been described in TDP-43 models of ALS and spinal cord samples of patients (Yu, Davidson et al. 2020, Kumar and Julien 2021). I therefore speculate that mt-DNA might be released following mitochondrial dysfunction, which could activate several pathways including cGAS-STING, TLR9 as well as the inflammasome pathway in our *chchd10* $^{P83L/P83L}$ model. This could subsequently lead to chronic inflammation,

which has long been thought to be involved in the pathogenesis of ALS (Correia, Patel et al. 2015, Liu and Wang 2017, McCauley and Baloh 2019, Béland, Markovinovic et al. 2020, Fu, Huang et al. 2022).

While the data presented here is not conclusive, further studies may focus research efforts on mt-DNA release. I propose that the observed inflammatory markers in the RNA sequencing dataset might result from mt-DNA release and subsequent activation of inflammatory pathways, which include cGAS-STING activation. This is relevant as several research groups are developing therapeutics to modulate cGAS-STING pathway (Cui, Zhang et al. 2019, Sheridan 2019, Ding, Song et al. 2020, Decout, Katz et al. 2021). Determining whether this pathway is a contributor to disease in CHCHD10 ^{P80L} patients could lead to new therapeutic avenues when modulators of the cGAS-STING pathway become clinically available.

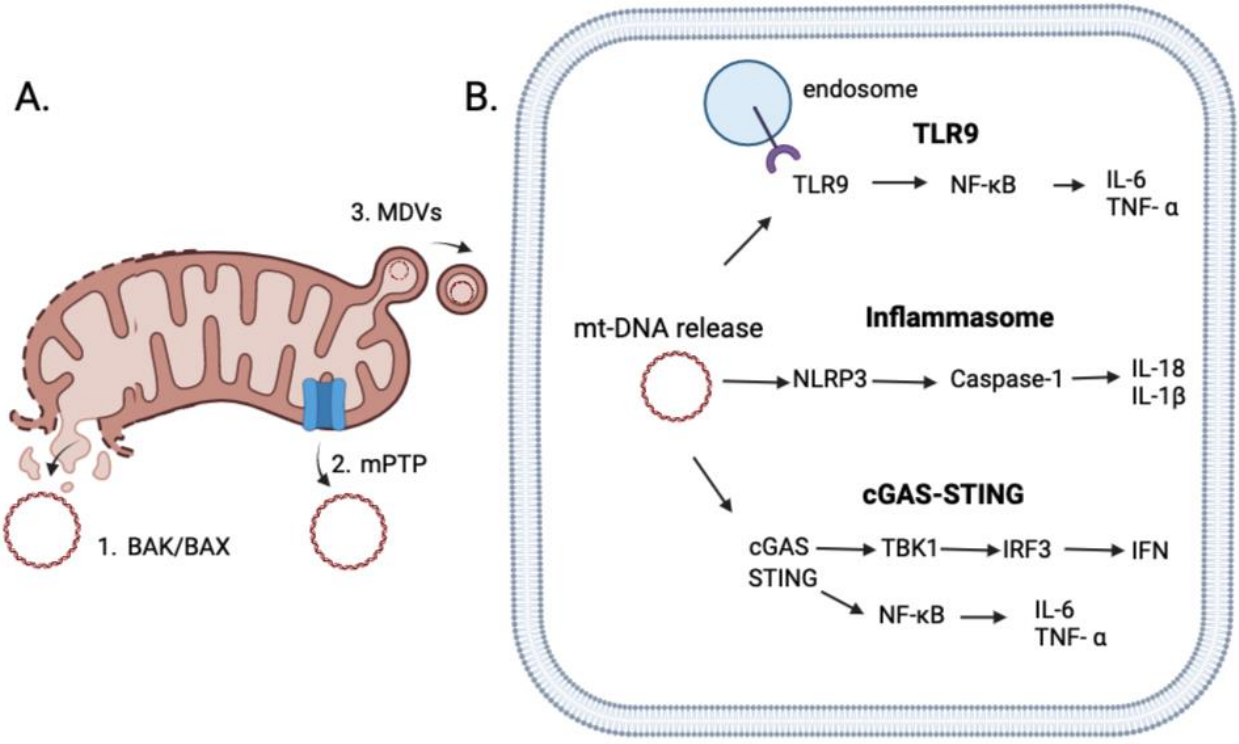

Figure 4.2. Mitochondrial dysfunction caused by Chchd10 ^{P83L} variant could trigger the release of mt-DNA leading to inflammation through various pathways.

A, mt-DNA release has been proposed to occur through various mechanisms, including BAK/BAX oligomerization (1) and mPTP formation (2). There is also some preliminary evidence that mt-DNA might also be released through MDVs (3). **B**, Following mt-DNA release into the cytoplasm, inflammation can be activated through TLR9 receptors on the endosomes, the inflammasome pathway, or the cGAS-STING pathway.

6. Zebrafish *chchd10* $^{P83L/P83L}$ develop ALS-like symptoms and pathology

In the last part of Chapter 3, I present research data that described how our symptomatic *chchd10* $^{P83L/P83L}$ zebrafish develop an ALS-like disease that is characterized by rapid deterioration of motor function and weight loss following symptom onset. We focused on symptomatic fish in the goal of capturing the main contributors to the degenerative phenotype. More particularly, as *in vivo* models allow for the examination of tissue-specific deficits, one of our main goals was to determine the site where the initial degeneration occurred as this may serve as an ideal point for therapeutic intervention.

In ALS, the primary site of degeneration occurs at the NMJ, which comprises the presynaptic motoneuron, and the postsynaptic muscle as well as a Schwan cell (Cappello and Francolini 2017). While much research attention has focused in the NMJ and motor neurons in the central nervous system, less research has been focused on muscle-specific dysfunction in ALS. The research I present in Chapter 3 underscores the importance of considering muscle pathology, especially in ALS cases where mitochondrial dysfunction is thought to play a central role. While muscle pathology was observed early, including in pre-symptomatic fish, no obvious changes in motoneurons cell body area or count were observed, even at late stages of disease. Yet, while we examined the motoneuron cell bodies and muscle, we did not focus on the NMJ, which could be affected in our models. Future studies should examine the NMJ in all genetic groupings as it would be interesting to note if and how NMJ pathology develops, and whether defects at the NMJ arise before muscle manifests pathology. Understanding the relative contribution of tissues to the disease-like state in our *chchd10* ^{P83L} fish may identify specific druggable targets.

Another area of research that may be important to explore is whether TDP-43 mislocalization in motoneurons, a hallmark of ALS, occurs in our ALS model. TDP-43

pathology has been reported in various models of CHCHD10 (Woo, Liu et al. 2017, Anderson, Bredvik et al. 2019, Genin, Madji Hounoum et al. 2019, Liu, Woo et al. 2022). While no TDP-43 pathology was observed in the spinal cord of patients carrying the CHCHD10 ^{R15L} variant, it could be that TDP-43 might not be a hallmark of CHCHD10-related ALS patients as is the case with other genetic cases.

It is also interesting to note that symptom onset of our KI model occurs at different ages as we observed symptom onset as early as 371 days and as late as 709 days despite our fish having a highly homogenous genetic background and being raised in the same environment. I propose that if mt-DNA deletion accumulation is the fundamental element of our models developing an ALS-like disease phenotype differing rates of accumulation of mt-DNA damage may underlie the varying onset of muscle degeneration and symptom expression. It would be of interest to determine, at these later stages of disease, whether there is increased accumulation of mt-DNA deletions in symptomatic fish and to explore whether mt-DNA release occurs.

In summation, future studies could examine how similar our KI *chchd10* $^{P83L/P83L}$ model is to other Chchd10 variants associated with ALS cases as this might aid in furthering our understanding of the biological role CHCHD10 plays in the cell. Furthermore, it would be of clinical interest to conduct drug screens using the fish model developed and presented in this thesis as there are currently few therapeutics to treat this disease.

Chapter 5: Conclusion

The mechanisms by which variants of CHCHD10 and CHCHD2 confer disease remain unknown and there remains considerable debate about whether the toxicity arises from a loss-of-function or gain-of-function disease mechanism. In this thesis, I present two research chapters that describe and characterize three KO models (*chchd10* $^{-/-}$, *chchd2* $^{-/-}$, and double *chchd10* $^{-/-}$ & *chchd2* $^{-/-}$), as well as a KI model (*chchd10* $^{P83L/P83L}$) that I believe will be useful for furthering our understanding of, and potentially, facilitate the development of therapeutics for ALS patients where mitochondrial dysfunction is thought to be involved.

I present data demonstrating that loss of either protein leads to similar phenotypes during zebrafish development. These results highlight that *in vivo* loss of either or both proteins results in detrimental consequences at larval stages characterized by reduced survival, impaired locomotor function, defects in NMJ integrity and mitochondrial respiratory chain assembly defects. This differs from most mouse studies which suggest that a toxic gain-of-function disease mechanism is mostly responsible for the phenotype. This thesis also presented data that suggest that the expression of the analogous CHCHD10 ^{P80L} variant in the fish (Chchd10 ^{P83L}) acts in a partial loss-of-function manner. This may have implications for therapeutic development as it implies that maintaining some CHCHD10 function is likely necessary for cellular homeostasis and survival. I also explored potential underlying causes leading to pathology in our models, and replicate findings that the mt-ISR is activated following loss of both proteins, but not when *chchd10* or *chchd2* is knocked out individually. To this point, I present data in this thesis that indicates that primary respiratory chain complex deficiency is independent of the mt-ISR, but that its activation in the double *chchd10* $^{-/-}$ & *chchd2* $^{-/-}$ could mitigate the respiratory chain deficiency. While the first research chapter of the thesis explored the biology of CHCHD10 and

CHCHD2 during development, the second research chapter examined adult-onset phenotypes and presented data implicating a muscle-specific deficiency arising before any conspicuous degenerative motor phenotype suggesting that muscle may be a potential therapeutic target for early intervention in patients. Using spinal cord RNA sequencing, I also identified chronic inflammation as another potential contributor to disease pathogenesis following expression of the ALS-associated Chchd10 ^{P83L} variant. I speculate that inflammation is potentially due to the release of mt-DNA and triggering of the cGAS-STING pathway notably. In summary, this thesis presents several robust zebrafish models that can be used as models to further study mitochondrial dysfunction in ALS and hopefully one day lead to the development of precision therapeutics for this dreadful disorder.

Appendices

1. Supplementary methods

Oxygen consumption rates measurement

Oxygen consumption rates were measured using a Seahorse Bioscience microplate-based extracellular flux (XFe24) analyzer SeaHorse set at 28.5 ºC as previously described (Stackley, Beeson et al. 2011). In brief, one larva aged 5 dpf per well was placed in 700 μL of E3 medium using XFe24 24-well islet capture plates. Basal oxygen measurement was measured 5 times in each larva.

H2A.X staining

Muscle sections extracted as described in Chapter 3 were incubated blocked and permeabilized with PBS solution containing 1% serum of respective secondary antibody and 0.1 % Triton X-100. Sections were then incubated overnight at 4°C with respective primary antibody: Phospho gamma H2A.X (S139) (abcam 228655) at a 1/100 concentration. After wash, secondary antibody, along with wheat germ agglutinin (1/100) was applied for 1 hour at room temperature. Slides were then mounted using ProLong™ Gold Antifade Mountant with DAPI (Thermo Fisher, P36931) and left to dry at room temperature overnight before imaging.

2. Supplementary figures

Supplementary Figure 1

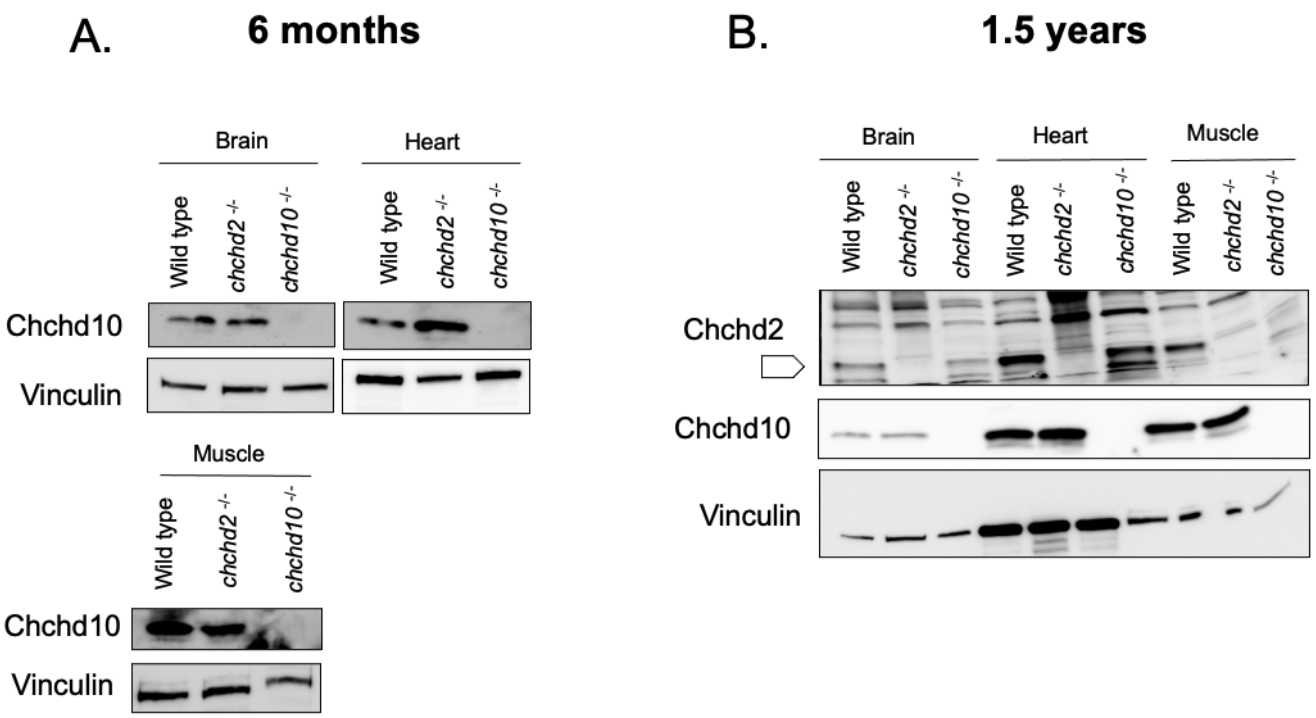

Supplementary Figure 5.1 Preliminary exploration of compensation by Chchd10 and Chchd2 in different tissues in adult zebrafish over time.

A, At 6 months of age, some compensation by Chchd10 in *chchd2* $^{-/-}$ fish seems to occur in brain and heart tissue but is not observed in muscle. **B**, At 1.5 year, increased levels of Chchd10 in *chchd2* $^{-/-}$ fish or of Chchd2 in *chchd10* $^{-/-}$ is not present in any probed tissue. Tissues were collected from one fish for each genotype per time point.

Supplementary Figure 2

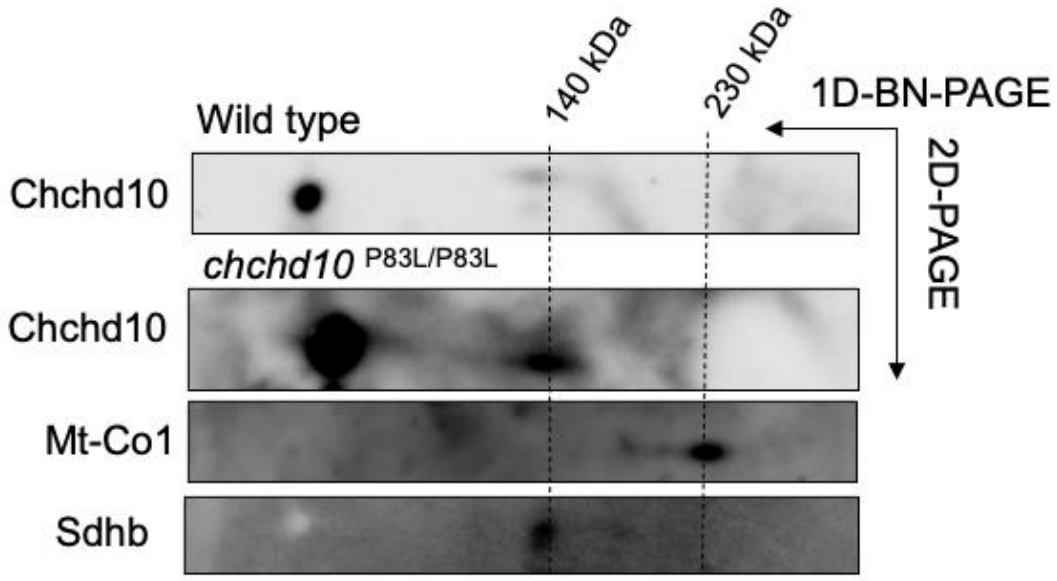

Supplementary Figure 5.2 2D- PAGE analysis of wild type and *chchd10* $^{P83L/P83L}$ zebrafish shows that Chchd10 forms a lower and higher molecular weight complex.

2D- PAGE, 5 larvae per genotype. mt-Co1 and Sdhb are used as molecular weight markers.

Supplementary Figure 3

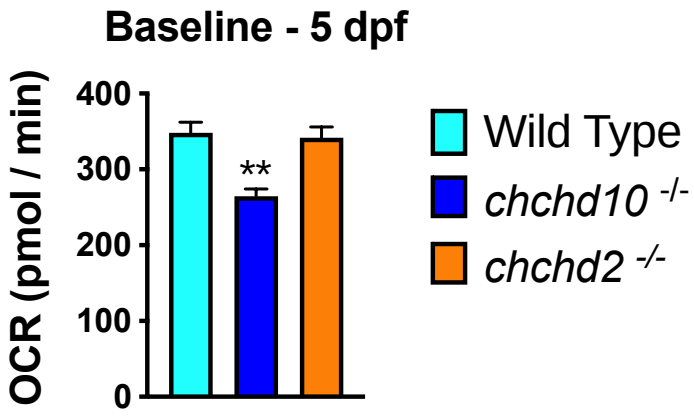

Supplementary Figure 5.3 Basal oxygen consumption rate (OCR) at 5 dpf shows a significantly reduced oxygen consumption in *chchd10*$^{-/-}$ larvae.

Significant difference in OCR between wild type and *chchd10*$^{-/-}$ larvae ($F(2, 23) = 16$, $p < 0.01$). Means were as follows: wild type = 348.1 pmol/min; *chchd10* $^{-/-}$ = 264.5 pmol/min ($p < 0.01$, Tuckey's); *chchd2* $^{-/-}$ = 342.0 5 pmol/min. (n = 6 larvae per genotype).

Supplementary Figure 4

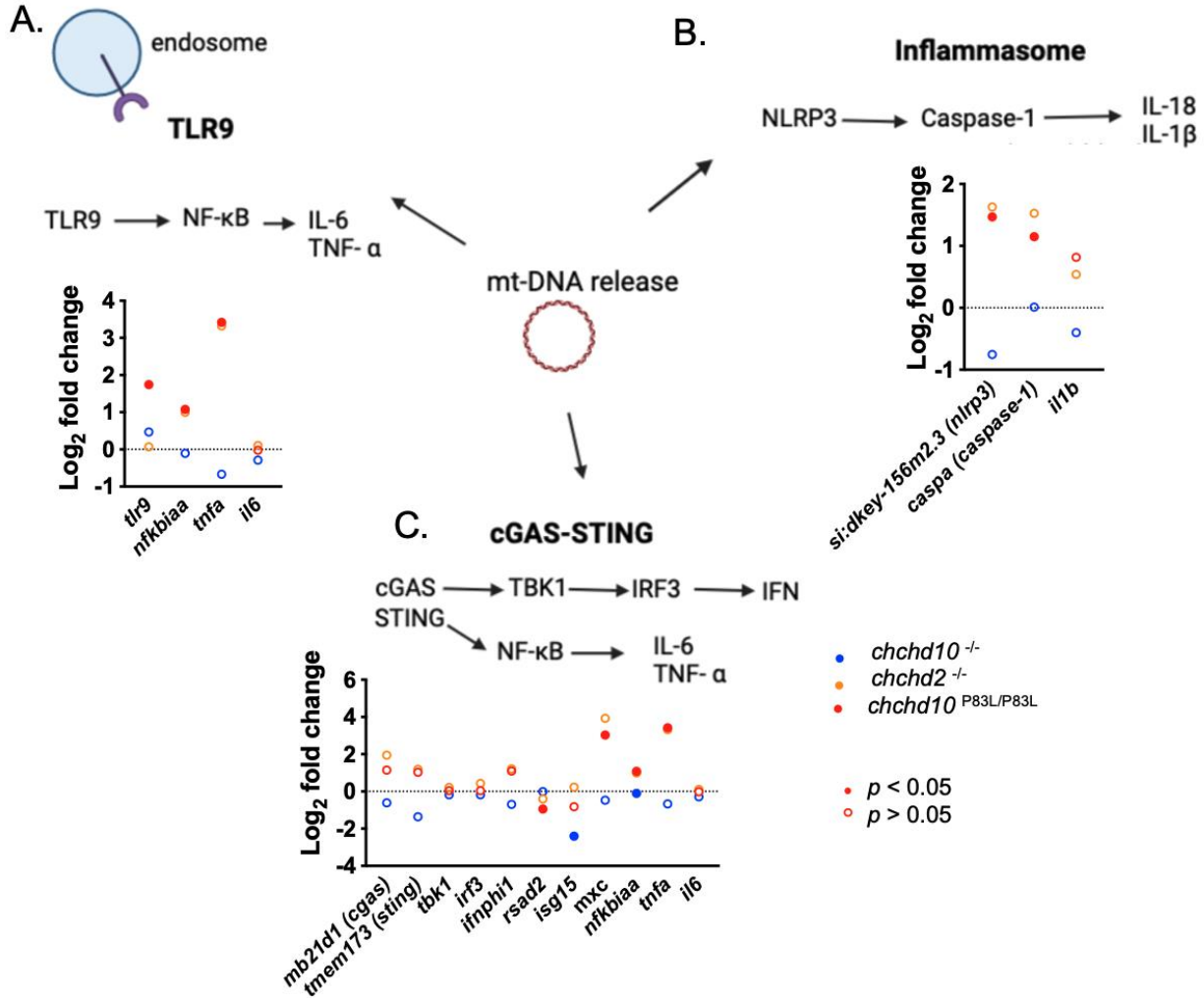

Supplementary Figure 5.4 Several transcripts related to mt-DNA release are significantly altered in *chchd10* $^{P83L/P83L}$ mutants.

Transcripts associated with TLR9 pathway **(A),** inflammasome **(B),** and cGAS-STING pathway **(C)**.

Supplementary Figure 5

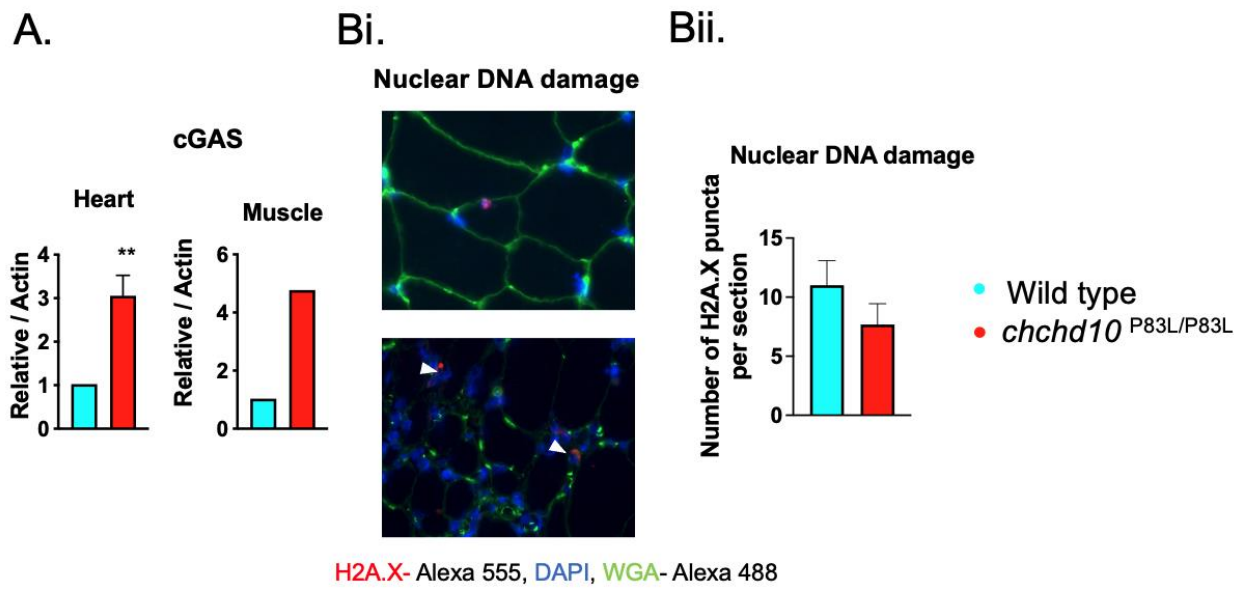

Supplementary Figure 5.5 Initial exploration of muscle tissue reveals an upregulation of *mb21d1* (orthologous to *cgas*) transcript, without nuclear DNA damage.

A, Transcript *mb21d1* encoding cGAS orthologue was upregulated in heart tissue (t (2) = 4.320, $p < 0.05$, n= 2 per genotype) and a tendency was observed in initial exploration of muscle tissue (n =1) in *chchd10* $^{P83L/P83L}$ zebrafish. **Bi**, Example of DNA damage found in muscle tissue**. Bii**, No significant increased nuclear DNA damage was observed in our *chchd10* $^{P83L/P83L}$ model compared to wild type (t (4), 1.22, $p > 0.05$, n =3 per genotype).

Master Reference List

Abe, K., M. Aoki, S. Tsuji, Y. Itoyama, G. Sobue, M. Togo, C. Hamada, M. Tanaka, M. Akimoto, K. Nakamura, F. Takahashi, K. Kondo, H. Yoshino, K. Abe, M. Aoki, S. Tsuji, Y. Itoyama, G. Sobue, M. Togo, C. Hamada, H. Sasaki, I. Yabe, S. Doi, H. Warita, T. Imai, H. Ito, M. Fukuchi, E. Osumi, M. Wada, I. Nakano, M. Morita, K. Ogata, Y. Maruki, K. Ito, O. Kano, M. Yamazaki, Y. Takahashi, H. Ishiura, M. Ogino, R. Koike, C. Ishida, T. Uchiyama, K. Mizoguchi, T. Obi, H. Watanabe, N. Atsuta, I. Aiba, A. Taniguchi, H. Sawada, T. Hazama, H. Fujimura, H. Kusaka, T. Kunieda, H. Kikuchi, H. Matsuo, H. Ueyama, K. Uekawa, M. Tanaka, M. Akimoto, M. Ueda, A. Murakami, R. Sumii, T. Kudou, K. Nakamura, K. Morimoto, T. Yoneoka, M. Hirai, K. Sasaki, H. Terai, T. Natori, H. Matsui, K. Kotani, K. Yoshida, T. Iwasaki, F. Takahashi, K. Kondo and H. Yoshino (2017). "Safety and efficacy of edaravone in well defined patients with amyotrophic lateral sclerosis: a randomised, double-blind, placebo-controlled trial." The Lancet Neurology **16**(7): 505-512.

Abe, K., Y. Itoyama, G. Sobue, S. Tsuji, M. Aoki, M. Doyu, C. Hamada, K. Kondo, T. Yoneoka and M. Akimoto (2014). "Confirmatory double-blind, parallel-group, placebo-controlled study of efficacy and safety of edaravone (MCI-186) in amyotrophic lateral sclerosis patients." Amyotrophic Lateral Sclerosis and Frontotemporal Degeneration **15**(7-8): 610-617.

Ajroud-Driss, S., F. Fecto, K. Ajroud, I. Lalani, S. E. Calvo, V. K. Mootha, H. X. Deng, N. Siddique, A. J. Tahmoush, T. D. Heiman-Patterson and T. Siddique (2015). "Mutation in the novel nuclear-encoded mitochondrial protein CHCHD10 in a family with autosomal dominant mitochondrial myopathy." Neurogenetics **16**(1): 1-9.

Alici, H., V. N. Uversky, D. E. Kang, J. A. Woo and O. Coskuner-Weber (2022). "Structures of the Wild-Type and S59L Mutant CHCHD10 Proteins Important in Amyotrophic Lateral Sclerosis–Frontotemporal Dementia." ACS Chemical Neuroscience **13**(8): 1273-1280.

Anderson, C. J., K. Bredvik, S. R. Burstein, C. Davis, S. M. Meadows, J. Dash, L. Case, T. A. Milner, H. Kawamata, A. Zuberi, A. Piersigilli, C. Lutz and G. Manfredi (2019). "ALS/FTD mutant CHCHD10 mice reveal a tissue-specific toxic gain-of-function and mitochondrial stress response." Acta Neuropathologica.

Arai, T., M. Hasegawa, H. Akiyama, K. Ikeda, T. Nonaka, H. Mori, D. Mann, K. Tsuchiya, M. Yoshida, Y. Hashizume and T. Oda (2006). "TDP-43 is a component of ubiquitin-positive tau-negative inclusions in frontotemporal lobar degeneration and amyotrophic lateral sclerosis." Biochem Biophys Res Commun **351**(3): 602-611.

Aras, S., M. Bai, I. Lee, R. Springett, M. Hüttemann and L. I. Grossman (2015). "MNRR1 (formerly CHCHD2) is a bi-organellar regulator of mitochondrial metabolism." Mitochondrion **20**: 43-51.

Aras, S., N. Purandare, S. Gladyck, M. Somayajulu-Nitu, K. Zhang, D. C. Wallace and L. I. Grossman (2020). "Mitochondrial Nuclear Retrograde Regulator 1 (MNRR1) rescues the cellular phenotype of MELAS by inducing homeostatic mechanisms." Proceedings of the National Academy of Sciences **117**(50): 32056-32065.

Arbour, D., C. Vande Velde and R. Robitaille (2017). "New perspectives on amyotrophic lateral sclerosis: the role of glial cells at the neuromuscular junction." J Physiol **595**(3): 647-661.

Armstrong, G. A. and P. Drapeau (2013). "Loss and gain of FUS function impair neuromuscular synaptic transmission in a genetic model of ALS." Hum Mol Genet **22**(21): 4282-4292.

Auranen, M., E. Ylikallio, M. Shcherbii, A. Paetau, S. Kiuru-Enari, J. P. Toppila and H. Tyynismaa (2015). "CHCHD10 variant p.(Gly66Val) causes axonal Charcot-Marie-Tooth disease." Neurology Genetics **1**(1): e1.

Babin, P. J., C. Goizet and D. Raldúa (2014). "Zebrafish models of human motor neuron diseases: Advantages and limitations." Progress in Neurobiology **118**: 36-58.

Baek, M., Y.-J. Choe, S. Bannwarth, J. Kim, S. Maitra, G. W. Dorn, J. P. Taylor, V. Paquis-Flucklinger and N. C. Kim (2021). "TDP-43 and PINK1 mediate CHCHD10S59L mutation–induced defects in Drosophila and in vitro." Nature Communications **12**(1): 1924.

Bai, J. and F. Liu (2022). "Nuclear cGAS: sequestration and beyond." Protein & Cell **13**(2): 90-101.

Bang, J., S. Spina and B. L. Miller (2015). "Frontotemporal dementia." The Lancet **386**(10004): 1672-1682.

Bannwarth, S., S. Ait-El-Mkadem, A. Chaussenot, E. C. Genin, S. Lacas-Gervais, K. Fragaki, L. Berg-Alonso, Y. Kageyama, V. Serre and D. G. Moore (2014). "A mitochondrial origin for frontotemporal dementia and amyotrophic lateral sclerosis through CHCHD10 involvement." Brain **137**(8): 2329-2345.

Beal, M. F. (2010). "Parkinson's disease: a model dilemma." Nature **466**(7310): S8-S10.

Becker, T., L. Böttinger and N. Pfanner (2012). "Mitochondrial protein import: from transport pathways to an integrated network." Trends in Biochemical Sciences **37**(3): 85-91.

Béland, L. C., A. Markovinovic, H. Jakovac, F. De Marchi, E. Bilic, L. Mazzini, J. Kriz and I. Munitic (2020). "Immunity in amyotrophic lateral sclerosis: blurred lines between excessive inflammation and inefficient immune responses." Brain Commun **2**(2): fcaa124.

Bensimon, G., L. Lacomblez and V. Meininger (1994). "A controlled trial of riluzole in amyotrophic lateral sclerosis. ALS/Riluzole Study Group." N Engl J Med **330**(9): 585-591.

Blokhuis, A. M., M. Koppers, E. J. N. Groen, D. M. A. van den Heuvel, S. Dini Modigliani, J. J. Anink, K. Fumoto, F. van Diggelen, A. Snelting, P. Sodaar, B. M. Verheijen, J. A. A. Demmers, J. H. Veldink, E. Aronica, I. Bozzoni, J. den Hertog, L. H. van den Berg and R. J. Pasterkamp (2016). "Comparative interactomics analysis of different ALS-associated proteins identifies converging molecular pathways." Acta Neuropathol **132**(2): 175-196.

Bose, P., G. A. B. Armstrong and P. Drapeau (2019). "Neuromuscular junction abnormalities in a zebrafish loss-of-function model of TDP-43." Journal of Neurophysiology **121**(1): 285-297.

Bourefis, A. R., M. L. Campanari, V. Buee-Scherrer and E. Kabashi (2020). "Functional characterization of a FUS mutant zebrafish line as a novel genetic model for ALS." Neurobiol Dis **142**: 104935.

Brockmann, S. J., A. Freischmidt, P. Oeckl, K. Müller, S. K. Ponna, A. M. Helferich, C. Paone, J. Reinders, K. Kojer, M. Orth, M. Jokela, M. Auranen, B. Udd, A. Hermann, K. M. Danzer, P. Lichtner, P. Walther, A. C. Ludolph, P. M. Andersen, M. Otto, P. Kursula, S. Just and J. H. Weishaupt (2018). "CHCHD10 mutations p.R15L and p.G66V cause motoneuron disease by haploinsufficiency." Human Molecular Genetics **27**(4): 706-715.

Broughton, R. E., J. E. Milam and B. A. Roe (2001). "The complete sequence of the zebrafish (Danio rerio) mitochondrial genome and evolutionary patterns in vertebrate mitochondrial DNA." Genome Res **11**(11): 1958-1967.

Brown, R. H. and A. Al-Chalabi (2017). "Amyotrophic Lateral Sclerosis." N Engl J Med **377**(2): 162-172.

Burstein, S. R., F. Valsecchi, H. Kawamata, M. Bourens, R. Zeng, A. Zuberi, T. A. Milner, S. M. Cloonan, C. Lutz, A. Barrientos and G. Manfredi (2018). "In vitro and in vivo studies of the ALS-FTLD protein CHCHD10 reveal novel mitochondrial topology and protein interactions." Human Molecular Genetics **27**(1): 160-177.

Butti, Z., Y. E. Pan, J. Giacomotto and S. A. Patten (2021). "Reduced C9orf72 function leads to defective synaptic vesicle release and neuromuscular dysfunction in zebrafish." Communications Biology **4**(1): 792.

Cappello, V. and M. Francolini (2017). "Neuromuscular Junction Dismantling in Amyotrophic Lateral Sclerosis." International Journal of Molecular Sciences **18**(10): 2092.

Cavallaro, G. (2010). "Genome-wide analysis of eukaryotic twin CX9C proteins." Molecular BioSystems **6**(12): 2459-2470.

Chaussenot, A., I. Le Ber, S. Ait-El-Mkadem, A. Camuzat, A. de Septenville, S. Bannwarth, E. C. Genin, V. Serre, G. Augé, A. Brice, J. Pouget and V. Paquis-Flucklinger (2014). "Screening of CHCHD10 in a French cohort confirms the involvement of this gene in frontotemporal dementia with amyotrophic lateral sclerosis patients." Neurobiology of Aging **35**(12): 2884.e2881-2884.e2884.

Che, X. Q., Q. H. Zhao, Y. Huang, X. Li, R. J. Ren, S. D. Chen, Q. H. Guo and G. Wang (2018). "Mutation Screening of the CHCHD2 Gene for Alzheimer's Disease and Frontotemporal Dementia in Chinese Mainland Population." J Alzheimers Dis **61**(4): 1283-1288.

Chung, M. J. and Y.-L. Suh (2002). "Ultrastructural Changes of Mitochondria in the Skeletal Muscle of Patients with Amyotrophic Lateral Sclerosis." Ultrastructural Pathology **26**(1): 3-7.

Consortium, P. M. A. S. (2018). "CHCHD10 variants in amyotrophic lateral sclerosis: Where is the evidence?" Ann Neurol **84**(1): 110-116.

Correia, A. S., P. Patel, K. Dutta and J.-P. Julien (2015). "Inflammation Induces TDP-43 Mislocalization and Aggregation." PLOS ONE **10**(10): e0140248.

Cruz, M. P. (2018). "Edaravone (Radicava): A Novel Neuroprotective Agent for the Treatment of Amyotrophic Lateral Sclerosis." P & T : a peer-reviewed journal for formulary management **43**(1): 25-28.

Cui, X., R. Zhang, S. Cen and J. Zhou (2019). "STING modulators: Predictive significance in drug discovery." Eur J Med Chem **182**: 111591.

De Gaetano, A., K. Solodka, G. Zanini, V. Selleri, A. V. Mattioli, M. Nasi and M. Pinti (2021). "Molecular Mechanisms of mtDNA-Mediated Inflammation." Cells **10**(11).

Decout, A., J. D. Katz, S. Venkatraman and A. Ablasser (2021). "The cGAS–STING pathway as a therapeutic target in inflammatory diseases." Nature Reviews Immunology **21**(9): 548-569.

DeJesus-Hernandez, M., I. R. Mackenzie, B. F. Boeve, A. L. Boxer, M. Baker, N. J. Rutherford, A. M. Nicholson, N. A. Finch, H. Flynn, J. Adamson, N. Kouri, A. Wojtas, P. Sengdy, G. Y. Hsiung, A. Karydas, W. W. Seeley, K. A. Josephs, G. Coppola, D. H. Geschwind, Z. K. Wszolek, H. Feldman, D. S. Knopman, R. C. Petersen, B. L. Miller, D. W. Dickson, K. B. Boylan, N. R. Graff-Radford and R. Rademakers (2011). "Expanded GGGGCC hexanucleotide repeat in noncoding region of C9ORF72 causes chromosome 9p-linked FTD and ALS." Neuron **72**(2): 245-256.

Ding, C., Z. Song, A. Shen, T. Chen and A. Zhang (2020). "Small molecules targeting the innate immune cGAS–STING–TBK1 signaling pathway." Acta Pharmaceutica Sinica B **10**(12): 2272-2298.

Dols-Icardo, O., I. Nebot, A. Gorostidi, S. Ortega-Cubero, I. Hernández, R. Rojas-García, A. García-Redondo, M. Povedano, A. Lladó, V. Álvarez, P. Sánchez-Juan, J. Pardo, I. Jericó, J. Vázquez-Costa, T. Sevilla, F. Cardona, B. Indakoechea, F. Moreno, R. Fernández-Torrón, L. Muñoz-Llahuna, S. Moreno-Grau, M. Rosende-Roca, Á. Vela, J. L. Muñoz-Blanco, O. Combarros, E. Coto, D. Alcolea, J. Fortea, A. Lleó, R. Sánchez-Valle, J. Esteban-Pérez, A. Ruiz, P. Pastor, A. López De Munain, J. Pérez-Tur, J. Clarimón and o. b. o. t. D. G. S. Consortium (2015). "Analysis of the CHCHD10 gene in patients with frontotemporal dementia and amyotrophic lateral sclerosis from Spain." Brain **138**(12): e400-e400.

Dupuis, L., J. L. Gonzalez de Aguilar, H. Oudart, M. de Tapia, L. Barbeito and J. P. Loeffler (2004). "Mitochondria in Amyotrophic Lateral Sclerosis: A Trigger and a Target." Neurodegenerative Diseases **1**(6): 245-254.

Fischer, L. R., D. G. Culver, P. Tennant, A. A. Davis, M. Wang, A. Castellano-Sanchez, J. Khan, M. A. Polak and J. D. Glass (2004). "Amyotrophic lateral sclerosis is a distal axonopathy: evidence in mice and man." Experimental Neurology **185**(2): 232-240.

Foo, J. N., J. Liu and E.-K. Tan (2015). "CHCHD2 and Parkinson's disease." The Lancet Neurology **14**(7): 681-682.

Fryer, A. L., A. Abdullah, J. M. Taylor and P. J. Crack (2021). "The Complexity of the cGAS-STING Pathway in CNS Pathologies." Frontiers in Neuroscience **15**.

Fu, J., Y. Huang, T. Bao, C. Liu, X. Liu and X. Chen (2022). "The role of Th17 cells/IL-17A in AD, PD, ALS and the strategic therapy targeting on IL-17A." Journal of Neuroinflammation **19**(1): 98.

Funayama, M., K. Ohe, T. Amo, N. Furuya, J. Yamaguchi, S. Saiki, Y. Li, K. Ogaki, M. Ando, H. Yoshino, H. Tomiyama, K. Nishioka, K. Hasegawa, H. Saiki, W. Satake, K. Mogushi, R. Sasaki, Y. Kokubo, S. Kuzuhara, T. Toda, Y. Mizuno, Y. Uchiyama, K. Ohno and N. Hattori (2015). "CHCHD2 mutations in autosomal dominant late-onset Parkinson's disease: a genome-wide linkage and sequencing study." The Lancet Neurology **14**(3): 274-282.

Ge, R., Y. Zhou, R. Peng, R. Wang, M. Li, Y. Zhang, C. Zheng and C. Wang (2015). "Conservation of the STING-Mediated Cytosolic DNA Sensing Pathway in Zebrafish." Journal of Virology **89**(15): 7696-7706.

Genin, E. C., S. Bannwarth, B. Ropert, F. Lespinasse, A. Mauri-Crouzet, G. Augé, K. Fragaki, C. Cochaud, E. Donnarumma, S. Lacas-Gervais, T. Wai and V. Paquis-Flucklinger (2022). "CHCHD10 and SLP2 control the stability of the PHB complex: a key factor for motor neuron viability." Brain.

Genin, E. C., B. Madji Hounoum, S. Bannwarth, K. Fragaki, S. Lacas-Gervais, A. Mauri-Crouzet, F. Lespinasse, J. Neveu, B. Ropert, G. Augé, C. Cochaud, C. Lefebvre-Omar, S. Bigou, A. Chiot, F. Mochel, S. Boillée, C. S. Lobsiger, D. Bohl, J.-E. Ricci and V. Paquis-Flucklinger (2019). "Mitochondrial defect in muscle precedes neuromuscular junction degeneration and motor neuron death in CHCHD10S59L/+ mouse." Acta Neuropathologica.

Genin, E. C., M. Plutino, S. Bannwarth, E. Villa, E. Cisneros-Barroso, M. Roy, B. Ortega-Vila, K. Fragaki, F. Lespinasse, E. Pinero-Martos, G. Augé, D. Moore, F. Burté, S. Lacas-Gervais, Y. Kageyama, K. Itoh, P. Yu-Wai-Man, H. Sesaki, J. E. Ricci, C. Vives-Bauza and V. Paquis-Flucklinger (2016). "CHCHD10 mutations promote loss of mitochondrial cristae junctions with impaired mitochondrial genome maintenance and inhibition of apoptosis." EMBO Molecular Medicine **8**(1): 58-72.

Hu, Y. W., J. Zhang, X. M. Wu, L. Cao, P. Nie and M. X. Chang (2018). "TANK-Binding Kinase 1 (TBK1) Isoforms Negatively Regulate Type I Interferon Induction by Inhibiting TBK1-IRF3 Interaction and IRF3 Phosphorylation." Frontiers in Immunology **9**.

Huang, X., B. P. Wu, D. Nguyen, Y.-T. Liu, M. Marani, J. Hench, P. Bénit, V. Kozjak-Pavlovic, P. Rustin and S. Frank (2018). "CHCHD2 accumulates in distressed mitochondria and facilitates oligomerization of CHCHD10Human Molecular Genetics, 2018, Vol. 00, No. 0Human Molecular Genetics, 2018, Vol. 00, No. 0." Human molecular genetics.

Ikeda, A., T. Matsushima, K. Daida, S. Nakajima, S. Conedera, Y. Li, H. Yoshino, G. Oyama, M. Funayama, K. Nishioka and N. Hattori (2017). "A novel mutation of CHCHD2 p.R8H in a sporadic case of Parkinson's disease." Parkinsonism Relat Disord **34**: 66-68.

Imai, Y., H. Meng, K. Shiba-Fukushima and N. Hattori (2019). "Twin CHCH Proteins, CHCHD2, and CHCHD10: Key Molecules of Parkinson's Disease, Amyotrophic Lateral Sclerosis, and Frontotemporal Dementia." International Journal of Molecular Sciences **20**(4): 908.

Iwata, M. and S. Sasaki (2007). "Mitochondrial Alterations in the Spinal Cord of Patients With Sporadic Amyotrophic Lateral Sclerosis." Journal of Neuropathology & Experimental Neurology **66**(1): 10-16.

Jansen, I. E., J. M. Bras, S. Lesage, C. Schulte, J. R. Gibbs, M. A. Nalls, A. Brice, N. W. Wood, H. Morris, J. A. Hardy, A. B. Singleton, T. Gasser, P. Heutink and M. Sharma (2015). "CHCHD2 and Parkinson's disease." Lancet Neurol **14**(7): 678-679.

Jiang, Z., W. Wang, G. Perry, X. Zhu and X. Wang (2015). "Mitochondrial dynamic abnormalities in amyotrophic lateral sclerosis." Translational neurodegeneration **4**: 14-14.

Kee, T. R., J. L. Wehinger, P. E. Gonzalez, E. Nguyen, K. C. McGill Percy, S. A. Khan, D. Chaput, X. Wang, T. Liu, D. E. Kang and J. A. Woo (2022). "Pathological characterization of a novel mouse model expressing the PD-linked CHCHD2-T61I mutation." Hum Mol Genet.

Keith, J. L., E. Swinkin, A. Gao, S. Alminawi, M. Zhang, P. McGoldrick, P. McKeever, J. Robertson, E. Rogaeva and L. Zinman (2020). "Neuropathologic description of CHCHD10 mutated amyotrophic lateral sclerosis." Neurology Genetics **6**(1): e394.

Khosravi, S. and M. E. Harner (2020). "The MICOS complex, a structural element of mitochondria with versatile functions." Biological Chemistry **401**(6-7): 765-778.

Kumar, D. R., F. Aslinia, S. H. Yale and J. J. Mazza (2011). "Jean-Martin Charcot: the father of neurology." Clinical medicine & research **9**(1): 46-49.

Kumar, S. and J. P. Julien (2021). "TDP-43 triggers immune response via mitochondrial DNA release." Cell Res **31**(4): 379-380.

Kurzwelly, D., M. T. Heneka, S. Biskup and S. Krüger (2015). "A distinct clinical phenotype in a German kindred with motor neuron disease carrying a CHCHD10 mutation." Brain **138**(9): e376-e376.

Kwiatkowski, T. J., Jr., D. A. Bosco, A. L. Leclerc, E. Tamrazian, C. R. Vanderburg, C. Russ, A. Davis, J. Gilchrist, E. J. Kasarskis, T. Munsat, P. Valdmanis, G. A. Rouleau, B. A. Hosler, P. Cortelli, P. J. de Jong, Y. Yoshinaga, J. L. Haines, M. A. Pericak-Vance, J. Yan, N. Ticozzi, T. Siddique, D. McKenna-Yasek, P. C. Sapp, H. R. Horvitz, J. E. Landers and R. H. Brown, Jr. (2009). "Mutations in the FUS/TLS gene on chromosome 16 cause familial amyotrophic lateral sclerosis." Science **323**(5918): 1205-1208.

Lehmer, C., M. H. Schludi, L. Ransom, J. Greiling, M. Junghänel, N. Exner, H. Riemenschneider, J. van der Zee, C. Van Broeckhoven and P. Weydt (2018). "A novel CHCHD10 mutation implicates a Mia40-dependent mitochondrial import deficit in ALS." EMBO molecular medicine **10**(6): e8558.

Lehtonen, J. M., S. Forsström, E. Bottani, C. Viscomi, O. R. Baris, H. Isoniemi, K. Höckerstedt, P. Österlund, M. Hurme, J. Jylhävä, S. Leppä, R. Markkula, T. Heliö, G. Mombelli, J. Uusimaa, R. Laaksonen, H. Laaksovirta, M. Auranen, M. Zeviani, J. Smeitink, R. J. Wiesner, K. Nakada, P. Isohanni and A. Suomalainen (2016). "FGF21 is a biomarker for mitochondrial translation and mtDNA maintenance disorders." Neurology **87**(22): 2290-2299.

Lezi, E. and R. H. Swerdlow (2012). "Mitochondria in neurodegeneration." Advances in experimental medicine and biology **942**: 269-286.

Lin, M.-m., N. Liu, Z.-h. Qin and Y. Wang (2022). "Mitochondrial-derived damage-associated molecular patterns amplify neuroinflammation in neurodegenerative diseases." Acta Pharmacologica Sinica.

Lin, Y.-F., A. M. Schulz, M. W. Pellegrino, Y. Lu, S. Shaham and C. M. Haynes (2016). "Maintenance and propagation of a deleterious mitochondrial genome by the mitochondrial unfolded protein response." Nature **533**(7603): 416-419.

Ling, S.-C., M. Polymenidou and Don W. Cleveland (2013). "Converging Mechanisms in ALS and FTD: Disrupted RNA and Protein Homeostasis." Neuron **79**(3): 416-438.

Liu, J. and F. Wang (2017). "Role of Neuroinflammation in Amyotrophic Lateral Sclerosis: Cellular Mechanisms and Therapeutic Implications." Front Immunol **8**: 1005.

Liu, T., J.-A. A. Woo, M. Z. Bukhari, X. Wang, Y. Yan, S. C. Buosi, A. Ermekbaeva, A. Sista, P. Kotsiviras, P. LePochat, A. Chacko, X. Zhao and D. E. Kang (2022). "Modulation of synaptic plasticity, motor unit physiology, and TDP-43 pathology by CHCHD10." Acta Neuropathologica Communications **10**(1): 95.

Liu, T., J. A. Woo, M. Z. Bukhari, P. LePochat, A. Chacko, M. B. Selenica, Y. Yan, P. Kotsiviras, S. C. Buosi, X. Zhao and D. E. Kang (2020). "CHCHD10-regulated OPA1-mitofilin complex mediates TDP-43-induced mitochondrial phenotypes associated with frontotemporal dementia." Faseb j **34**(6): 8493-8509.

Liu, W., X. Duan, L. Xu, W. Shang, J. Zhao, L. Wang, J.-C. Li, C.-H. Chen, J.-P. Liu and C. Tong (2020). "Chchd2 regulates mitochondrial morphology by modulating the levels of Opa1." Cell Death & Differentiation **27**(6): 2014-2029.

Liu, Y., H. V. Clegg, P. L. Leslie, J. Di, L. A. Tollini, Y. He, T. H. Kim, A. Jin, L. M. Graves, J. Zheng and Y. Zhang (2014). "CHCHD2 inhibits apoptosis by interacting with Bcl-x L to regulate Bax activation." Cell Death And Differentiation **22**: 1035.

Liu, Y., B. S. Samuel, P. C. Breen and G. Ruvkun (2014). "Caenorhabditis elegans pathways that surveil and defend mitochondria." Nature **508**(7496): 406-410.

Liu, Y. T., X. Huang, D. Nguyen, M. K. Shammas, B. P. Wu, E. Dombi, D. A. Springer, J. Poulton, S. Sekine and D. P. Narendra (2020). "Loss of CHCHD2 and CHCHD10 activates OMA1 peptidase to disrupt mitochondrial cristae phenocopying patient mutations." Hum Mol Genet **29**(9): 1547-1567.

Longen, S., M. Bien, K. Bihlmaier, C. Kloeppel, F. Kauff, M. Hammermeister, B. Westermann, J. M. Herrmann and J. Riemer (2009). "Systematic analysis of the twin cx(9)c protein family." J Mol Biol **393**(2): 356-368.

Lopez-Gonzalez, R., Y. Lu, T. F. Gendron, A. Karydas, H. Tran, D. Yang, L. Petrucelli, B. L. Miller, S. Almeida and F. B. Gao (2016). "Poly(GR) in C9ORF72-Related ALS/FTD Compromises Mitochondrial Function and Increases Oxidative Stress and DNA Damage in iPSC-Derived Motor Neurons." Neuron **92**(2): 383-391.

Luna, L. G. (1968). "Manual of histologic staining methods of the Armed Forces Institute of Pathology."

Magrané, J., C. Cortez, W. B. Gan and G. Manfredi (2014). "Abnormal mitochondrial transport and morphology are common pathological denominators in SOD1 and TDP43 ALS mouse models." Hum Mol Genet **23**(6): 1413-1424.

Magrané, J., I. Hervias, M. S. Henning, M. Damiano, H. Kawamata and G. Manfredi (2009). "Mutant SOD1 in neuronal mitochondria causes toxicity and mitochondrial dynamics abnormalities." Human molecular genetics **18**(23): 4552-4564.

Mao, C., H. Wang, H. Luo, S. Zhang, H. Xu, S. Zhang, J. Rosenblum, Z. Wang, Q. Zhang, M. Tang, M. J. Shepard, X. Wang, Y. Wang, Z. Zhuang, C. Shi and Y. Xu (2019). "CHCHD10 is involved in the development of Parkinson's disease caused by CHCHD2 loss-of-function mutation p.T61I." Neurobiology of Aging **75**: 38-41.

Matsui, H., J. Ito, N. Matsui, T. Uechi, O. Onodera and A. Kakita (2021). "Cytosolic dsDNA of mitochondrial origin induces cytotoxicity and neurodegeneration in cellular and zebrafish models of Parkinson's disease." Nat Commun **12**(1): 3101.

McArthur, K., L. Whitehead, J. Heddleston, L. Li, B. Padman, V. Oorschot, N. Geoghegan, S. Chappaz, S. Davidson and H. San Chin (2018). BAK/BAX macropores facilitate mitochondrial herniation and mtDNA efflux during apoptosis. Science. 359: eaao6047.

McCauley, M. E. and R. H. Baloh (2019). "Inflammation in ALS/FTD pathogenesis." Acta Neuropathologica **137**(5): 715-730.

Meng, H., C. Yamashita, K. Shiba-Fukushima, T. Inoshita, M. Funayama, S. Sato, T. Hatta, T. Natsume, M. Umitsu, J. Takagi, Y. Imai and N. Hattori (2017). "Loss of Parkinson's disease-associated protein CHCHD2 affects mitochondrial crista structure and destabilizes cytochrome c." Nature communications **8**: 15500-15500.

Miller, R. G., J. D. Mitchell and D. H. Moore (2012). "Riluzole for amyotrophic lateral sclerosis (ALS)/motor neuron disease (MND)." Cochrane Database Syst Rev **2012**(3): Cd001447.

Modjtahedi, N., K. Tokatlidis, P. Dessen and G. Kroemer (2016). "Mitochondrial Proteins Containing Coiled-Coil-Helix-Coiled-Coil-Helix (CHCH) Domains in Health and Disease." Trends in Biochemical Sciences **41**(3): 245-260.

Moloney, E. B., F. de Winter and J. Verhaagen (2014). "ALS as a distal axonopathy: molecular mechanisms affecting neuromuscular junction stability in the presymptomatic stages of the disease." Frontiers in neuroscience **8**: 252.

Motwani, M., S. Pesiridis and K. A. Fitzgerald (2019). "DNA sensing by the cGAS-STING pathway in health and disease." Nat Rev Genet **20**(11): 657-674.

Müller, K., P. M. Andersen, A. Hübers, N. Marroquin, A. E. Volk, K. M. Danzer, T. Meitinger, A. C. Ludolph, T. M. Strom and J. H. Weishaupt (2014). "Two novel mutations in conserved codons indicate that CHCHD10 is a gene associated with motor neuron disease." Brain **137**(12): e309-e309.

Nakahira, K., S. Hisata and A. M. Choi (2015). "The Roles of Mitochondrial Damage-Associated Molecular Patterns in Diseases." Antioxid Redox Signal **23**(17): 1329-1350.

Neumann, M., D. M. Sampathu, L. K. Kwong, A. C. Truax, M. C. Micsenyi, T. T. Chou, J. Bruce, T. Schuck, M. Grossman, C. M. Clark, L. F. McCluskey, B. L. Miller, E. Masliah, I. R. Mackenzie, H. Feldman, W. Feiden, H. A. Kretzschmar, J. Q. Trojanowski and V. M. Lee (2006). "Ubiquitinated TDP-43 in frontotemporal lobar degeneration and amyotrophic lateral sclerosis." Science **314**(5796): 130-133.

Nguyen, M. K., K. McAvoy, S. C. Liao, Z. Doric, I. Lo, H. Li, G. Manfredi and K. Nakamura (2022). "Mouse midbrain dopaminergic neurons survive loss of the PD-associated mitochondrial protein CHCHD2." Hum Mol Genet **31**(9): 1500-1518.

Nicoletti, G., M. Gagliardi, R. Procopio, G. Iannello, M. Morelli, G. Annesi and A. Quattrone (2018). "A new CHCHD2 mutation identified in a southern italy patient with multiple system atrophy." Parkinsonism Relat Disord **47**: 91-93.

Ogaki, K., S. Koga, M. G. Heckman, F. C. Fiesel, M. Ando, C. Labbé, O. Lorenzo-Betancor, E. L. Moussaud-Lamodière, A. I. Soto-Ortolaza, R. L. Walton, A. J. Strongosky, R. J. Uitti, A. McCarthy, T. Lynch, J. Siuda, G. Opala, M. Rudzinska, A. Krygowska-Wajs, M. Barcikowska, K. Czyzewski, A. Puschmann, K. Nishioka, M. Funayama, N. Hattori, J. E. Parisi, R. C. Petersen, N. R. Graff-Radford, B. F. Boeve, W. Springer, Z. K. Wszolek, D. W. Dickson and O. A. Ross (2015). "Mitochondrial targeting sequence variants of the CHCHD2 gene are a risk for Lewy body disorders." Neurology **85**(23): 2016-2025.

Orsini, M., A. B. Oliveira, O. J. M. Nascimento, C. H. M. Reis, M. A. A. Leite, J. A. de Souza, C. Pupe, O. G. de Souza, V. H. Bastos, M. R. G. de Freitas, S. Teixeira, C. Bruno, E. Davidovich and B. Smidt (2015). "Amyotrophic Lateral Sclerosis: New Perpectives and Update." Neurology international **7**(2): 5885-5885.

Oskarsson, B., T. F. Gendron and N. P. Staff (2018). "Amyotrophic Lateral Sclerosis: An Update for 2018." Mayo Clin Proc **93**(11): 1617-1628.

Paganoni, S., S. Hendrix, S. P. Dickson, N. Knowlton, J. D. Berry, M. A. Elliott, S. Maiser, C. Karam, J. B. Caress, M. A. Owegi, A. Quick, J. Wymer, S. A. Goutman, D. Heitzman, T. D. Heiman-Patterson, C. Jackson, C. Quinn, J. D. Rothstein, E. J. Kasarskis, J. Katz, L. Jenkins, S.

S. Ladha, T. M. Miller, S. N. Scelsa, T. H. Vu, C. Fournier, K. M. Johnson, A. Swenson, N. Goyal, G. L. Pattee, S. Babu, M. Chase, D. Dagostino, M. Hall, G. Kittle, M. Eydinov, J. Ostrow, L. Pothier, R. Randall, J. M. Shefner, A. V. Sherman, E. Tustison, P. Vigneswaran, H. Yu, J. Cohen, J. Klee, R. Tanzi, W. Gilbert, P. Yeramian and M. Cudkowicz (2022). "Effect of sodium phenylbutyrate/taurursodiol on tracheostomy/ventilation-free survival and hospitalisation in amyotrophic lateral sclerosis: long-term results from the CENTAUR trial." Journal of Neurology, Neurosurgery & Psychiatry **93**(8): 871-875.

Paganoni, S., S. Hendrix, S. P. Dickson, N. Knowlton, E. A. Macklin, J. D. Berry, M. A. Elliott, S. Maiser, C. Karam, J. B. Caress, M. A. Owegi, A. Quick, J. Wymer, S. A. Goutman, D. Heitzman, T. D. Heiman-Patterson, C. E. Jackson, C. Quinn, J. D. Rothstein, E. J. Kasarskis, J. Katz, L. Jenkins, S. Ladha, T. M. Miller, S. N. Scelsa, T. H. Vu, C. N. Fournier, J. D. Glass, K. M. Johnson, A. Swenson, N. A. Goyal, G. L. Pattee, P. L. Andres, S. Babu, M. Chase, D. Dagostino, M. Hall, G. Kittle, M. Eydinov, M. McGovern, J. Ostrow, L. Pothier, R. Randall, J. M. Shefner, A. V. Sherman, M. E. St Pierre, E. Tustison, P. Vigneswaran, J. Walker, H. Yu, J. Chan, J. Wittes, Z.-F. Yu, J. Cohen, J. Klee, K. Leslie, R. E. Tanzi, W. Gilbert, P. D. Yeramian, D. Schoenfeld and M. E. Cudkowicz (2021). "Long-term survival of participants in the CENTAUR trial of sodium phenylbutyrate-taurursodiol in amyotrophic lateral sclerosis." Muscle & Nerve **63**(1): 31-39.

Paganoni, S., E. A. Macklin, S. Hendrix, J. D. Berry, M. A. Elliott, S. Maiser, C. Karam, J. B. Caress, M. A. Owegi, A. Quick, J. Wymer, S. A. Goutman, D. Heitzman, T. Heiman-Patterson, C. E. Jackson, C. Quinn, J. D. Rothstein, E. J. Kasarskis, J. Katz, L. Jenkins, S. Ladha, T. M. Miller, S. N. Scelsa, T. H. Vu, C. N. Fournier, J. D. Glass, K. M. Johnson, A. Swenson, N. A. Goyal, G. L. Pattee, P. L. Andres, S. Babu, M. Chase, D. Dagostino, S. P. Dickson, N. Ellison, M. Hall, K. Hendrix, G. Kittle, M. McGovern, J. Ostrow, L. Pothier, R. Randall, J. M. Shefner, A. V. Sherman, E. Tustison, P. Vigneswaran, J. Walker, H. Yu, J. Chan, J. Wittes, J. Cohen, J. Klee, K. Leslie, R. E. Tanzi, W. Gilbert, P. D. Yeramian, D. Schoenfeld and M. E. Cudkowicz (2020). "Trial of Sodium Phenylbutyrate-Taurursodiol for Amyotrophic Lateral Sclerosis." N Engl J Med **383**(10): 919-930.

Patrushev, M., V. Kasymov, V. Patrusheva, T. Ushakova, V. Gogvadze and A. Gaziev (2004). "Mitochondrial permeability transition triggers the release of mtDNA fragments." Cell Mol Life Sci **61**(24): 3100-3103.

Pellegrino, M. W., A. M. Nargund, N. V. Kirienko, R. Gillis, C. J. Fiorese and C. M. Haynes (2014). "Mitochondrial UPR-regulated innate immunity provides resistance to pathogen infection." Nature **516**(7531): 414-417.

Penttilä, S., M. Jokela, H. Bouquin, A. M. Saukkonen, J. Toivanen and B. Udd (2015). "Late onset spinal motor neuronopathy is caused by mutation in CHCHD10." Ann Neurol **77**(1): 163-172.

Perrone, F., H. P. Nguyen, S. Van Mossevelde, M. Moisse, A. Sieben, P. Santens, J. De Bleecker, M. Vandenbulcke, S. Engelborghs, J. Baets, P. Cras, R. Vandenberghe, P. De Jonghe, P. P. De Deyn, J.-J. Martin, P. Van Damme, C. Van Broeckhoven and J. van der Zee (2017).

"Investigating the role of ALS genes CHCHD10 and TUBA4A in Belgian FTD-ALS spectrum patients." Neurobiology of Aging **51**: 177.e179-177.e116.

Peterson, T. S., J. M. Spitsbergen, S. W. Feist and M. L. Kent (2011). "Luna stain, an improved selective stain for detection of microsporidian spores in histologic sections." Dis Aquat Organ **95**(2): 175-180.

Poewe, W., K. Seppi, C. M. Tanner, G. M. Halliday, P. Brundin, J. Volkmann, A.-E. Schrag and A. E. Lang (2017). "Parkinson disease." Nature Reviews Disease Primers **3**(1): 17013.

Purandare, N., M. Somayajulu, M. Hüttemann, L. I. Grossman and S. Aras (2018). "The cellular stress proteins CHCHD10 and MNRR1 (CHCHD2): Partners in mitochondrial and nuclear function and dysfunction." Journal of Biological Chemistry **293**(17): 6517-6529.

Riley, J. S., G. Quarato, C. Cloix, J. Lopez, J. O'Prey, M. Pearson, J. Chapman, H. Sesaki, L. M. Carlin, J. F. Passos, A. P. Wheeler, A. Oberst, K. M. Ryan and S. W. Tait (2018). "Mitochondrial inner membrane permeabilisation enables mtDNA release during apoptosis." Embo j **37**(17).

Ronchi, D., G. Riboldi, R. Del Bo, N. Ticozzi, M. Scarlato, D. Galimberti, S. Corti, V. Silani, N. Bresolin and G. P. Comi (2015). "CHCHD10 mutations in Italian patients with sporadic amyotrophic lateral sclerosis." Brain **138**(8): e372-e372.

Rosen, D. R., T. Siddique, D. Patterson, D. A. Figlewicz, P. Sapp, A. Hentati, D. Donaldson, J. Goto, J. P. O'Regan, H.-X. Deng, Z. Rahmani, A. Krizus, D. McKenna-Yasek, A. Cayabyab, S. M. Gaston, R. Berger, R. E. Tanzi, J. J. Halperin, B. Herzfeldt, R. Van den Bergh, W.-Y. Hung, T. Bird, G. Deng, D. W. Mulder, C. Smyth, N. G. Laing, E. Soriano, M. A. Pericak–Vance, J. Haines, G. A. Rouleau, J. S. Gusella, H. R. Horvitz and R. H. Brown (1993). "Mutations in Cu/Zn superoxide dismutase gene are associated with familial amyotrophic lateral sclerosis." Nature **362**(6415): 59-62.

Ruan, Y., J. Hu, Y. Che, Y. Liu, Z. Luo, J. Cheng, Q. Han, H. He and Q. Zhou (2022). "CHCHD2 and CHCHD10 regulate mitochondrial dynamics and integrated stress response." Cell Death & Disease **13**(2): 156.

Ryan, É. B., J. Yan, N. Miller, S. Dayanidhi, Y. C. Ma, H.-X. Deng and T. Siddique (2021). "Early death of ALS-linked CHCHD10-R15L transgenic mice with central nervous system, skeletal muscle, and cardiac pathology." iScience **24**(2): 102061.

Sakowski, S. A., J. S. Lunn, A. S. Busta, S. S. Oh, G. Zamora-Berridi, M. Palmer, A. A. Rosenberg, S. G. Philip, J. J. Dowling and E. L. Feldman (2012). "Neuromuscular effects of G93A-SOD1 expression in zebrafish." Molecular Neurodegeneration **7**(1): 44.

Sato, S., S. Noda, S. Torii, T. Amo, A. Ikeda, M. Funayama, J. Yamaguchi, T. Fukuda, H. Kondo, N. Tada, S. Arakawa, M. Watanabe, Y. Uchiyama, S. Shimizu and N. Hattori (2021). "Homeostatic p62 levels and inclusion body formation in CHCHD2 knockout mice." Hum Mol Genet **30**(6): 443-453.

Sayles, N. M., N. Southwell, K. McAvoy, K. Kim, A. Pesini, C. J. Anderson, C. Quinzii, S. Cloonan, H. Kawamata and G. Manfredi (2022). "Mutant CHCHD10 causes an extensive metabolic rewiring that precedes OXPHOS dysfunction in a murine model of mitochondrial cardiomyopathy." Cell Reports **38**(10): 110475.

Schmid, B., A. Hruscha, S. Hogl, J. Banzhaf-Strathmann, K. Strecker, J. van der Zee, M. Teucke, S. Eimer, J. Hegermann, M. Kittelmann, E. Kremmer, M. Cruts, B. Solchenberger, L. Hasenkamp, F. van Bebber, C. Van Broeckhoven, D. Edbauer, S. F. Lichtenthaler and C. Haass (2013). "Loss of ALS-associated TDP-43 in zebrafish causes muscle degeneration, vascular dysfunction, and reduced motor neuron axon outgrowth." Proc Natl Acad Sci U S A **110**(13): 4986-4991.

Shammas, M. K., X. Huang, B. P. Wu, E. Fessler, I. Y. Song, N. P. Randolph, Y. Li, C. K. Bleck, D. A. Springer, C. Fratter, I. A. Barbosa, A. F. Powers, P. M. Quirós, C. Lopez-Otin, L. T. Jae, J. Poulton and D. P. Narendra (2022). "OMA1 mediates local and global stress responses against protein misfolding in CHCHD10 mitochondrial myopathy." J Clin Invest **132**(14).

Shaw, M. P., A. Higginbottom, A. McGown, L. M. Castelli, E. James, G. M. Hautbergue, P. J. Shaw and T. M. Ramesh (2018). "Stable transgenic C9orf72 zebrafish model key aspects of the ALS/FTD phenotype and reveal novel pathological features." Acta Neuropathol Commun **6**(1): 125.

Sheridan, C. (2019). "Drug developers switch gears to inhibit STING." Nature Biotechnology **37**(3): 199-201.

Shi, C.-h., C.-y. Mao, S.-y. Zhang, J. Yang, B. Song, P. Wu, C.-t. Zuo, Y.-t. Liu, Y. Ji, Z.-h. Yang, J. Wu, Z.-p. Zhuang and Y.-m. Xu (2016). "CHCHD2 gene mutations in familial and sporadic Parkinson's disease." Neurobiology of Aging **38**: 217.e219-217.e213.

Shpilka, T. and C. M. Haynes (2018). "The mitochondrial UPR: mechanisms, physiological functions and implications in ageing." Nature Reviews Molecular Cell Biology **19**(2): 109-120.

Smeyers, J., E.-G. Banchi and M. Latouche (2021). "C9ORF72: What It Is, What It Does, and Why It Matters." Frontiers in Cellular Neuroscience **15**.

Sreedharan, J., I. P. Blair, V. B. Tripathi, X. Hu, C. Vance, B. Rogelj, S. Ackerley, J. C. Durnall, K. L. Williams, E. Buratti, F. Baralle, J. de Belleroche, J. D. Mitchell, P. N. Leigh, A. Al-Chalabi, C. C. Miller, G. Nicholson and C. E. Shaw (2008). "TDP-43 mutations in familial and sporadic amyotrophic lateral sclerosis." Science **319**(5870): 1668-1672.

Stackley, K. D., C. C. Beeson, J. J. Rahn and S. S. L. Chan (2011). "Bioenergetic Profiling of Zebrafish Embryonic Development." PLoS ONE **6**(9): e25652.

Straub, I. R., A. Janer, W. Weraarpachai, L. Zinman, J. Robertson, E. Rogaeva and E. A. Shoubridge (2018). "Loss of CHCHD10–CHCHD2 complexes required for respiration underlies the pathogenicity of a CHCHD10 mutation in ALS." Human Molecular Genetics **27**(1): 178-189.

Straub, I. R., W. Weraarpachai and E. A. Shoubridge (2021). "Multi-OMICS study of a CHCHD10 variant causing ALS demonstrates metabolic rewiring and activation of endoplasmic reticulum and mitochondrial unfolded protein responses." Hum Mol Genet **30**(8): 687-705.

Taylor, J. P., R. H. Brown, Jr. and D. W. Cleveland (2016). "Decoding ALS: from genes to mechanism." Nature **539**(7628): 197-206.

Taylor, R. W. and D. M. Turnbull (2005). "Mitochondrial DNA mutations in human disease." Nat Rev Genet **6**(5): 389-402.

Tian, Y., C. Merkwirth and A. Dillin (2016). "Mitochondrial UPR: A Double-Edged Sword." Trends Cell Biol **26**(8): 563-565.

Tio, M., R. Wen, Y. L. Lim, Z. H. B. Zukifli, S. Xie, P. Ho, Z. Zhou, T.-W. Koh, Y. Zhao and E.-K. Tan (2017). "Varied pathological and therapeutic response effects associated with CHCHD2 mutant and risk variants." Human Mutation **38**(8): 978-987.

Todkar, K., L. Chikhi, V. Desjardins, F. El-Mortada, G. Pépin and M. Germain (2021). "Selective packaging of mitochondrial proteins into extracellular vesicles prevents the release of mitochondrial DAMPs." Nature Communications **12**(1): 1971.

Traynor, B. J., J. O. Johnson, S. M. Glynn, J. R. Gibbs, M. A. Nalls, M. Sabatelli, G. Restagno, V. E. Drory, A. Chiò and E. Rogaeva (2014). "Mutations in the CHCHD10 gene are a common cause of familial amyotrophic lateral sclerosis." Brain **137**(12): e311-e311.

Van Langenhove, T., J. van der Zee and C. Van Broeckhoven (2012). "The molecular basis of the frontotemporal lobar degeneration-amyotrophic lateral sclerosis spectrum." Ann Med **44**(8): 817-828.

Vande Velde, C., K. K. McDonald, Y. Boukhedimi, M. McAlonis-Downes, C. S. Lobsiger, S. Bel Hadj, A. Zandona, J.-P. Julien, S. B. Shah and D. W. Cleveland (2011). "Misfolded SOD1 Associated with Motor Neuron Mitochondria Alters Mitochondrial Shape and Distribution Prior to Clinical Onset." PLOS ONE **6**(7): e22031.

Vinsant, S., C. Mansfield, R. Jimenez-Moreno, V. Del Gaizo Moore, M. Yoshikawa, T. G. Hampton, D. Prevette, J. Caress, R. W. Oppenheim and C. Milligan (2013). "Characterization of early pathogenesis in the SOD1(G93A) mouse model of ALS: part II, results and discussion." Brain Behav **3**(4): 431-457.

Wang, W., L. Wang, J. Lu, S. L. Siedlak, H. Fujioka, J. Liang, S. Jiang, X. Ma, Z. Jiang, E. L. da Rocha, M. Sheng, H. Choi, P. H. Lerou, H. Li and X. Wang (2016). "The inhibition of TDP-43 mitochondrial localization blocks its neuronal toxicity." Nat Med **22**(8): 869-878.

Wang, Y., E. Xu, P. R. Musich and F. Lin (2019). "Mitochondrial dysfunction in neurodegenerative diseases and the potential countermeasure." CNS Neurosci Ther **25**(7): 816-824.

West, A. P. and G. S. Shadel (2017). "Mitochondrial DNA in innate immune responses and inflammatory pathology." Nature Reviews Immunology **17**(6): 363-375.

West, R. J. H., R. Furmston, C. A. C. Williams and C. J. H. Elliott (2015). "Neurophysiology of Drosophila Models of Parkinson's Disease." Parkinson’s Disease **2015**: 381281.

Woo, J.-A., T. Liu, C. Trotter, C. C. Fang, E. De Narvaez, P. LePochat, D. Maslar, A. Bukhari, X. Zhao and A. Deonarine (2017). "Loss of function CHCHD10 mutations in cytoplasmic TDP-43 accumulation and synaptic integrity." Nature Communications **8**: 15558.

Woo, J. A., T. Liu, C. Trotter, C. C. Fang, E. De Narvaez, P. LePochat, D. Maslar, A. Bukhari, X. Zhao, A. Deonarine, S. D. Westerheide and D. E. Kang (2017). "Loss of function CHCHD10 mutations in cytoplasmic TDP-43 accumulation and synaptic integrity." Nat Commun **8**: 15558.

Xia, W., J. Qiu, Y. Peng, M. M. Snyder, L. Gu, K. Huang, N. Luo, F. Yue and S. Kuang (2022). "Chchd10 is dispensable for myogenesis but critical for adipose browning." Cell Regeneration **11**(1): 14.

Xiao, T., B. Jiao, W. Zhang, C. Pan, J. Wei, X. Liu, Y. Zhou, L. Zhou, B. Tang and L. Shen (2017). "Identification of CHCHD10 Mutation in Chinese Patients with Alzheimer Disease." Molecular Neurobiology **54**(7): 5243-5247.

Xiao, Y., J. Zhang, X. Shu, L. Bai, W. Xu, A. Wang, A. Chen, W.-Y. Tu, J. Wang, K. Zhang, B. Luo and C. Shen (2019). "Loss of mitochondrial protein CHCHD10 in skeletal muscle causes neuromuscular junction impairment." Human Molecular Genetics **29**(11): 1784-1796.

Xiao, Y., J. Zhang, X. Shu, L. Bai, W. Xu, A. Wang, A. Chen, W. Y. Tu, J. Wang, K. Zhang, B. Luo and C. Shen (2020). "Loss of mitochondrial protein CHCHD10 in skeletal muscle causes neuromuscular junction impairment." Hum Mol Genet **29**(11): 1784-1796.

Yang, N., Y. Zhao, Z. Liu, R. Zhang, Y. He, Y. Zhou, Q. Xu, Q. Sun, X. Yan, J. Guo and B. Tang (2019). "Systematically analyzing rare variants of autosomal-dominant genes for sporadic Parkinson's disease in a Chinese cohort." Neurobiol Aging **76**: 215.e211-215.e217.

Youle, R. J. and A. M. van der Bliek (2012). "Mitochondrial Fission, Fusion, and Stress." Science **337**(6098): 1062-1065.

Yu, C. H., S. Davidson, C. R. Harapas, J. B. Hilton, M. J. Mlodzianoski, P. Laohamonthonkul, C. Louis, R. R. J. Low, J. Moecking, D. De Nardo, K. R. Balka, D. J. Calleja, F. Moghaddas, E. Ni, C. A. McLean, A. L. Samson, S. Tyebji, C. J. Tonkin, C. R. Bye, B. J. Turner, G. Pepin, M. P. Gantier, K. L. Rogers, K. McArthur, P. J. Crouch and S. L. Masters (2020). "TDP-43 Triggers Mitochondrial DNA Release via mPTP to Activate cGAS/STING in ALS." Cell **183**(3): 636-649.e618.

Zhang, M., Z. Xi, L. Zinman, A. C. Bruni, R. G. Maletta, S. A. M. Curcio, I. Rainero, E. Rubino, L. Pinessi, B. Nacmias, S. Sorbi, D. Galimberti, A. E. Lang, S. Fox, E. I. Surace, M. Ghani, J. Guo, C. Sato, D. Moreno, Y. Liang, J. Keith, B. J. Traynor, P. St George-Hyslop and E. Rogaeva

(2015). "Mutation analysis of CHCHD10 in different neurodegenerative diseases." Brain **138**(9): e380-e380.

Zhong, Z., S. Liang, E. Sanchez-Lopez, F. He, S. Shalapour, X.-j. Lin, J. Wong, S. Ding, E. Seki and B. Schnabl (2018). "New mitochondrial DNA synthesis enables NLRP3 inflammasome activation." Nature **560**(7717): 198-203.

Zhou, Q., Y. Chen, Q. Wei, B. Cao, Y. Wu, B. Zhao, R. Ou, J. Yang, X. Chen, S. Hadano and H. F. Shang (2017). "Mutation Screening of the CHCHD10 Gene in Chinese Patients with Amyotrophic Lateral Sclerosis." Mol Neurobiol **54**(5): 3189-3194.

Zhou, W., D. Ma, A. X. Sun, H.-D. Tran, D.-l. Ma, B. K. Singh, J. Zhou, J. Zhang, D. Wang, Y. Zhao, P. M. Yen, E. Goh and E.-K. Tan (2018). "PD-linked CHCHD2 mutations impair CHCHD10 and MICOS complex leading to mitochondria dysfunction."

Zhou, W., D. Ma and E. K. Tan (2020). "Mitochondrial CHCHD2 and CHCHD10: Roles in Neurological Diseases and Therapeutic Implications." Neuroscientist **26**(2): 170-184.

Zou, Z. Y., Z. R. Zhou, C. H. Che, C. Y. Liu, R. L. He and H. P. Huang (2017). "Genetic epidemiology of amyotrophic lateral sclerosis: a systematic review and meta-analysis." J Neurol Neurosurg Psychiatry **88**(7): 540-549.